Solitary wave interaction and evolution

Sayed Mohammad Hoseini
University of Wollongong

Solitary wave interaction and evolution

Sayed Mohammad Hoseini
B.Sc., M.Sc. Mathematics

A thesis submitted in fulfilment of the requirements for the award of the degree of Doctor of Philosophy

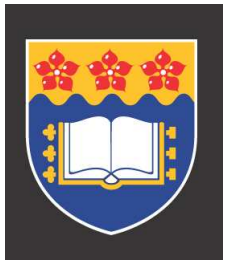

School of Mathematics and Applied Statistics
University of Wollongong
Wollongong 2522, New South Wales, Australia
June 2007

Dedicated to

My wife, Amir Ali, newborn Fatemeh Sadat,
my father and my mother.

In The Name of Allah

Abstract

Asymptotic theory is applied to examine solitary wave interaction for three higher-order model equations, which represent small perturbations to integrable equations. The higher-order equations considered are the higher-order Nonlinear Schrödinger equation and the focusing and defocusing higher-order Hirota equations. The asymptotic theory, which involves a transformation, allows the straightforward determination of parameter choices, for which the higher-order equations are asymptotically integrable, and of the higher-order phase and coordinate shifts due to the collision, in the asymptotically integrable cases. For the higher-order Hirota equations, direct soliton perturbation theory is also used, to determine the details of the evolving solitary waves; in particular analytical expressions are found for the solitary wave tails.

An important feature of the asymptotic and perturbation theories is that they allow cross-validation of the theoretical results and also allow families of asymptotic embedded solitons to be identified.

Numerical solutions of the governing equations are also obtained. For solitary wave interaction, asymptotically elastic and inelastic cases are considered. When the higher-order coefficients satisfy the appropriate algebraic relationship then the numerical results confirm the prediction of the asymptotic theory. Numerical solutions for evolving solitary waves are also used to confirm the results of the soliton perturbation theory.

Declaration

I, Sayed M. Hoseini, declare that this thesis, submitted in partial fulfilment of the requirements for the award of Doctor of Philosophy, in the school of Mathematics and Applied Statistics, University of Wollongong, is wholly my own work unless otherwise referenced or acknowledged. The document has not been submitted for qualifications at any other academic institution.

Sayed M. Hoseini

June 2007

Acknowledgements

First of all I want to thank God and my dear wife *Somayeh Zahedi Nejad*, to whom this thesis is dedicated, for her encouragement and patience. It is the least you deserve for putting up with countless late nights, and for steadying frayed nerves.

To my dear kids, *Amir Ali* and *Fatemeh Sadat* whose love and support provided me the energy to attain my study.

To my supervisor A/Prof *Timothy Marchant* for the excellent supervision he provided and for all the help, advice and assistance which he gave besides those related to academic matters. I whole-heartedly appreciate all of this assistance. This help opened up my eyes and mind to the topic of solitary waves and his teaching led me to a deeper understanding of solitons and solitary wave interaction. He also taught me how to gain a better relationship with other people. Without his guidance, this thesis could not come to fruition.

List of publications

The following publications have been published by the author during his studies.

[**1**] S. M. Hoseini and T. R. Marchant. Solitary wave interaction and evolution for a higher-order Hirota equation. *Wave Motion.*, 44:92-106, 2006.

[**2**] B. Whiten , M. McGuiness and S. M. Hoseini. Sustainable water management in the minerals industry. *Proceedings of the Mathematics-In-Industry-Study Group.*, ISBN 0-473-11068-7, 2006.

[**3**] S. M. Hoseini and T. R. Marchant. Solitary wave interaction for a higher-order nonlinear Schrödinger equation. *IMA Journal of Applied Mathematics*, 72:206-222, 2007.

[**4**] S. M. Hoseini and T. R. Marchant. Gray soliton interaction and evolution for a higher-order Hirota equation. to be submitted.

[**5**] S. M. Hoseini and T. R. Marchant. Soliton perturbation theory on a higher-order Hirota equation. submitted to *Mathematics and Computers in Simulation*, submitted, 2007.

Papers 1, 3, 4 and 5 are included in this thesis. Papers 1 and 5 are Chapter 3, paper 3 is Chapter 2 and paper 4 is Chapter 4.

Table of Contents

List of Figures

Chapter 1

Introduction

In recent years there has been a great deal of interest in the development of solitary wave solutions of higher-order model equations and in the determination of the effects of the collision which the higher-order solitary waves suffer. The interest in higher-order models for some physical systems occurring in oceanography and nonlinear optics results from their improved accuracy. As is well known, for a wide class of higher-order dispersive wave equations, for which the leading order equations are completely integrable, the higher-order equations can be asymptotically transformed into higher-order integrable equations, to the same order of approximation. The first significant work in soliton solutions, involving asymptotic transformations was Kodama's pioneering work [21]. By using a canonical map he obtained an approximate Hamiltonian for the higher-order Korteweg-de Vries (KdV)

$$\eta_t + 6\eta\eta_x + \eta_{xxx} + \epsilon c_1\eta^2\eta_x + \epsilon c_2\eta_x\eta_{xx} + \epsilon c_3\eta\eta_{xxx} + \epsilon c_4\eta_{xxxxx} = 0, \quad \epsilon \ll 1, \quad (1.1)$$

where ϵ is a measure of the importance of the higher-order terms and the real parameters c_i depend on the physical context. The Hamiltonian was exact for the integrable version of the higher-order KdV equation and accurate to $O(\epsilon)$ in the general case, which implies that the higher-order KdV equation with arbitrary coefficients is approximately integrable. The asymptotic transformation used included a nonlocal term. More recently, Fokas and Liu [7], showed that asymptotic transformations can be developed by considering the master symmetries of the associated integrable equation.

Marchant and Smyth [28] also transformed the higher-order KdV equation (1.1) with arbitrary coefficients, to the associated higher-order integrable KdV equation. In contrast to Kodama [21], a local asymptotic transformation was used. The higher-order two-soliton solution for (1.1) was considered well before and after interaction and found to consist of two higher-order solitary waves of (1.1), which were unchanged in shape. Moreover, no dispersive radiation was present; hence, it was concluded that the collision was elastic to at least $O(\epsilon)$. The $O(\epsilon)$ corrections to the phase shifts of the higher-order solitary waves after collision were also found.

Marchant [26] applied an asymptotic transformation to the higher-order modified equation

$$\begin{aligned}&\eta_t + 24\eta^2\eta_x + \eta_{xxx} + \epsilon c_1\eta^4\eta_x + \epsilon c_2\eta_x^3\\&+\epsilon c_3\eta^2\eta_{xxx} + \epsilon c_4\eta\eta_x\eta_{xx} + \epsilon c_5\eta_{xxxxx} = 0, \quad \epsilon \ll 1,\end{aligned} \tag{1.2}$$

and hence examined solitary wave interaction for (1.2). The higher-order mKdV (1.2) was asymptotically transformed to the mKdV equation (when $\epsilon = 0$ in (1.2)), when the higher-order coefficients satisfy a certain algebraic relationship. This is in contrast to the higher-order KdV, which can be asymptotically transformed for all choices of c_i . This allowed the higher-order mKdV two-soliton solution to be found, including predictions for the higher-order phase shifts.

This thesis considers three higher-order wave equations, the higher-order nonlinear Schrödinger (NLS) equation

$$\begin{aligned}&i\omega_t + \omega_{xx} + \omega|\omega|^2 + \epsilon(c_1|\omega|^4\omega + c_2\omega^2\overline{\omega}_{xx} + c_3\overline{\omega}\omega_x^2 + c_4|\omega_x|^2\omega\\&+c_5|\omega|^2\omega_{xx} + c_6\omega_{xxxx}) = 0, \quad \epsilon \ll 1,\end{aligned} \tag{1.3}$$

and the higher-order Hirota equations with positive and negative signs (focusing and defocusing)

$$\begin{aligned}&\eta_t + 3\alpha|\eta|^2\eta_x \pm \gamma\eta_{xxx} + \epsilon(c_1\alpha^2|\eta|^4\eta_x + c_2\alpha\gamma(\eta|\eta_x|^2)_x + c_3\alpha\gamma\eta^*(\eta\eta_{xx})_x\\&+c_4\alpha\gamma\eta^*\eta_x\eta_{xx} + c_5\alpha\gamma\eta\eta_x\eta_{xx}^* + c_6\gamma^2\eta_{5x}) = 0, \quad \epsilon \ll 1,\end{aligned} \tag{1.4}$$

where the parameters α and γ are real and positive. The physical applications of (1.3) and (1.4) are discussed in the chapters 2, 3, 4. These higher-order wave

equations are generalized versions of a member of the integrable hierarchies, see for example Kano [17]. Note that for $\epsilon = 0$, (1.3) and (1.4) become the usual NLS and Hirota equations, respectively. Those are integrable and are exactly solvable by the inverse scattering transform (IST), see for example Hirota [13] and Mihalache *et. al.* [31]. However, Hirota [13] developed his 'direct method' with which he was able to build multi-soliton solutions of (1.3) and (1.4).

The main technique to study the effects of the the higher-order terms in the wave equations considered in this thesis, is an extension of the normal form theory developed by Kodama [21] and Marchant [26]. Here we would like to roughly describe the characteristic features of this method. The idea of the method is very simple; by using an asymptotic transformation the higher-order wave equations with arbitrary coefficients are transformed into an integrable higher-order equation. It is shown that the asymptotic transformation is valid if the higher-order coefficients satisfy an algebraic relationship. Using the asymptotic transformations, one and two-soliton solutions of the higher-order integrable equations can be transformed to one and two higher-order solitary wave solutions for (1.3) and (1.4). For the two-soliton solutions the transformation also allows the higher-order phase and coordinate shifts, which the solitary waves suffer during collision, to be found analytically.

In this thesis, it is assumed that the asymptotic transformation used relate the corresponding solutions of the integrable and higher-order equations. This is analytically and numerically verified for one and two soliton solutions considered here, but no proof exists for more general types of solutions. However, as the transform involves neglecting terms at second-order ($O(\epsilon^2)$), it is likely that any transformed solution remains a valid solution of the higher-order equation on a timescale up to $t \sim O(\frac{1}{\epsilon^2})$.

When the asymptotic theory is not applicable, the direct soliton perturbation method based on the IST shall be used to describe the evolution of the higher-order solitary waves, see sections 3.4 and 4.4. Some general features of this approach can be seen from the papers of Hereman [12] for bright solitons and Chen *et. al.* [3] for dark solitons with non-vanishing boundary conditions. According to the direct perturbation theory the solution of the inhomogeneous linear operator associated

with the higher-order problem is expanded in the complete set of eigenfunctions of the related homogenous linear operator. Hence, we construct the linearisation operator for the higher-order problem by expanding the initial one-soliton solution in powers of ϵ. In particular, for the higher-order Hirota equation (1.4), to solve for the ϵ coefficients in the expansion, the eigenstates of the adjoint operator are needed. For (1.4), it can be shown that the eigenfunctions of the linear operator and adjoint operator are squared Jost solutions of the Lax equations related to the unperturbed problems. The method allows, in order to eliminate the secular terms in the expansion, the effects of higher-order nonlinearities on the soliton parameters to be found. In sections 3.4 and 4.4, the solitary wave solutions of the higher-order Hirota equation at $O(\epsilon)$ are found but a similar procedure could be applied to find the solution at $O(\epsilon^2)$ and beyond.

In chapter 2, solitary wave interaction for the higher-order NLS equation (1.3) is examined. By using a nonlocal asymptotic transformation, (1.3) is transformed to a higher-order member of NLS hierarchy of integrable equations, if the higher-order coefficients satisfy a linear algebraic relationship. This transformation is used to find the single and two-soliton solutions for (1.3) to be found. Due to the complexity of NLS two-soliton solution, the higher-order two-soliton solutions are investigated well before and after interaction. The interaction is shown to be elastic and higher-order corrections to the coordinate and phase shifts, which the higher-order solitary waves suffer, are found. The numerical simulations are considered for two different examples; one satisfies the algebraic relationship derived from asymptotic theory, and the other does not. For the first example which satisfies the relationship, the numerical solutions confirm that the collision is elastic and the theoretical coordinate and phase shifts predictions are confirmed. For the second example which does not satisfy the relationship, a symmetric head on collision of solitary waves is considered. For this example radiation is shed by the solitary wave collision and forms a bed on which the solitary waves sit. The shelf height is shown to be slowly decaying (like $t^{-\frac{1}{2}}$), which indicates that computations to calculate the final phase and coordinate shifts are infeasible. And in the meantime, the noteworthy result is that for this example the collision is inelastic; radiation is shed by the solitary wave collision.

In chapter 3, solitary wave interaction and evolution for the focusing higher-order Hirota equation, (1.4) with positive sign, is examined. For the focusing case, bright solitons exist which propagate on a zero background. A similar procedure to chapter 2 is used to derive the single and two-soliton higher-order solutions for (1.4). Numerical simulations are again used to confirm the higher-order corrections to the coordinate and phase shifts. An example which satisfies the algebraic relationship derived from asymptotic theory is used for this purpose.

Hirota solitons are embedded in the linear wave spectrum. For the higher-order Hirota equation (1.4), the resonant interactions between the solitary wave and the linear radiation leads to radiation loss and the formation of a tail behind the solitary wave. Soliton perturbation theory is used to determine the details of the evolving wave and it's tail. In 3.4 the soliton perturbation theory involves expanding the ϵ-order solitary wave solution as a sum of the localized (discrete) and non-localized (continuous) eigenstates of the unperturbed Hirota equation. In particular, an integral expression is found for the first-order correction to the solitary wave profile. Moreover, an asymptotic expansion, valid for large time, allows a simple analytical expression to be found for the solitary wave tail. It is found that a two-parameter family of higher-order asymptotic solitons exists (when the solitary wave tail vanishes). An excellent comparison is found between the theoretical and numerical solutions, for the solitary wave tail. Another noteworthy result is that the two parameter family of higher-order asymptotic embedded solitons found from perturbation theory, exist when the higher-order coefficients satisfy the algebraic relationship derived from asymptotic theory.

In chapter 4, we extend our discussion to the case of the defocusing higher-order Hirota equation (1.4) with the negative sign. Here, for simplicity, we assume $\alpha = 2$ and $\gamma = 1$ and re-scale the higher-order coefficients c_i. It has been previously shown that the defocusing Hirota equation has dark soliton solutions which are stable on a nonzero continuous background, see for example Mahalingam and Porsezian [25] and Li *et. al.* [24]. By using an asymptotic transformation the dark one-soliton solution of the integrable higher-order Hirota equation is transformed to the dark soliton solution of higher-order Hirota equation (1.4). For two-soliton solution of

(1.4), it is seen that the absolute value of the two-soliton solution for defocusing Hirota equation at $|\eta|^q$ can be considered as sum of the absolute values of the two Hirota one-soliton solutions well before and after the collision. Using this fact and asymptotic transformation derived in section 4.3, the higher-order phase shifts are found, if the higher-order coefficients satisfy an algebraic relationship. Analogous to the higher-order bright Hirota solitons, the direct perturbation theory is used to study the evolution of dark higher-order Hirota solitary wave solutions. The perturbation theory shows that a subtle and complex picture of solitary wave tail evolution occurs.

In Appendix A, the Lax equations related to the defocusing Hirota equation considered in section 4.4 and the Jost solutions are presented. It is shown that the non-localized (continuous) eigenstate of the linearized operator related to the defocusing Hirota equation is just the squared Jost solution. It is also shown that the first Lax equation in the zero curvature representation for Hirota equation is shared with the NLS counterpart, so a similar procedure can be used to find the Hirota Jost solutions.

In Appendix B, the numerical scheme for the higher-order defocusing Hirota equation, discussed in chapter 4, is presented. The numerical scheme is a hybrid fourth order Runge-Kutta finite-difference scheme with fourth-order centered finite differences in the spatial coordinate.

Lastly, we would like to point out that there are slight differences between notations and parameters used in each chapter.

Chapter 2

Solitary wave interaction for a higher-order NLS equation

In this chapter solitary wave interaction for the higher-order NLS equation (1.3) is examined. The results of this chapter appear in Hoseini and Marchant [15]. An asymptotic transformation is used to transform the higher-order NLS equation (1.3) to a higher-order member of the NLS integrable hierarchy, if an algebraic relationship between the higher-order coefficients is satisfied. The transformation is used to derive the higher-order one and two-soliton solutions; in general the N-soliton solution can be derived. It is shown that the higher-order collision is asymptotically elastic and analytical expressions are found for the higher-order phase and coordinate shifts. Numerical simulations of the interaction of two higher-order solitary waves are also performed. Two examples are considered, one satisfies the algebraic relationship derived from asymptotic theory, and the other does not. For the example which satisfies the algebraic relationship, the numerical results confirm that the collision is elastic. The numerical and theoretical predictions for the higher-order phase and coordinate shifts are also in strong agreement. For the example which does not satisfy the algebraic relationship, the numerical results show that the collision is inelastic; radiation is shed by the solitary wave collision. As the bed of radiation shed by the waves decays very slowly (like $t^{-\frac{1}{2}}$), it is computationally infeasible to calculate the final phase and coordinate shifts for the inelastic example. An asymptotic conservation law is derived and used to test the finite-difference scheme

for the numerical solutions.

2.1 Introduction

One of the most important model equations in modern nonlinear science is the nonlinear Schrödinger (NLS) equation,

$$iu_t + u_{xx} + u|u|^2 = 0. \tag{2.1}$$

In the late 1960's, the NLS equation was used to describe the modulation of weakly-nonlinear wavetrains in deep water. It was shown by Benjamin and Feir [1] that an uniform wavetrain is unstable to longwave perturbations. See Peregrine [35] and Yuen and Lake [44] for reviews of fluid mechanics applications of the NLS equation.

In the optical context, the NLS equation was derived by Hasegawa and Tappert [11]. It describes the evolution of the slowly varying envelope of an optical pulse. Derived asymptotically from Maxwell's equations it assumes slow variation in the carrier frequency and the Kerr dependence (where the nonlinear refractive index $\eta = \eta_0 + \eta_1|w|^2$). The NLS equation is central to understanding soliton propagation in optical fibres, which is of critical importance to the field of fibre-based telecommunications, see for example, Wabnitz and Kodama [38].

The NLS equation is integrable; this means that a collision between NLS solitons is elastic; after the collision the solitons retain their original shape with the only memory of the collision being shifts in position and phase. The explicit N-soliton solution for the NLS equation was developed using the bilinear transformation method, see Hirota [13].

An important higher-order NLS equation was derived by Kodama [21] to describe short pulses in optical fibres,

$$iu_t + \alpha_1 u_{xx} + \alpha_2 u|u|^2 + i\epsilon(\beta_1 u_{xxx} + \beta_2|u|^2 u_x + \beta_3 u|u|_x^2) = 0, \quad \epsilon \ll 1, \tag{2.2}$$

where the α_i and β_i coefficients are all real and the β_i represent the various higher-order corrections for the short pulse. (2.2) can be asymptotically transformed to a member of the NLS integrable hierarchy, which has the higher-order coefficients

$$(\beta_1, \beta_2, \beta_3) = (\alpha_1, 3\alpha_2, 0). \tag{2.3}$$

Hence solitary wave collisions of (2.2) are asymptotically elastic, see Kano [17] or Kodama [23] for details of the transformation. Hirota's equation, the Sasa-Satsuma equation and the derivative NLS equation are all integrable special cases of (2.2).

The focus of this chapter is the higher-order NLS equation (1.3). The higher-order coefficients

$$(c_1, c_2, c_3, c_4, c_5, c_6) = (\frac{3}{8}, \frac{1}{4}, \frac{3}{4}, \frac{1}{2}, 1, \frac{1}{4}), \tag{2.4}$$

represent the next member of the NLS integrable hierarchy, after (2.3), see Kano [17] or Kodama and Mikhailov [23]. The higher-order NLS equation (1.3) is a generalization of the hierarchy member (2.4) and appears as a model for classical Heisenberg ferromagnetic spin chains, with biquadratic exchange interactions along the spin lattice, see Kavitha and Daniel [18]. The near-continuum limit of various forms of the discrete NLS equation are also governed by (1.3), see, for example, Dmitriev *et. al.* [4] or Kivshar and Salerno [20]. Discrete NLS equations are used to model optical waveguide arrays and Bose-Einstein condensates. Another application of (1.3) is the numerical analysis of finite-difference schemes for the NLS equation as the leading-order discretization error for many schemes includes higher-order terms from (1.3).

Zhu and Yang [46] examined the weak interaction in the generalized NLS equations context where the solitary waves both stable, well-separated, and having almost the same velocities and amplitudes. A similar collision is considered in this chapter (see example 2 in subsection 2.3). In fact, we study interaction of equal-amplitude solitary waves. They numerical simulated weak interaction for the generalized NLS equation with various nonlinearities such as the cubic-quintic (by letting $\gamma = 0$ in their (3.5) the higher-order NLS (2.2) is obtained), exponential, and saturable nonlinearities and made detailed predictions on the dynamics of their weak interactions. They also analytically derived a universal system of dynamical equations for parameters of interacting solitary waves using asymptotic methods and showed that these dynamical equations accurately describe the weak interaction in generalized NLS equation with arbitrary nonlinearities. Using the Karpman-Solov'ev method, they treated the interference as a small perturbation to each solitary wave. The evolution of a single solitary wave for the focusing and defocusing Hirota equations

by using perturbation theory will be successfully done in chapters 3 and 4. They also investigated the fractal-scattering phenomenon which appear in the system of dynamical equations when its single parameter is not zero.

Frauenkron *et. al.* [8] considered the NLS equation perturbed by a quintic nonlinearity ((1.3) with only the parameter c_1 nonzero). Physical applications for this equation include optical waveguides in which the refractive index deviates from the Kerr dependence. This is the case for various semiconductor and nonlinear polymer waveguides. The collisions between two and three solitary waves was considered using an accurate symplectic numerical method. For two solitary waves the effect of the inelastic collision is a small radiation loss only. However, for the collision of three solitary waves, a nontrivial energy exchange can occur between the solitary waves.

Dmitriev *et. al.* [4] considered the discrete version of the NLS equation with a small quintic perturbation. This was shown to be equivalent to the higher-order NLS equation (1.3) with the parameters c_1 and c_6 nonzero. It was shown that nontrivial inelastic behaviour can occur even when two solitary waves interact, leading to chaotic soliton scattering. Kivshar and Salerno [20] considered the stability of a travelling wave solution for an alternative discrete NLS model. The near-continuum limit of their model is (1.3) with the parameters c_5 and c_6 both non-zero.

Kano [17] considered a higher-order NLS equation (a generalization of (1.3)) and used an asymptotic transformation to consider the interaction of bound higher-order NLS solitary waves, governed by (1.3) with only c_1 nonzero. Perturbed inverse scattering theory was used to show the inelastic nature of the collision. Kodama and Mikhailov [23] considered the higher-order NLS and KP equations and identified the conditions for asymptotic integrability, by considering the existence of asymptotic conservation laws and symmetries. An example of the inelastic interaction of bound higher-order NLS solitary waves was also considered.

Kodama [21] described a method for the asymptotic transformation of a second-order KdV equation (one order beyond the KdV approximation) to a member of the KdV integrable hierarchy. Hence the second-order KdV equation is nearly integrable and the solitary waves are asymptotic solitons. Kodama [22] considered solitary wave

interaction for the BBM equation. This equation was transformed to a member of the KdV integrable hierarchy plus inelastic terms at third-order. The inverse scattering perturbation method was then used to show that the inelastic terms at third-order generate a fifth-order change in solitary wave amplitude.

Marchant and Smyth [28] asymptotically transformed a higher-order KdV equation to an integrable member of the KdV hierarchy. The higher-order KdV two-soliton solution was found using the transformation, including analytical expressions for the phase shift corrections. A good comparison was found between the predicted and numerically obtained higher-order phase shifts. Marchant [26] considered solitary wave interaction for a higher-order mKdV equation via a combination of analytical results, again obtained using an asymptotic transformation, and numerical solutions.

The resonant interaction between solitary waves and linear radiation has been the subject of much recent research. This resonance can result from the linear phase velocity being the same as the soliton velocity or from the frequency of the solitary wave being embedded in the continuous wave spectrum. This resonance normally leads to radiation loss from the solitary wave, special cases where no radiation loss occurs are called embedded solitons, see Pelinovsky and Yang [33] or Champneys *et. al.* [2]. The dispersion relation for the higher-order NLS equation (1.3) is $\omega = k^2 - \epsilon c_6 k^4$, hence when $\omega = 0$ the phase speed of the radiation (allowing for the Doppler shift) will correspond to the soliton velocity. This means resonance will occur for (1.3) when $k = (\epsilon c_6)^{-\frac{1}{2}}$.

Yang and Akylas [42] considered the NLS equation with a higher-order term of the form iu_{xxx}. They found infinite families of embedded, double-humped solitons and plotted the soliton profiles by solving the governing ode numerically. Their stability was also considered numerically. It was found that for an energy increasing perturbation the embedded solitons are stable while energy decreasing perturbations lead to decay of the soliton. Minzoni *et. al.* [32] considered a higher-order NLS equation which also included the iu_{xxx} term. They considered a double humped wave, joined by linear radiation and used a Lagrangian averaging technique to determine the details of the embedded soliton. They showed that the humped wave has an

oscillatory one-sided stability.

In this chapter we consider solitary wave interaction for the higher-order NLS equation (1.3). In section 2.2 a nonlocal asymptotic transformation is used to transform (1.3) to the integrable member of the NLS hierarchy (2.4). The transformation is valid if the higher-order coefficients satisfy a certain algebraic relationship. For this special case higher-order single and two-soliton solutions are derived, using the transformation. The higher-order collision is found to be asymptotically elastic for this special case and analytical expressions are derived for both the higher-order phase and coordinate shift corrections, due to the collision.

In section 2.3 numerical solutions are presented for two examples. For the example of an elastic collision, the theoretical predictions of section 2.2 are confirmed. In particular, the theoretical and numerical values for the higher-order phase and coordinate shifts are in close agreement. For the inelastic example radiation is shed during the collision. The coordinate and phase shifts interact with this bed of radiation, which causes the shifts to continue evolving long after collision. It is shown numerically that this bed of radiation decays like $t^{-\frac{1}{2}}$, the theoretically predicted rate. Because the rate of decay of the bed to zero height is so slow, it is computationally infeasible to calculate the final, steady-state, values of the phase and coordinate shifts. In section 2.4, the conclusion, the implications of the results found here, for two applications of (1.3), optical waveguide arrays and finite-difference schemes for the NLS equation, are discussed.

2.2 The asymptotic theory

We consider the transformation

$$\begin{aligned} u = g &+ \epsilon(c_1 - \frac{3}{2}c_2)|g|^2 g + \epsilon(c_1 - \frac{3}{2}c_2 + \frac{1}{2}c_3 - \frac{3}{2}c_6)g_{xx} \\ &+\epsilon(c_2 - c_1 + c_3 - \frac{1}{2}c_4 - \frac{3}{2}c_6)g_x \int_{-\infty}^{x} |g(p,t)|^2 dp + \epsilon x h, \quad \epsilon \ll 1, \qquad (2.5) \\ \text{where} \quad h &= (c_1 - c_2 - \frac{1}{2}c_6)(g_{xxx} + 3g_x|g|^2), \end{aligned}$$

and $g(x,t) \to 0$ as $x \to \pm\infty$. If (2.5) is substituted into (1.3), and terms of $O(\epsilon^2)$ are neglected, then $g(x,t)$ is a solution of the integrable higher-order NLS equation

$$ig_t + g_{xx} + g|g|^2 + \epsilon'(\frac{3}{2}|g|^4 g + g^2\overline{g}_{xx} + 3\overline{g}g_x^2 + 2|g_x|^2 g \qquad (2.6)$$
$$+4|g|^2 g_{xx} + g_{xxxx}) = 0, \quad \text{where} \quad \epsilon' = 2\epsilon(c_1 - c_2),$$

if the algebraic relationship

$$-4c_1 + 4c_2 + 2c_3 - c_4 + c_5 - 6c_6 = 0, \qquad (2.7)$$

is satisfied. Kano [17] and Kodama and Mikhailov [23] also considered an asymptotic transformation for the higher-order NLS equation (1.3) and obtained the algebraic relationship (2.7) for asymptotic integrability of the higher-order NLS equation.

The expression (2.5) and that of Kano [17] each contain four transformation terms, of which three are common. The term $\epsilon x h$ in not present in Kano [17] while his transformation contains a term not present here. Combining the five independent terms of (2.5) and Kano [17] lead to an expression which transforms (1.3) to the NLS equation, subject to the condition (2.7). This is in contrast to (2.5) and Kano [17] which both transform (1.3) to a member of the NLS integrable hierarchy.

The transformation term $\epsilon x h$ is secular, which means that the transformation (2.5) is only valid for $x \ll O(\epsilon^{-1})$. However, we note the Taylor series expansion

$$g(x + \epsilon x\frac{h}{g_x}, t) = g(x,t) + \epsilon x h, \quad \epsilon \ll 1, \qquad (2.8)$$

so it is possible to rewrite the secular transformation term in (2.5) as a transformation of the spatial variable, x, instead. Hence, replacing $g + \epsilon x h$ by (2.8) in (2.5) leads to a nonsecular form of the asymptotic transformation.

As (2.6) is integrable, the collision of higher-order solitary waves of (1.3) is asymptotically elastic when the higher-order coefficients satisfy (2.7). Dmitriev *et. al.* [4] considered a version of (1.3) with $\epsilon = 1$, $c_1 = \epsilon$, $c_6 = -\frac{\Delta\tau^2}{6}$ and the other c_i all zero. The parameters ϵ and τ are measures of the small higher-order nonlinearity and discreteness in their model. They find numerically that the solitary wave collisions are almost elastic when $c_1 = -1.525c_6$. Note that with only c_1 and c_6 non-zero that (2.7) implies $c_1 = -1.5c_6$ for an asymptotically elastic collision. Hence the prediction of the asymptotic theory is very close to the numerically obtained results of Dmitriev *et. al.* [4].

2.2.1 A single higher-order solitary wave

The soliton solution of the integrable higher-order NLS equation (2.6) is

$$\begin{aligned} &g = Ae^{i\varphi}\,\mathrm{sech}\,\theta, \quad \text{where} \\ &\varphi = a(x-s_1)+bt+\xi_1, \quad \theta = \kappa(x-s_1-vt), \\ &A = \sqrt{2}\kappa, \quad v = 2a-4\epsilon^{'}(a^2-\kappa^2)a, \\ &b = \kappa^2-a^2+\epsilon^{'}(\kappa^4+a^4-6\kappa^2a^2), \end{aligned} \tag{2.9}$$

and A is the amplitude of the wave, κ is related to the width of the wave envelope, v is the velocity and a and b determine the temporal and spatial dependence of the soliton's phase. Also, the soliton is located at $x = s_1$ at $t = 0$ and ξ_1 is the initial phase. For $\epsilon^{'}$ =0, (2.9) becomes the NLS soliton. Using the soliton (2.9) in the transformation (2.5) gives

$$\begin{aligned} &u = e^{i\varphi}A\,\mathrm{sech}\,\theta+\epsilon e^{i\varphi}(B\,\mathrm{sech}\,\theta+C\,\mathrm{sech}\,\theta\tanh\theta+D\,\mathrm{sech}^3\,\theta, \\ &+Ex\,\mathrm{sech}\,\theta+Fx\,\mathrm{sech}\,\theta\tanh\theta), \quad \text{where} \\ &B = \frac{1}{\sqrt{2}}\kappa a^2(3c_6+3c_2-2c_1-c_3)+\sqrt{2}a\kappa^2(2c_3-3c_6-2c_1+2c_2-c_4) \\ &+\frac{1}{\sqrt{2}}\kappa^3(6c_1-7c_2+2c_4-3c_3+3c_6), \\ &C = i\sqrt{2}\kappa^2a\,(c_3-c_4-4c_1+5c_2)+\sqrt{2}\kappa^3\,(2c_1-2c_2-2c_3+c_4+3c_6)\,, \\ &D = \sqrt{2}\kappa^3\,(c_3-c_4-2c_1+2c_2)\,, \quad E = \frac{1}{\sqrt{2}}ia\kappa(a^2-3\kappa^2)(2c_2-2c_1+c_6), \\ &F = \frac{1}{\sqrt{2}}\kappa^2(\kappa^2-3a^2)(2c_2-2c_1+c_6), \end{aligned} \tag{2.10}$$

and φ, θ and A are given by (2.9).

Using the nonsecular form of the transformation leads to a complicated implicit form for the one-soliton solution. Algebraically, it is easier to use the form (2.5) as the secular terms in (2.10) (with coefficients E and F) represent phase and velocity corrections only. Hence they can be absorbed into the phase functions θ and φ, which is achieved by rescaling a and κ,

$$\begin{aligned} \kappa &= \kappa^*(1-\epsilon(\kappa^{*^2}-3a^{*^2})(c_2-c_1+\frac{1}{2}c_6)), \\ a &= a^*(1+\epsilon(a^{*^2}-3\kappa^{*^2})(c_2-c_1+\frac{1}{2}c_6)), \end{aligned} \tag{2.11}$$

where a^* and κ^* are the rescaled values. This rescaling process is similar to the Poincaré-Lindstedt technique for the elimination of secular terms in the solution of odes.

The higher-order NLS solitary wave can then be written (after using the relationship (2.7)) as (after dropping the stars)

$$\begin{aligned}
&u = Ae^{i\varphi}\,\mathrm{sech}\,\theta + \epsilon Be^{i\varphi}\,\mathrm{sech}\,\theta + \epsilon Ce^{i\varphi}\,\mathrm{sech}\,\theta\tanh\theta + \epsilon De^{i\varphi}\,\mathrm{sech}^3\,\theta,\\
&\text{where}\quad \varphi = a\big[x - s_1 - \epsilon s_1(a^2-3\kappa^2)(c_2 - c_1 + \frac{1}{2}c_6)\big]\\
&+bt + \epsilon a\kappa(-3c_6 - 2c_1 + 2c_2 - c_4 + 2c_3) + \xi_1,\\
&\theta = \kappa\big[x - s_1(1 + \epsilon(\kappa^2 - 3a^2)(c_2 - c_1 + \frac{1}{2}c_6)),\\
&+\epsilon\kappa(2c_3 - 3c_6 - 2c_1 + 2c_2 - c_4) - vt\big],
\end{aligned} \tag{2.12}$$

and the various coefficients are given by

$$\begin{aligned}
&A = \sqrt{2}\kappa,\quad B = \frac{\sqrt{2}}{2}\kappa a^2(c_2 - c_4 + c_3 - 6c_6 + c_5)\\
&+\frac{\sqrt{2}}{6}\kappa^3(c_4 + 5c_2 + c_3 + 5c_5 - 8c_1 - 18c_6),\\
&C = i\sqrt{2}\kappa^2 a\,(c_2 - c_5 - c_3 + 6c_6)\,,\\
&D = \frac{\sqrt{2}}{3}\kappa^3(2c_1 + 12c_6 - 2c_2 - 2c_5 - c_4 - c_3)\\
&v = 2a - 4\epsilon c_6(a^2 - \kappa^2)a,\quad b = \kappa^2 - a^2 + \epsilon c_6(\kappa^4 + a^4 - 6\kappa^2 a^2).
\end{aligned} \tag{2.13}$$

Moreover, the higher-order solitary wave has been shifted from $x = s_1$ to

$$x = s_1(1 + \epsilon(\kappa^2 - 3a^2)(c_2 - c_1 + \frac{1}{2}c_6)) - \epsilon\kappa(2c_3 - 3c_6 - 2c_1 + 2c_2 - c_4), \tag{2.14}$$

at $t = 0$, by the transformation. The expressions (2.12) and (2.13) agree with the expression for a single higher-order NLS solitary wave, derived directly from (1.3). Hence the asymptotic transformation works correctly when applied to a single solitary wave.

2.2.2 The higher-order two-soliton solution

Here the two-soliton solution of (1.3) is examined for the elastic case when the higher-order coefficients satisfy (2.7). The two-soliton solution of the integrable

higher-order equation (2.6) has the explicit form as

$$\begin{aligned} g(x,t) &= \frac{g_1(x,t)}{f_1(x,t)} \quad \text{where} \\ f_1(x,t) &= \cosh\vartheta + \sinh\vartheta \tanh\theta_1 \tanh\theta_2 \\ &- \sinh\vartheta \,\mathrm{sech}\,\theta_1 \,\mathrm{sech}\,\theta_2 \cos(\varphi_1 - \varphi_2), \\ g_1 &= A_1 \,\mathrm{sech}\,\theta_1 e^{i\varphi_1}(\cos\psi_1 + i\sin\psi_1 \tanh\theta_2) \\ &+ A_2 \,\mathrm{sech}\,\theta_2 e^{i\varphi_2}(\cos\psi_2 + i\sin\psi_2 \tanh\theta_1), \\ \vartheta &= \frac{1}{2}\ln\frac{(a_1-a_2)^2+(\kappa_1-\kappa_2)^2}{(a_1-a_2)^2+(\kappa_1+\kappa_2)^2}. \end{aligned} \tag{2.15}$$

The various other parameters are

$$\begin{aligned} &A_j = \sqrt{2}\kappa_j, \quad v_j = 2a_j - 4\epsilon^{'}(a_j^2 - \kappa_j^2)a_j, \\ &\psi_j = \arg(\kappa_j^2 - \kappa_{3-j}^2 + (a_j - a_{3-j})^2 + 2i\kappa_{3-j}(a_j - a_{3-j})), \\ &\theta_j = \kappa_j(x - v_j t - s_j), \quad \varphi_j = a_j(x - s_j) + b_j t + \xi_j, \\ &b_j = \kappa_j^2 - a_j^2 + \epsilon^{'}(\kappa_j^4 + a_j^4 - 6\kappa_j^2 a_j^2), \quad j = 1, 2. \end{aligned} \tag{2.16}$$

The velocity of the jth soliton by the position $s_j + v_j t$ is v_j. The initial phase at the centre of the soliton is determined by $\varphi_j(s_j, 0) = \xi_j$. For the integrable NLS equation when $\epsilon^{'} = 0$ the higher-order two-soliton solution (2.15) becomes the NLS two-soliton solution, see Hirota [13]. The only affects of higher-order terms are on the velocities v_j and the parameters b_j of the two solitons. This is similar to the two-soliton solution of the integrable higher-order KdV equation, in which only the velocities of the solitons have a correction term at $\mathrm{O}(\epsilon)$.

Let $v_1 > v_2$ and without lose of generality we assume that the soliton with amplitude A_1 is initially well to the left of the soliton with amplitude A_2. Well before and after collision the two-soliton solution is just the supperposition of two well separated solitons; hence the collision is elastic with no radiation being shed as a result of the collision. However, the collision makes some changes on the phase and coordinate shifts that the solitons suffer. In fact these are

$$\text{coordinate shifts}: \; -\frac{2\vartheta}{\kappa_1}, \; \frac{2\vartheta}{\kappa_2}, \quad \text{phase shifts}: \; -2\psi_1, \; 2\psi_2, \tag{2.17}$$

for the waves with amplitudes A_1 and A_2, respectively. Of course, the coordinate shift (2.17) represents a shift in the position of the solitary waves profiles associated

with a change in θ_j while the phase shift shows a change in the phase of the wave, φ_j.

The form of the higher-order two-soliton solution, to O(ϵ), which describes the behavior of the higher-order NLS solitary waves during the interaction, is just the integrable higher-order NLS two-soliton solution (2.15), transformed by (2.5). However, the form of the higher-order two-soliton solution is slightly complicated, so the explicit higher-order two-soliton solution is negotiated and the nature of the collision will be determined with the solution well before and after interaction. Well before and after interaction, the two soliton solution (2.15) is just comprised of the superposion of two well separated single higher-order waves (2.9). Transforming the sum of these two solitary waves of the form (2.9) by the transformation (2.5) gives two higher-order waves of the form (2.12) with (2.13). Hence as any cross or product terms are zero for well separated solitons, the transformation works in the same manner as for the single soliton.

However, the nonlocal term in the transformation (2.5), which an integral from far behind the solitary wave to its current location, does lead to a collision dependent term in the transformation. Hence before interaction the wave with amplitude A_2 on the right will include a term representing the integration of the wave with amplitude A_1 on the left, whilst after interaction the wave with amplitude A_1 is on the right, so it contains a terms representing the integration of the wave with amplitude A_2. It can be easily shown that the relevant integral of the wave on the left is $\int_{-\infty}^{\infty} |g(x,t)|^2 dx = 4\kappa_j$ ($j = 1$ before collision and $j = 2$ after) while the interaction dependent term in the transformation is $\epsilon 4\kappa_j g_x$. We define the phase and coordinate shifts, due to the nonlocal term, as $\xi_j^{'}$ and $s_j^{'}$. Before collision (as $t \to -\infty$) these shifts are

$$\begin{aligned} (\xi_1^{'}, \xi_2^{'}) &= (-\epsilon\Omega\kappa_1 a_1, -\epsilon\Omega a_2(\kappa_2 + 2\kappa_1)), \\ (s_1^{'}, s_2^{'}) &= (-\epsilon\Omega\kappa_1, -\epsilon\Omega(\kappa_2 + 2\kappa_1)), \end{aligned} \tag{2.18}$$

while after collision (as $t \to \infty$)

$$\begin{aligned} &(\xi_1^{'}, \xi_2^{'}) = (-\epsilon\Omega a_1(\kappa_1 + 2\kappa_2), -\epsilon\Omega a_2\kappa_2), \\ &(s_1^{'}, s_2^{'}) = (-\epsilon\Omega(\kappa_1 + 2\kappa_2), -\epsilon\Omega\kappa_2), \\ &\text{where} \quad \Omega = -3c_6 - 2c_1 + 2c_2 - c_4 + 2c_3. \end{aligned} \tag{2.19}$$

Taking the difference in the phase and coordinate shifts (2.18) and (2.19) and combining them with the contribution from the rescaling (2.11) gives

$$\begin{aligned}
&\text{coordinate shifts}: \quad -\frac{2\vartheta}{\kappa_1} - 2\epsilon\lambda\kappa_2, \quad \frac{2\vartheta}{\kappa_2} + 2\epsilon\lambda\kappa_1, \\
&\text{phase shifts}: \quad -2\psi_1 - 8\epsilon\rho\kappa_2 a_2 - 2\epsilon\lambda\kappa_2 a_1, \\
&\qquad\qquad 2\psi_2 + 8\epsilon\rho\kappa_1 a_1 + 2\epsilon\lambda\kappa_1 a_2, \\
&\text{where} \quad \lambda = (4c_2 - 4c_1 - 2c_6 - c_4 + 2c_3), \quad \rho = (c_2 - c_1 + \frac{1}{2}c_6).
\end{aligned} \tag{2.20}$$

as the higher-order coordinate and phase shifts of the waves with amplitudes $A_1 = \sqrt{2}\kappa_1$ and $A_2 = \sqrt{2}\kappa_2$, respectively. For the integrable hierarchy (2.4) $\lambda = \rho = 0$ and the higher-order shifts are all zero. Also, it is worth noting that the higher-order corrections to the coordinate shifts are qualitatively similar to those for the higher-order mKdV equation, see (16) of Marchant [26]. In their (16), as in (2.20), the higher-order coordinate shift is proportional to the amplitude of the solitary wave it has collided with.

In summary, when (2.7) is satisfied, the higher-order NLS solitary wave collision is asymptotically elastic with the higher-order phase and coordinate shifts given by (2.20).

2.3 Numerical results

In this section the interaction of higher-order NLS solitary waves is examined numerically. This allows the theoretical results, which apply when (2.7) is satisfied, to be verified and allows the nature of the collision to be determined for an example not covered by the asymptotic theory.

The numerical method used here is based on a perturbation technique, similar to that used by Zou and Su [47] or Marchant [26]. In both these applications, of higher-order KdV and mKdV equations, the lowest-order solution, about which the perturbation was based, is the appropriate exact two-soliton solution. This type of numerical method is useful as it allows higher-order phase and coordinate shifts, and any inelastic effects, to be accurately identified.

The higher-order NLS equation (1.3) is expanded using

$$u = v + \epsilon p, \tag{2.21}$$

where v is the two-soliton solution of the NLS equation ((2.15) and (2.16) with $\epsilon^{'} = 0$) and p is the O(ϵ) correction term of interest here. The expansion (2.21) is substituted into the higher-order NLS equation (1.3), which leads to a linear NLS-type equation with forcing terms

$$\begin{aligned} &ip_t + p_{xx} + v^2\overline{p} + 2|v|^2 p = -f, , \qquad (2.22)\\ &\text{where} \quad f = c_1|v|^4 v + c_2 v^2 \overline{v}_{xx} + c_3 \overline{v} v_x^2 + c_4 |v_x|^2 v + c_5 |v|^2 v_{xx} + c_6 v_{xxxx}. \end{aligned}$$

The linear NLS equation (2.22) is solved by an explicit central-time central-space finite-difference scheme with second-order accuracy. The stability of the scheme is $\Delta t < \Delta x^2/4$, where Δt and Δx are the time and space discretizations, see Taha and Ablowitz [37].

When solving (2.22), there is in general, a secular growth in p, due to the forcing f not being orthogonal to the eigenfunctions of the adjoint homogeneous equation. As we wish to only focus on the effects of the solitary wave collision we need to ensure that no secular growth occurs for a single solitary wave. Hence we require $f = 0$ well before and after the collision of the waves. The contribution to the perturbation p, from a single higher-order NLS solitary wave (2.12), needs to be considered. The parameter choices

$$\begin{aligned} &(c_1, c_2, c_3, c_4, c_5, c_6) = (3q, 2q, 2q+1, 1, -1, 0), \qquad (2.23)\\ &\text{where} \quad q = \frac{1+2r}{8r-4}, \quad r = \frac{a_1^2}{2\kappa_1^2} = \frac{a_2^2}{2\kappa_2^2},\\ &\text{and} \quad (c_1, c_2, c_3, c_4, c_5, c_6) = (1, 0, -2, 0, 2, 0), \qquad (2.24) \end{aligned}$$

are used for the numerical examples as they have no O(ϵ) amplitude, velocity or phase corrections in (2.12) and (2.13). Moreover, as $c_6 = 0$, the solitary waves for these two special cases will not be subject to any resonance with linear radiation, which can only occur for $\epsilon c_6 > 0$.

The special case (2.23) satisfies (2.7), hence is asymptotically elastic and can be used to verify the theoretical results. The special case (2.24) does not satisfy (2.7),

hence is not covered by the asymptotic theory. For these special cases, the forcing $f = 0$ well before and after collision so the perturbation p after interaction represents only the higher-order coordinate and phase shifts, plus any inelastic effects, such as shed radiation.

The higher-order solitary wave solution of (1.3) for the special cases (2.23) and (2.24) is the NLS soliton

$$u = Ae^{i\varphi}\operatorname{sech}\theta, \quad \varphi = ax + (\kappa^2 - a^2)t - \epsilon\xi_1, \quad \theta = \kappa(x - \epsilon s_1 - 2at), \tag{2.25}$$

where s_1 and ξ_1 are higher-order corrections to the position and phase of the solitary wave. Applying a Taylor series expansion to (2.25) gives

$$u = Ae^{i\varphi}\operatorname{sech}\theta + \epsilon Ae^{i\varphi}(\kappa s_1 \operatorname{sech}\theta\tanh\theta - i\xi_1\operatorname{sech}\theta). \tag{2.26}$$

Hence if $\mathrm{O}(\epsilon)$ coordinate and phase shifts of s_1 and ξ_1 are applied to the solitary wave then the perturbation is given by the functions $p_1 = A\kappa s_1 e^{i\varphi}\operatorname{sech}\theta\tanh\theta$ and $p_2 = -iA\xi_1 e^{i\varphi}\operatorname{sech}\theta$ respectively. As $e^{-i\varphi}$ is a known analytical expression from the NLS two-soliton solution (2.15), the quantity $e^{-i\varphi}p$ can be determined. By considering the real and imaginary parts of $e^{-i\varphi}p$ after interaction, the higher-order coordinate and phase shifts s_1 and ξ_1 can be determined, by measuring the amplitudes of the sech tanh and sech functions, respectively.

The averaged quantity

$$\int_{-\infty}^{+\infty}(|u|^2 + \frac{\epsilon}{2}a_5|u|^4)dx, \quad \text{where} \quad a_5 = (c_2 + c_3 - c_5), \tag{2.27}$$

is asymptotically conserved by the higher-order NLS equation (1.3). The quantity $|u|^2$ is deemed mass density by some authors and energy density by others. In the optical context it relates to conservation of norm or photon number while in the water wave context it is energy. Here, for simplicity, the quantity $|u|^2$ is deemed mass density, even though it does not physically represent mass. Also note that (2.27) represents an averaged asymptotic mass density so the mass density $|u|^2$ is only conserved if $a_5 = 0$. If the mass of the system is written as $M_0 + \epsilon M_1$, then the equation for the first-order mass, at $\mathrm{O}(\epsilon)$, is

$$M_1 = \int_{-\infty}^{\infty}(p\overline{v} + \overline{p}v)dx = a_6 - \frac{a_5}{2}\int_{-\infty}^{+\infty}|v|^4dx, \tag{2.28}$$

where v is a solution of the NLS equation and a_6 is a constant. The expression (2.28) for the first-order mass is equivalent to the expression developed in [38] for the adiabatic variation of energy in a perturbed NLS equation, see their (65). For the special cases of solitary wave interactions considered here there are no $O(\epsilon)$ corrections to the solitary wave's profile, so $M_1 = 0$ for a single solitary wave. Hence before interaction the constant a_6 is chosen so that M_1 is initially zero. During interaction the quartic term in (2.28) will cause the first-order mass M_1 to vary before returning to zero after interaction.

Hence mass is not conserved during a collision of higher-order NLS solitary waves, but is conserved, if times well before and after the collision (as $t \to \pm\infty$) are considered. This is similar to the result in Marchant [26] in which mass was not conserved during a collision of higher-order mKdV solitary waves, but was conserved well before and after collision.

Example 1 is of the higher-order NLS equation (1.3) with coefficients (2.23), hence it satisfies (2.7) and is asymptotically elastic. The parameters of the two solitary waves are chosen as

$$\begin{aligned} (\kappa_1, a_1, s_1, \xi_1) &= (\frac{1}{\sqrt{2}}, \frac{1}{\sqrt{6}}, -20, 0), \\ (\kappa_2, a_2, s_2, \xi_2) &= (\frac{1}{2\sqrt{2}}, -\frac{1}{2\sqrt{6}}, 20, 0). \end{aligned} \tag{2.29}$$

The wave on the left is located at $x = -20$ initially and has amplitude $A_1 = 1$ and moves to the right with velocity 0.816. The wave on the right is located at $x = 20$ initially and has amplitude $A_2 = 0.5$ and moves to the left with velocity 0.408. The initial phases, ξ_j, of both waves are zero. Hence this is an example of a head-on collision between the two waves. As $A_1 > A_2$ the waves with amplitudes A_1 and A_2 will be referred to as the larger and smaller waves, respectively, in the discussion of results in this section.

Initially the perturbation $p = 0$, which corresponds to a time well before interaction. The forced linear NLS-type equation (2.22) is solved numerically, from $t = 0$ up until $t = 60$, which represents a time well after interaction. The spatial and temporal grid spacings used are $\triangle x = 2.5 \times 10^{-2}$ and $\triangle t = 1.5625 \times 10^{-4}$.

Figure (2.1) shows the absolute value of the perturbation, $|p|$, for example 1 at

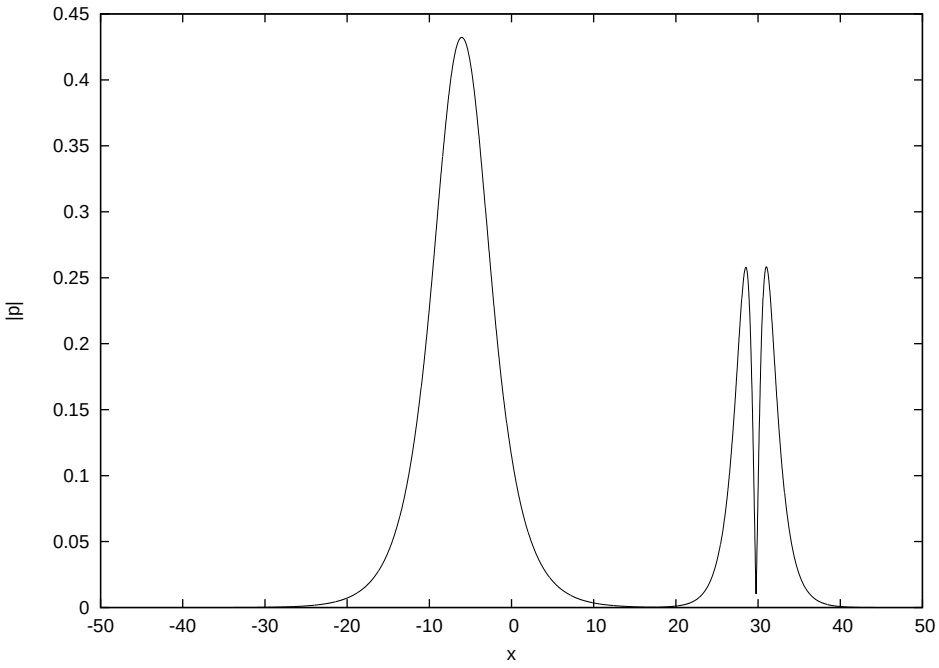

Figure 2.1: $|p|$ at $t = 60$ for example 1

time $t = 60$. The figure shows that after interaction $|p|$ comprises two, well separated humps, which represent the phase and coordinate shifts of the two solitary waves. From (2.26) we know that the coordinate shift is described by the sech tanh curve while the phase shift is described by the sech curve, so clearly the magnitude of the coordinate shift, relative to the phase shift, is much greater for the larger wave than the smaller wave.

Figure (2.2) shows the real and imaginary parts of $pe^{-i\varphi}$, at $t = 60$ for example 1. The perturbation has been scaled to eliminate the phase $e^{i\varphi}$ of the wave, so that real and imaginary parts represent the coordinate and phase shifts respectively. Also note that the expressions for the larger and smaller waves have been scaled by slightly different forms of the phase, as the NLS solitons suffer a phase shift of the form (2.17). It can be seen from figure (2.2) that the real part is anti-symmetric and the imaginary part is symmetric. Moreover, fitting $\operatorname{sech}\theta\tanh\theta$ and $\operatorname{sech}\theta$ curves to the numerical profiles, by using least squares, verifies that the numerical profiles are the same, to graphical accuracy, as the phase and coordinate shifts (2.26).

The numerical estimates of the higher-order phase and coordinate shifts are obtained by measuring the amplitudes of the symmetric and antisymmetric curves in

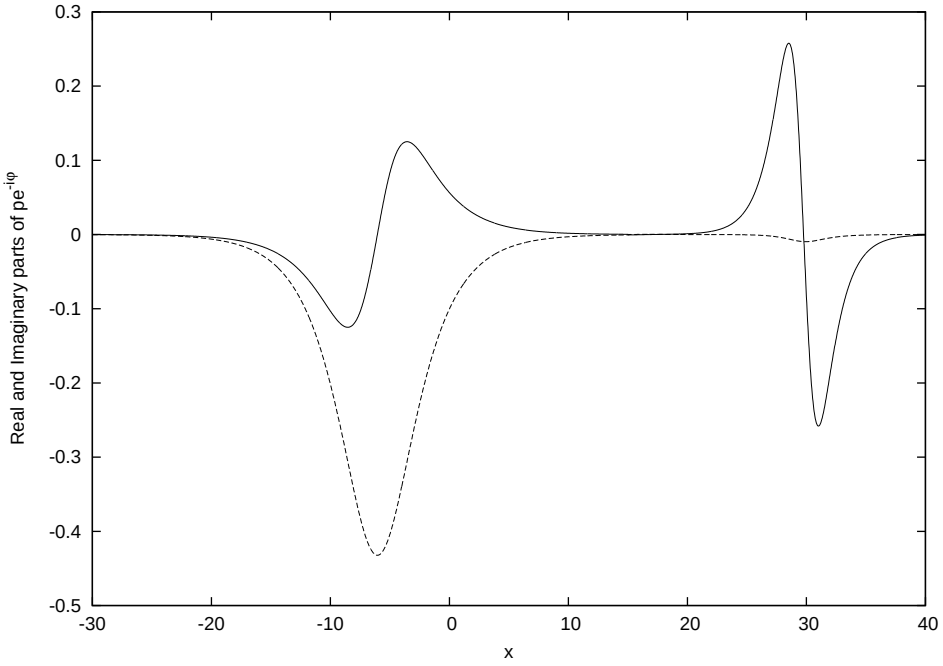

Figure 2.2: Real (solid lines) and imaginary parts (dashed lines) of $pe^{-i\varphi}$ at $t = 60$ for example 1

figure (2.2). The amplitudes are also measured using values of $\triangle x$ and $\triangle t$ double the values quoted above. Richardson extrapolation is then used to obtain a converged estimate of the phase and coordinate phase shifts. The numerically obtained phase shifts are -8.67×10^{-5} and -0.8660278 for the larger and smaller waves, respectively. The corresponding theoretical predictions from (2.20) are 0 and -0.8660254. For the coordinate shifts the numerical predictions are -0.7067908 and 1.414196, while the theoretical predictions are -0.7071068 and 1.414214, for the larger and smaller waves, respectively. In absolute terms the largest error is 3×10^{-4}. The errors are extremely small, verifying the theoretical predictions and confirming the accuracy of the numerical scheme.

Examination of the free surface behind, in front of, and in between the solitary waves after interaction shows that p is essentially flat, with no dispersive wave train produced. The amplitude of the largest oscillation in $|p|$ behind the waves is $O(10^{-5})$. Richardson extrapolation indicates the converged amplitudes of the oscillations are $O(10^{-6})$, confirming that it is merely a result of the discretization. Hence, no dispersive wave train occurs as a result of the collision, so it is elastic to

$O(\epsilon)$.

For example 1 $a_5 = 0$, hence mass is conserved during the collision. As the amplitude and velocity corrections are zero, (2.28) indicates that the first-order mass, M_1, is zero throughout the interaction of the higher-order waves. The values of M_1 are calculated numerically from the finite-difference solution at each time step, by using Simpson's method. The numerical results indicate, that for the spatial and time-discretizations used, that the magnitude of M_1 is never greater than 5.1×10^{-3}. This represents an extremely small change to the total mass of $4(\kappa_1 + \kappa_2) = 4.2426$, of the interacting solitary waves. Moreover, Richardson extrapolation indicates the converged value of M_1 is no greater than 1.1×10^{-4}. Hence the numerical scheme conserves the mass extremely accurately throughout the interaction.

In summary, it can be seen that the theoretical predictions have been confirmed for this example. The numerical results show that the collision is asymptotically elastic to $O(\epsilon)$ and the numerical estimates for the higher-order phase and coordinate shifts are extremely close to the theoretical predictions (2.20). These results also show that the numerical scheme is an extremely accurate method of determining the phase and coordinate shifts, which will now be used for the special case (2.24), which is not asymptotically elastic.

Example 2 is of the higher-order NLS equation (1.3) with coefficients (2.24), hence it does not satisfy the algebraic condition (2.7) and the asymptotic theory of §2.2 does not apply. The solitary wave parameters are given by

$$\begin{aligned} (\kappa_1, a_1, s_1, \xi_1) &= (\frac{1}{\sqrt{2}}, \frac{\sqrt{6}}{2}, -20, 0), \\ (\kappa_2, a_2, s_2, \xi_2) &= (\frac{1}{\sqrt{2}}, -\frac{\sqrt{6}}{2}, 20, 0). \end{aligned} \tag{2.30}$$

The amplitudes of the waves are unity, the velocities are ± 2.45 and the waves are located at $x = \pm 20$ initially. Hence, this represents a symmetric head on collision of solitary waves. A symmetric collision is chosen for analysis as only the solution in $x \geq 0$ needs to be calculated and $x = 0$ is the centre point of the radiation shelf. The values of $\Delta x = 5 \times 10^{-2}$ and $\Delta t = 4 \times 10^{-4}$.

Figure (2.3) shows the absolute value of the perturbation, $|p|$, for example 2 at times $t = 20, 50$ and 70. Due to the symmetry only the solution $x \geq 0$ is shown,

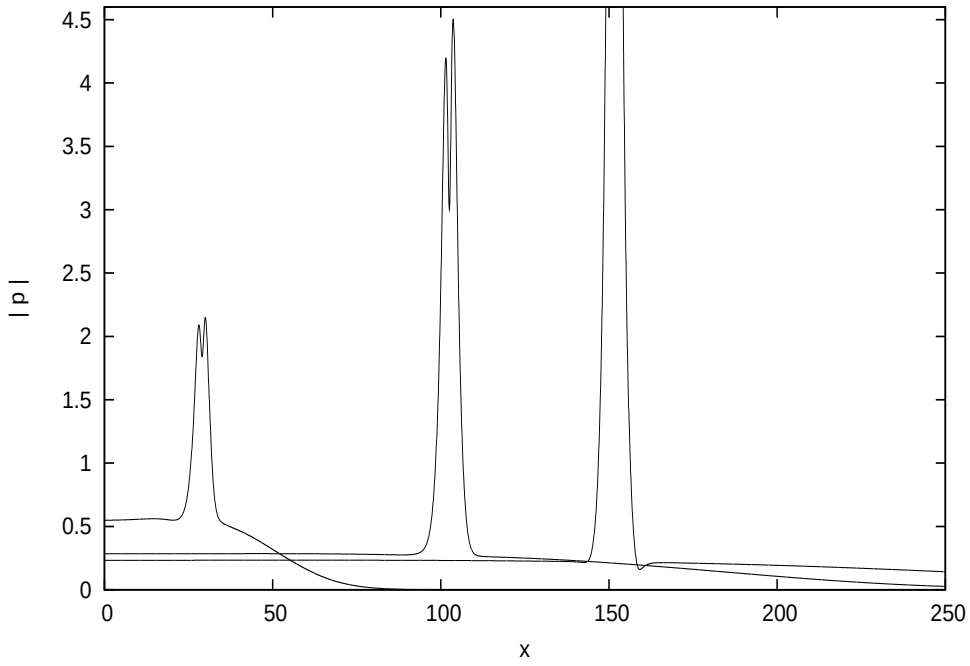

Figure 2.3: $|p|$, at $t = 20$, 50 and 70, for example 2

hence only the hump corresponding to the right moving solitary wave is visible. For this example the collision is inelastic and it can be clearly seen that the hump is sitting on a bed of radiation, which was shed during the collision. The height of the radiation bed is decreasing with time, as $|p(0,t)|$ is 0.55, 0.28 and 0.23 at the times $t = 20, 50$ and 70. Moreover, it can been that the amplitudes of the hump, corresponding to the phase and coordinate shifts, is increasing with time. The maximum values of $|p|$ are 2.15, 4.5 and 8.47, for the three different humps shown in figure (2.3).

Figure (2.4) shows the logarithm of the shelf height $|p|$ at $x = 0$ versus the logarithm of time t, up to $t = 150$. for example 2. This figure shows the rate of decrease of the shelf height with time. The slope of the curve is -0.53, at $t = 150$. Hence, at long time, the shelf height is decaying at close to the theoretically expected slope, of -0.5. See, for example, Gordon [10], whose theoretical solutions show that radiative perturbations of the NLS equation suffer a $t^{-\frac{1}{2}}$ decay rate. The similarity solution for the NLS equation has the form $u = t^{-\frac{1}{2}} f(xt^{-\frac{1}{2}})$, which also illustrates the appropriate decay rate of the shelf.

Fitting the numerical data gives the shelf height as $p(0,t) = 2.214t^{-0.53}$. For the

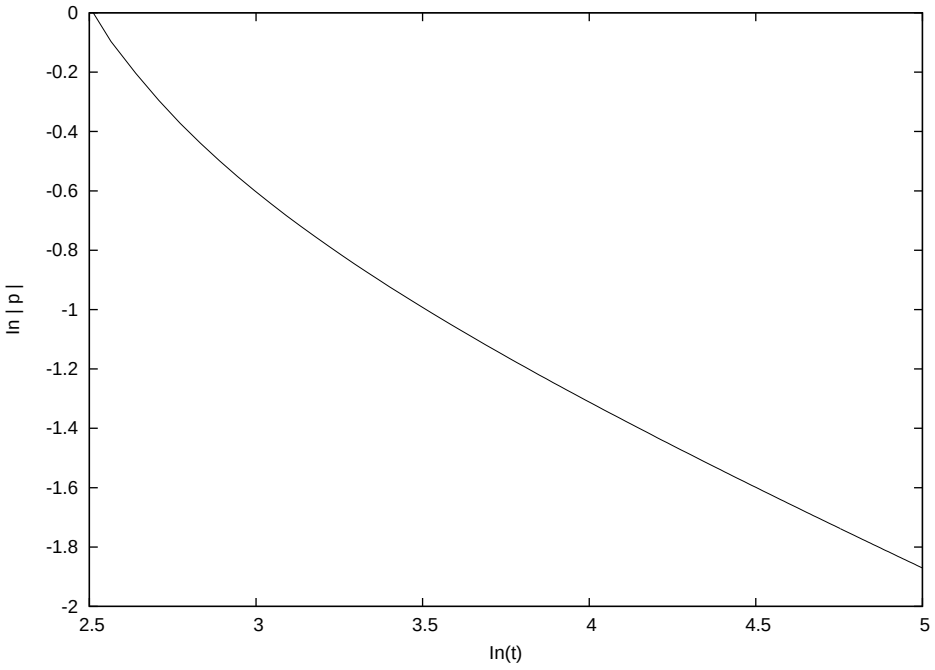

Figure 2.4: The logarithm of the shelf height $|p(0,t)|$, versus the logarithm of time t, up to $t = 150$, for example 2.

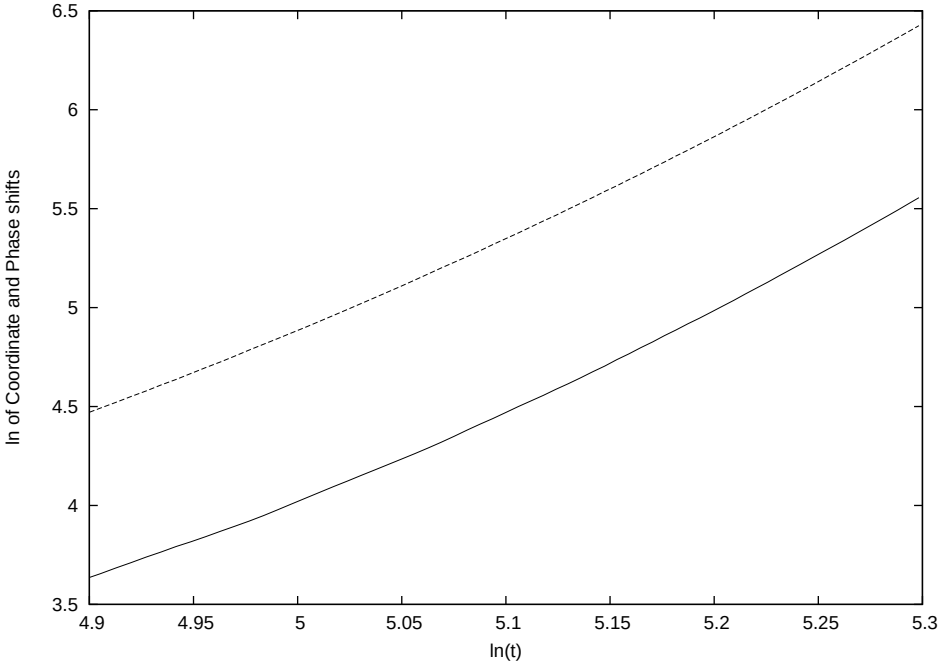

Figure 2.5: The logarithm of the phase (dashed curve) and coordinate (solid curve) shifts, versus the logarithm of time t, up to $t = 200$, for example 2

steady-state coordinate and phase shifts to be obtained the shelf height must be close to zero. For example, requiring the shelf height $|p| < 1 \times 10^{-3}$ and using the fitted power law relationship, implies that time $t > 6,700$, to obtain steady-state values, well beyond the limit of what is computationally feasible.

Figure (2.5) shows the logarithms of the phase and coordinate shifts, versus the logarithm of time t, up to $t = 200$. These shifts are related to the amplitudes of the real and imaginary parts of $pe^{-i\varphi}$, with the absolute values of the shifts being used. The curves show that both the phase and coordinate shifts are increasing in an approximately linear manner at $t = 200$. At this time $|p(0)| \approx 0.13$, hence the phase and coordinate shifts are still evolving as they interact with the bed of radiation. Note that the solitary waves have completed interacting at time $t \approx 15$, so the forcing term $f = 0$ for $\ln(t) > 2.7$. Hence the growth of the phase and coordinate shifts shown in Figure 2. 5 is not due to secular forcing terms in f.

As explained above, it is not practical to numerically determine the steady-state phase and coordinate shifts, as the steady-states are approached at very long times. Moreover, the perturbation method used here is valid for $p \ll O(\epsilon^{-1})$. Hence at long times, the validity of the perturbation method will break down, as the growth in the magnitude of the phase and coordinate shifts causes $|p|$ to reach $\mathrm{O}(\epsilon^{-1})$.

Inelastic collisions of higher-order NLS solitary waves are quite different to inelastic collisions for the higher-order KdV (or mKdV) equation. The linear NLS group velocity is $c_g = 2k$, while the linear KdV group velocity is $c_g = -3k^2$. Hence, the radiation shed at the point of a NLS collision will propagate in both the positive and negative x-directions, forming the shelf on which the solitary waves (and its associated hump) must propagate.

For the KdV equation the radiation shed at the point of collision will only propagate in the negative x-direction whilst the solitary waves (and the humps associated with the phase shifts) propagate in the positive x-direction (the KdV equation is a model for unidirectional propagation). So, for the KdV (or mKdV) equation, separation of the radiation and the solitary waves occurs at a much faster rate, than for the NLS equation, and the phase shifts due to the inelastic collision can be numerically determined. See, for example, Marchant [26], who tabulated the phase shifts

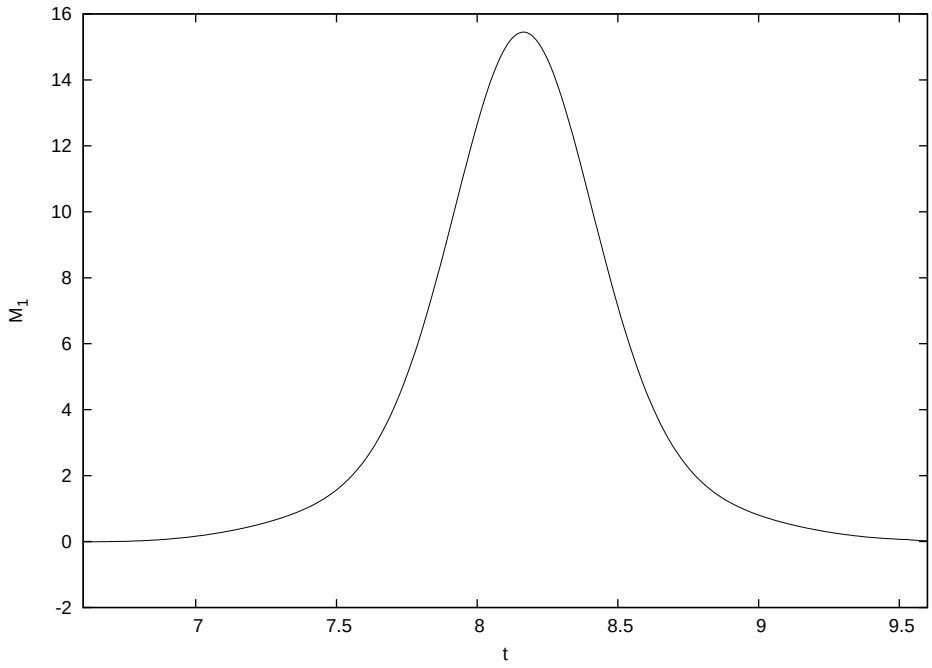

Figure 2.6: The first-order mass M_1, versus t, during the interaction, for example 2

for an inelastic higher-order mKdV equation.

Also note that alternative approaches to calculating the higher-order phase and coordinate shifts are the inverse scattering perturbation method or a direct multi-soliton perturbation theory. See, for example, Matsuno [30] who determined phase shifts for a higher-order Benjamin-Ono equation by a direct perturbation method.

Figure (2.6) shows the first-order mass M_1, versus time t, for example 2. Shown is the solution of (2.28) with v the NLS two-soliton solution. The direct numerical calculation of M_1, from the finite-difference solution is not shown as it is the same as (2.28) to graphical accuracy. For this example $a_5 = -4$, hence mass is not conserved. The first-order mass M_1 is not zero through the interaction, but increases up to a maximum value of 15.4522 at time $t \approx 8.2$. The variation between this prediction for the mass, and that from the numerical scheme, is very small, being only 9.1×10^{-4} or 0.06%. Hence the numerical scheme accurately predicts the first-order mass throughout the collision.

2.4 Conclusion

An asymptotic transformation has been applied to a higher-order NLS equation (1.3). It is found that the higher-order NLS solitary waves are asymptotic solitons when an algebraic relationship (2.7) involving the higher-order coefficients is satisfied. Analytical expressions for the higher-order phase and coordinate shifts are determined.

Numerical solutions of the higher-order NLS equation confirm the asymptotic results, namely, the elastic nature of the collision and the values of the higher-order phase and coordinate shifts. Moreover, numerical solutions, for an example not satisfying (2.7) shows strong evidence of inelastic behaviour, via the shedding of radiation. Final steady-state phase and coordinate shifts, after collision, could not be determined numerically because the bed of radiation on which each travels decays very slowly.

The numerical results presented here show the effects of an inelastic higher-order NLS collision are long-lasting. Moreover, the numerical results of Frauenkron *et. al.* [8] and Dmitriev *et. al.* [4], who solved their version of the higher-order NLS equation directly, also found strong inelastic effects, such as chaotic soliton scattering. For many physical applications strong or long-lasting inelastic effects may not be desirable, in which case it is important for the higher-order parameters to satisfy (2.7). This could be achieved by tuning the physical system in some manner to vary the higher-order parameters. One telecommunications example, is of a coupled optical fibre array, which is governed by (1.3) in the near-continuum limit. In this case the higher-order parameters could be varied by doping the fibre appropriately, in order to change its properties.

This work may also form a useful tool in the numerical analysis of finite-difference schemes for the NLS equation. For some schemes the leading-order truncation error is higher-order terms from (1.3). Inelastic effects, due to the discretization, should be avoided, hence a numerical scheme which satisfies the condition for asymptotic integrability (2.7) is highly desirable. Moreover, the numerical errors in the phase shifts can be easily estimated, using (2.20).

Chapter 3

Bright solitary wave interaction and evolution for a higher-order focusing Hirota equation

In this chapter, bright solitary wave interaction and evolution for the higher-order focusing Hirota equation (1.4) is examined. The results of this chapter appear in Hoseini and Marchant [14]. Similar to the higher-order NLS equation (1.3), the higher-order Hirota equation is asymptotically transformed to a higher-order member of the NLS hierarchy of integrable equations, if the higher-order coefficients satisfy a certain algebraic relationship. The transformation is used to derive higher-order one and two bright soliton solutions. It is shown that the interaction is asymptotically elastic and the higher-order corrections to the coordinate and phase shifts are derived. For the higher-order Hirota equation considered here, resonance occurs between the solitary waves and linear radiation, so soliton perturbation theory is used to determine the details of the evolving wave and its tail. An analytical expression for the solitary wave tail is derived and it is found that the tail vanishes when the the algebraic relationship from the asymptotic theory is satisfied. Hence a two-parameter family of higher-order asymptotic embedded solitons exists. A comparison between the theoretical predictions and numerical solutions shows strong agreement for both solitary wave interaction, where the higher-order coordinate and phase shifts are compared, and solitary wave evolution, with comparisons made of

the solitary wave tail.

3.1 Introduction

The Hirota equation is an integrable equation which has a number of physical applications, such as the propagation of optical pulses in nematic liquid crystal waveguides, see Rodriguez *et. al.* [36], and for a certain parameter regime, femtosecond pulse propagation in optical fibres, see Yang [41]. The focusing Hirota equation is

$$\eta_t + 3\alpha|\eta|^2\eta_x + \gamma\eta_{xxx} = 0, \tag{3.1}$$

where the parameters α and γ are positive real constants. As mentioned above it is integrable, see Hirota [13] for a derivation of the N-soliton solution. Note that, for simplicity, in this chapter the notions 'soliton' and 'solitary wave' are used instead of 'bright soliton' and 'bright solitary wave', respectively.

The Hirota equation is closely related to both the NLS and modified KdV (mKdV) equations, as it is a complex generalization of the mKdV equation and it is part of the NLS hierarchy of integrable equations. Also, its soliton solution has a very similar form to the NLS soliton. The Hirota equation is also called the complex modified KdV (cmKdV) equation although this name is shared with a non-integrable variant, in which the nonlinear term in (3.1) is replaced by $(|\eta|^2\eta)_x$. The non-integrable cmKdV equation has physical applications such as Langmuir solitons in a plasma, see Dysthe *et. al.* [5], and transverse waves in a elastic solid, see Erbay [6].

Hasegawa and Tappert [11] derived the NLS equation to describe the evolution of the slowly varying envelope of an optical pulse. Again, for the higher-order NLS equation (2.2) (with $\epsilon = 1$), if $3\beta_1\alpha_2 = \beta_2\alpha_1$ and $\beta_3 = 0$, then the higher-order NLS equation (2.2) reduces to the Hirota equation (3.1) via a gauge transformation, see Gilson *et. al.* [9].

The higher-order focusing Hirota equation

$$\begin{aligned}&\eta_t + 3\alpha|\eta|^2\eta_x + \gamma\eta_{xxx} + \epsilon(c_1\alpha^2|\eta|^4\eta_x + c_2\alpha\gamma(\eta|\eta_x|^2)_x + c_3\alpha\gamma\eta^*(\eta\eta_{xx})_x\\ &+c_4\alpha\gamma\eta^*\eta_x\eta_{xx} + c_5\alpha\gamma\eta\eta_x\eta^*_{xx} + c_6\gamma^2\eta_{5x}) = 0, \quad \epsilon \ll 1,\end{aligned} \tag{3.2}$$

is considered in this chapter, where starred quantities are complex conjugates and ϵ is a measure of the importance of the higher-order terms. If the higher-order coefficients are given by

$$(c_1, c_2, c_3, c_4, c_5, c_6) = (1, \frac{2}{3}, \frac{2}{3}, \frac{2}{3}, 0, \frac{2}{15}), \tag{3.3}$$

then (3.2) is a member of the NLS integrable hierarchy, see Kano [17]. Hence (3.2) represents a generalization of a member of the integrable hierarchy (3.3).

Marchant [26] examined solitary wave interaction for a higher-order mKdV equation (obtained by taking η to be real in (3.2)). The higher-order equation was asymptotically transformed to the mKdV equation, when the higher-order coefficients satisfy an algebraic relationship. This allowed the higher-order mKdV two-soliton solution to be found, including predictions for the higher-order phase shifts. Numerical modelling of the interaction of two higher-order waves, for elastic and inelastic examples, confirmed the theoretical predictions.

Marchant [27] considered the interaction of the higher-order mKdV solitons on a nonzero mean level. By using an asymptotic transformation, valid if the higher-order coefficients satisfy an algebraic relationship, he examined the collision between solitary waves with sech-type and algebraic (which only exist on a non-zero mean level) profiles. The transformation was used to show that the higher-order collision is asymptotically elastic and to derive the higher-order phase shifts. He also numerically showed that for the example covered by the asymptotic theory, the collision is elastic and the theoretical predictions for higher-order phase shifts were confirmed by numerical simulations. For the example not covered by the asymptotic theory, the interaction was shown numerically to be inelastic.

The resonant interaction between solitary waves and linear radiation can result from the linear phase velocity being the same as the soliton velocity or from the frequency of the solitary wave being embedded in the linear wave spectrum. This resonance normally leads to radiation loss and the formation of a tail behind the solitary wave. Special cases where the tail vanishes and no radiation loss occurs are called embedded solitons, see Pelinovsky and Yang [33] or Champneys *et. al.* [2].

The Hirota equation (3.1) has a two-parameter soliton family, with arbitrary amplitude and velocity, which are embedded in the linear wave spectrum. Rodriguez

et. al. [36] explains why these embedded solitons do not emit radiation and proves their stability. Yang [41] considered solitary wave evolution for a higher-order Hirota equation of the form

$$\eta_t + 6|\eta|^2\eta_x + \eta_{xxx} + i\epsilon(c_1|\eta|^2\eta + c_2\eta(|\eta|^2)_x), \quad \epsilon \ll 1. \tag{3.4}$$

Using perturbation theory he found that there exists a one-parameter family, of arbitrary amplitude, of embedded solitons. An expression for the amplitude of the solitary wave tail and ordinary differential equations (odes), describing the evolution of the wave amplitude and frequency, were found. Pelinovsky and Yang [34] also considered the higher-order Hirota equation (3.4) and performed a comprehensive stability analysis.

In this chapter we examine solitary wave interaction and evolution for the higher-order Hirota equation (3.2). In section 3.2 a nonlocal asymptotic transformation is used to transform (3.2) to the integrable member of the NLS hierarchy (3.3). The asymptotic transformation for the higher-order Hirota equation (3.2) is valid if the algebraic relationship

$$c_1 - \frac{3}{2}c_3 - c_4 - c_5 + 5c_6 = 0, \tag{3.5}$$

is satisfied. In section 3.2 higher-order single and two-soliton solutions are derived, using the transformation. For the single wave, the transformation predicts the existence of a two-parameter family of higher-order asymptotic embedded solitons. For the two-soliton collision the higher-order collision is found to be asymptotically elastic and analytical expressions are derived for both the higher-order phase and coordinate shifts, due to the collision. The asymptotic transformation represents a technique for analysing higher-order two-soliton collisions which is simpler to apply than alternative approaches, such as perturbation methods based on inverse scattering. Moreover, it establishes the existence of the embedded soliton family in a simple manner.

In section 3.3 numerical solutions are presented for an elastic collision of higher-order Hirota solitary waves. In particular, the theoretical and numerical values for the higher-order phase and coordinate shifts are in close agreement.

In section 3.4 soliton perturbation theory is used to derive the details of an

evolving solitary wave, governed by (3.2). An analytical expression is found for the solitary wave tail. An excellent comparison is found between the theoretical and numerical solutions, for the solitary wave tail. Moreover, the perturbation theory shows that the tail vanishes when (3.5) is satisfied and confirms the existence of the two-parameter family of higher-order asymptotic embedded solitons. This provides cross-validation of both theoretical approaches as the algebraic relationship (3.5) occurs in both the asymptotic transformation and the soliton perturbation method.

3.2 Asymptotic theory for solitary wave interaction

If the transformation

$$\begin{aligned}
&\eta = \psi + \frac{\alpha\epsilon}{12}(2c_1 - 4c_2 - c_3 + 10c_6 - 4c_5)|\psi|^2\psi \\
&+\frac{\gamma\epsilon}{6}(2c_1 - 2c_2 - 2c_3 + 5c_6 - 3c_5)\psi_{xx} \\
&+\frac{\alpha\epsilon}{12}(2c_1 - 2c_2 - 5c_3 + 20c_6 - 2c_5)\psi_x \int_{-\infty}^{x} |\psi(p,t)|^2 dp, \\
&\tau = t - \frac{\epsilon}{12}(2c_1 - 2c_2 - c_3 - 2c_5)x, \quad \xi = x, \quad \epsilon \ll 1,
\end{aligned} \tag{3.6}$$

where $\psi(x,t) \to 0$ as $x \to \pm\infty$, is substituted into (3.2) and terms of $O(\epsilon^2)$ are neglected, then $\psi(x,t)$ is a solution of the higher-order member of the Hirota hierarchy of integrable equations

$$\begin{aligned}
&\psi_\tau + 3\alpha|\psi|^2\psi_\xi + \gamma\psi_{\xi\xi\xi} + \epsilon^{'}\alpha^2|\psi|^4\psi_\xi + \frac{2\epsilon^{'}}{3}\alpha\gamma(\psi|\psi_\xi|^2)_\xi \\
&+\frac{2\epsilon^{'}}{3}\alpha\gamma\psi^*(\psi\psi_{\xi\xi})_\xi + \frac{2\epsilon^{'}}{3}\alpha\gamma\psi^*\psi_\xi\psi_{\xi\xi} + \frac{2\epsilon^{'}}{15}\gamma^2\psi_{5\xi} = 0, \\
&\text{where} \quad \epsilon^{'} = \frac{15\epsilon}{8}(2c_1 - 2c_2 - c_3 + 4c_6 - 2c_5) \ll 1,
\end{aligned} \tag{3.7}$$

if the algebraic relationship (3.5) is satisfied. Note that this transformation is an appropriate combination of (2.5) used for the higher-order NLS equation and that for the KdV equation, see Marchant and Smyth [28].

The form of transformation (3.6) is appropriate for solutions which approach zero far up and downstream, such as the solitary wave solutions considered here. For other forms of solutions, such as periodic solutions, the nonlocal term in the

transformation (3.6) needs to be modified slightly. The form of the transformation is qualitatively similar to the transformation (2.5). Note that a similar form of transformation (3.6) was used for a higher-order KdV equation, see Marchant and Smyth [28], and a higher-order mKdV equation, see Marchant [26]. For example, when η and ψ are real, (3.6) is equivalent to the transformation used by Marchant [26]. By appropriate scalings of the higher-order coefficients, the algebraic relationship (3.5) becomes the algebraic relation found by Marchant [26] for the higher-order mKdV equation (see his (6)).

3.2.1 A single higher-order soliton

The soliton solution of the integrable higher-order Hirota equation (3.7) is

$$\begin{aligned}
&\psi = Ae^{i\varphi}\operatorname{sech}\theta, \quad \text{where} \quad A = (\frac{2\gamma}{\alpha})^{\frac{1}{2}}\kappa,\\
&\varphi = a(\xi - b\tau - s) + \varphi_0, \quad \theta = \kappa(\xi - s - v\tau),\\
&v = \gamma(\kappa^2 - 3a^2) + \frac{2}{3}\epsilon^{'}\gamma^2(a^4 + \frac{1}{5}\kappa^4 - 2a^2\kappa^2),\\
&b = \gamma(3\kappa^2 - a^2) + \frac{2}{3}\epsilon^{'}\gamma^2(\frac{1}{5}a^4 + \kappa^4 - 2a^2\kappa^2).
\end{aligned} \tag{3.8}$$

A is the amplitude of the wave, κ is related to the width of the wave envelope and and v is the velocity. The parameter a is the wavenumber of the phase and b is related to the frequency of the phase. Also the soliton is at $\xi = s$ at $t = 0$ and φ_0 is the initial phase. For $\epsilon^{'} = 0$, (3.8) becomes the Hirota soliton which moves to the right when $\kappa^2 > 3a^2 + \epsilon^{'}\frac{32}{15}\gamma a^4$, and to the left when $\kappa^2 < 3a^2 + \epsilon^{'}\frac{32}{15}\gamma a^4$.

Using (3.8) in the transformation (3.6) gives

$$\begin{aligned}
&\eta = Ae^{i\varphi}\operatorname{sech}\theta + \epsilon Ae^{i\varphi}(B\operatorname{sech}\theta + C\operatorname{sech}\theta\tanh\theta + D\operatorname{sech}^3\theta),\\
&\text{where} \quad B = \frac{i\gamma}{6}(-2c_2 + 2c_1 + 20c_6 - 5c_3 - 2c_5)a\kappa\\
&+\frac{\gamma}{6}(2c_2 - 2c_1 - 5c_6 + 2c_3 + 3c_5)a^2 + \frac{\gamma}{6}(3c_3 - 15c_6 - c_5)\kappa^2,\\
&C = \frac{\gamma}{6}(-2c_1 + 2c_2 + 5c_3 - 20c_6 + 2c_5)\kappa^2\\
&+\frac{i\gamma}{6}(10c_6 + 2c_2 - c_3 - 2c_1 + 4c_5)a\kappa, \quad D = \frac{\gamma}{3}(10c_6 - c_3 - c_2)\kappa^2,\\
&\varphi = a[(1 + \frac{\epsilon\gamma}{4}(2c_1 - c_3 - 2c_2 - 2c_5)(\kappa^2 - \frac{a^2}{3}))x - bt - s] + \varphi_0,\\
&\theta = \kappa[(1 - \frac{\epsilon\gamma}{4}(2c_1 - c_3 - 2c_2 - 2c_5)(a^2 - \frac{\kappa^2}{3}))x - vt - s).
\end{aligned} \tag{3.9}$$

We rescale a and κ by

$$\begin{aligned} a &= a^*(1+\frac{\epsilon\gamma}{4}(\kappa^{*^2}-\frac{a^{*^2}}{3})(2c_1-c_3-2c_2-2c_5)), \\ \kappa &= \kappa^*(1-\frac{\epsilon\gamma}{4}(a^{*^2}-\frac{\kappa^{*^2}}{3})(2c_1-c_3-2c_2-2c_5)), \end{aligned} \tag{3.10}$$

where a^* and κ^* are the rescaled values. This gives, after dropping the stars, the higher-order Hirota wave in the form

$$\begin{aligned} &\eta = Ae^{i\varphi}\operatorname{sech}\theta + \epsilon Ae^{i\varphi}(B\operatorname{sech}\theta + C\operatorname{sech}\theta\tanh\theta + D\operatorname{sech}^3\theta), \\ &A = (\frac{2\gamma}{\alpha})^{\frac{1}{2}}\kappa, \quad D = \frac{\gamma}{3}(10c_6-c_3-c_2)\kappa^2, \\ &B = \frac{\gamma}{12}(2c_1-2c_2-10c_6+c_3)a^2 + \frac{\gamma}{12}(7c_3-30c_6-2c_1+2c_2)\kappa^2, \\ &C = \frac{i\gamma}{6}(10c_6+2c_2-c_3-2c_1+4c_5)a\kappa, \\ &\varphi = a[x - s(1-\frac{\epsilon\gamma}{4}(\kappa^2-\frac{a^2}{3})(2c_1-c_3-2c_2-2c_5)) \\ &+\frac{\epsilon\gamma}{6}(2c_1-2c_2+20c_6-5c_3-2c_5)\kappa - bt] + \varphi_0, \\ &\theta = \kappa[x - s(1+\frac{\epsilon\gamma}{4}(a^2-\frac{\kappa^2}{3})(2c_1-c_3-2c_2-2c_5)) \\ &+\frac{\epsilon\gamma}{6}(2c_1-2c_2+20c_6-5c_3-2c_5)\kappa - vt], \\ &v = \gamma(\kappa^2-3a^2) + \epsilon\gamma^2c_6(\kappa^4+5a^4-10\kappa^2a^2), \\ &b = \gamma(3\kappa^2-a^2) + \epsilon\gamma^2c_6(a^4+5\kappa^4-10\kappa^2a^2). \end{aligned} \tag{3.11}$$

The higher-order Hirota solitary wave (3.11), derived using the transformation (3.6), is the same as that found directly, if (3.5) is satisfied. Note that the transformation has shifted the wave from $\xi = s$ at $\tau = 0$ to

$$x = s[1+\frac{\epsilon\gamma}{4}(a^2-\frac{\kappa^2}{3})(2c_1-c_3-2c_2-2c_5)] - \frac{\epsilon\gamma}{6}(2c_1-2c_2+20c_6-5c_3-2c_5)\kappa, \tag{3.12}$$

at $t = 0$. As $\eta \to 0$ as $\theta \to \pm\infty$ in (3.11) it is a localised higher-order solitary wave. Hence when (3.5) is satisfied a two-parameter family of higher-order asymptotic embedded solitons exists. When (3.5) is not true, then mass and energy are shed, see section 3.4 for a derivation of the solitary wave tail. The condition (3.5) does not imply that exact higher-order embedded solitons occur as a tail is likely to form at second-order, $O(\epsilon^2)$, for waves satisfying (3.5).

3.2.2 The higher-order two-soliton solution

In this section the two-soliton solution of the higher-order Hirota equation (3.2), with coefficients satisfying (3.5), is found. The two-soliton solution of the integrable higher-order Hirota equation (3.7) is

$$\begin{aligned}
&\psi(\xi,\tau)=\frac{\Phi(\xi,\tau)}{\Psi(\xi,\tau)},\quad \text{where}\quad \Psi(\xi,\tau)=\\
&\cosh\vartheta+\sinh\vartheta(\tanh\theta_1\tanh\theta_2-\operatorname{sech}\theta_1\operatorname{sech}\theta_2\cos(\varphi_1-\varphi_2)),\\
&\Phi(\xi,\tau)=A_1\operatorname{sech}\theta_1 e^{i\varphi_1}(\cos\psi_1+i\sin\psi_1\tanh\theta_2)\\
&+A_2\operatorname{sech}\theta_2 e^{i\varphi_2}(\cos\psi_2+i\sin\psi_2\tanh\theta_1),\\
&\vartheta=\frac{1}{2}\ln\frac{(a_1-a_2)^2+(\kappa_1-\kappa_2)^2}{(a_1-a_2)^2+(\kappa_1+\kappa_2)^2}.
\end{aligned}\tag{3.13}$$

The various other parameters (for $j=1,2$) are

$$\begin{aligned}
&A_j=(\frac{2\gamma}{\alpha})^{\frac{1}{2}}\kappa_j,\quad \theta_j=\kappa_j(\xi-v_j\tau-s_j),\quad \varphi_j=a_j(\xi-b_j\tau-s_j)+\varphi_{0_j},\\
&\psi_j=\arg(\kappa_j^2-\kappa_{3-j}^2+(a_j-a_{3-j})^2+2i\kappa_{3-j}(a_j-a_{3-j})),\\
&v_j=\gamma(\kappa_j^2-3a_j^2)+\frac{2}{3}\epsilon'\gamma^2(a_j^4+\frac{1}{5}\kappa_j^4-2a_j^2\kappa_j^2),\\
&b_j=\gamma(3\kappa_j^2-a_j^2)+\frac{2}{3}\epsilon'\gamma^2(\frac{1}{5}a_j^4+\kappa_j^4-2a_j^2\kappa_j^2),
\end{aligned}\tag{3.14}$$

see Hirota [13]. Note that the two-soliton solution (3.13) is similar to (2.15). The velocity of the jth soliton is v_j and its position is s_j at $\tau=0$. The initial phase at the centre of the soliton is $\varphi_j(s_j,0)=\varphi_{0_j}$. When $\epsilon'=0$ it becomes the Hirota two-soliton solution. The higher-order terms only affect the velocities v_j and the parameters b_j of the two solitons. This is similar to the two-soliton solution of the integrable higher-order KdV and mKdV equations, for which only the velocities have a correction term at $O(\epsilon)$. Also, the Hirota two-soliton solution is remarkably similar to the form of the NLS two-soliton solution.

The phase and coordinate shifts for the higher-order integrable equation are

$$\text{coordinate shifts}:\ \frac{2\vartheta}{\kappa_1},\ -\frac{2\vartheta}{\kappa_2},\quad \text{phase shifts}:\ \frac{2\psi_1}{a_1},\ -\frac{2\psi_2}{a_2},\tag{3.15}$$

for the waves with amplitudes A_1 and A_2, respectively. The coordinate shift refers to a shift in the position of the wave envelope (associated with a change in θ_j) while the phase shift refers to a change in the phase of the wave, φ_j.

The higher-order two-soliton solution, to $O(\epsilon)$, describing the interaction of two higher-order Hirota solitons is just the integrable higher-order Hirota two-soliton solution (3.13), transformed by (3.6). The collision is considered well before and after interaction, where it is comprised of the sum of two well separated single higher-order waves (3.8). Substituting the sum of these two solitary waves of the form (3.8) into the transformation (3.6) gives two higher-order waves of the form (3.11).

However, the nonlocal term in (3.6) does lead to a collision dependent term in the transformation. The nonlocal term is an integral from far behind the solitary wave to its current location. The relevant integral of the wave on the left is $\int_{-\infty}^{\infty} |\psi(x,t)|^2 dx = (\frac{4\gamma}{\alpha})\kappa_j$ ($j = 1$ before collision and $j = 2$ after) and the interaction dependent term in the transformation is $(\frac{4\gamma}{\alpha})\epsilon\kappa_j\psi_x$. This term represents both a coordinate and phase shift at higher-order. Also, there is a contribution from the rescaling (3.10), to the higher-order coordinate and phase shifts. Combining these contributions gives

$$\begin{aligned}
&\text{coordinate shifts}: \quad \frac{2\vartheta}{\kappa_1} - \frac{1}{3}\epsilon\gamma\kappa_2\mu, \quad -\frac{2\vartheta}{\kappa_2} + \frac{1}{3}\epsilon\gamma\kappa_1\mu, \\
&\text{phase shifts}: \quad \frac{2\psi_1}{a_1} + \frac{1}{3a_1}\epsilon\gamma\kappa_2(a_1+2a_2)\rho - \frac{1}{3}\epsilon\gamma\kappa_2\triangle, \\
&\qquad\qquad -\frac{2\psi_2}{a_2} - \frac{1}{3a_2}\epsilon\gamma\kappa_1(a_2+2a_1)\rho + \frac{1}{3}\epsilon\gamma\kappa_1\triangle, \\
&\text{where} \quad \mu = -20c_6 + 4c_3, \quad \rho = 2c_1 - c_3 - 2c_2 - 2c_5, \\
&\qquad\qquad \triangle = -2c_2 + 2c_1 + 20c_6 - 5c_3 - 2c_5,
\end{aligned} \tag{3.16}$$

as the higher-order coordinate and phase shifts of the waves with amplitudes A_1 and A_2, respectively. For the member of the NLS integrable hierarchy (3.3), then $\mu = \rho = \triangle = 0$ and the higher-order shifts are all zero. Also, when $a_1 = a_2 = 0$ and (3.2) becomes a higher-order mKdV equation, the higher-order corrections to the coordinate shifts are the same as those for the higher-order mKdV equation, see (16) of Marchant [26]. In his (16), as in (3.16), the higher-order coordinate shift is proportional to the amplitude of the solitary wave it has collided with.

In summary, when (3.5) is satisfied, the higher-order Hirota solitary wave collision is asymptotically elastic, to first-order, with the higher-order phase and coordinate shifts given by (3.16). Inelastic effects, due to the collision, are likely to occur at second-order.

3.3 Numerical interaction of solitary waves

In this subsection the interaction of higher-order Hirota solitary waves is examined numerically. This allows the theoretical results for a solitary wave collision, which apply when (3.5) is satisfied, to be verified. The numerical method used is similar to section 2.3.

The higher-order Hirota equation (3.2) is expanded using

$$\eta = u + \epsilon p, \tag{3.17}$$

where u is the two-soliton solution of the Hirota equation ($\epsilon^{'} = 0$ in (3.13)) and p is the $O(\epsilon)$ correction term of interest here. The expansion (3.17) is substituted into the higher-order Hirota equation (3.2), which gives a linear KdV-type equation by the form

$$\begin{aligned} &p_t + \gamma p_{xxx} + 3\alpha|u|^2 p_x + 3\alpha u u_x p^* + 3\alpha u^* u_x p = -f, \\ &\text{where} \quad f = c_1\alpha^2|u|^4 u_x + c_2\alpha\gamma(u|u_x|^2)_x + c_3\alpha\gamma u^*(uu_{xx})_x \\ &+c_4\alpha\gamma u^* u_x u_{xx} + c_5\alpha\gamma u u_x u^*_{xx} + c_6\gamma^2 u_{5x}. \end{aligned} \tag{3.18}$$

To avoid secular terms the contribution to the perturbation p, from a single higher-order Hirota wave (3.2) needs to be considered. In general asymptotic solitons, which occur when (3.5) is satisfied, have $O(\epsilon)$ corrections to their amplitude, velocity and other parameters. However, the special case

$$\begin{aligned} &(c_1, c_2, c_3, c_4, c_5, c_6) = (3 - \frac{\beta}{2}, -2 + \beta, 2 - \beta, -3 + 2\beta, 3 - \beta, 0), \\ &\text{where} \quad \beta = \frac{(1 + 3\delta)}{(1 + \delta)}, \quad \delta = \frac{a_1^2}{\kappa_1^2} = \frac{a_2^2}{\kappa_2^2}, \end{aligned} \tag{3.19}$$

has no $O(\epsilon)$ corrections to the amplitude, velocity or the parameter b, in (3.11). Hence (3.19) is used for the numerical study of solitary wave interaction, using (3.18). The linear KdV-type equation (3.18) is solved by an implicit, three level, finite-difference scheme with second-order accuracy and unconditional stability. The special case (3.19), which satisfies (3.5), shows an asymptotically elastic and shall be employed to verify the theoretical results (3.16) obtained in 3.2.2 for the higher-order coordinate and phase shifts. For this special case the forcing $f = 0$ well before after

collision so the the perturbation p after interaction only represents the higher-order coordinate and phase shifts. The higher-order solution for the special case (3.19) is the Hirota soliton

$$\eta = Ae^{i\varphi}\operatorname{sech}\theta, \quad \varphi = a(x - bt - \epsilon\Lambda_2), \quad \theta = \kappa(x - vt - \epsilon\Lambda_1), \tag{3.20}$$

where Λ_1 and Λ_2 are higher-order corrections to the position and phase of the solitary wave. The description after (2.26) details how the higher-order corrections Λ_1 and Λ_2 can be measured from the solution of (3.18).

The higher-order Hirota equation (3.2) asymptotically conserves the averaged quantity

$$\int_{-\infty}^{+\infty}(|\eta|^2 + \frac{\epsilon\alpha\gamma}{6}c_7|\eta_x|^2)dx, \quad \text{where} \quad c_7 = (c_2 - 2c_3 + c_4 + c_5). \tag{3.21}$$

In the optical context it implies the conservation of photon number, see Yang [41]. Here we assign it no physical meaning but, for simplicity, call $|\eta|^2$ mass density. Note that (3.21) represents an asymptotic mass density as the mass density is only conserved if $c_7 = 0$. If the mass of the system is written as $M_0 + \epsilon M_1$, then the equation for the first-order mass is

$$M_1 = \int_{-\infty}^{+\infty}(p\overline{u} + \overline{p}u)dx = c_8 - \frac{\alpha\gamma}{6}c_7\int_{-\infty}^{+\infty}|u_x|^2dx, \tag{3.22}$$

where u is an solution of the Hirota equation (in the example here, the two-soliton solution) and c_8 is a constant. For the special case considered here there are no $O(\epsilon)$ corrections to the solitary wave's profile, so $M_1 = 0$ for a single solitary wave. Hence before interaction the constant c_8 is chosen so that M_1 is initially zero. During interaction the term $|u_x|^2$ in (3.22) will cause the first-order mass M_1 to vary before returning to zero after interaction. The expression (3.22) will be used as an additional check on the accuracy of the numerical results.

Example 1 is of the higher-order Hirota equation (3.2) with $\alpha = 2$, $\gamma = 1$ and coefficients (3.19), hence it satisfies (3.5) and is asymptotically elastic. The parameters of the two solitons are $(\kappa_1, a_1) = (1, 2)$ and $(\kappa_2, a_2) = (\frac{1}{2}, 1)$, so $\delta = 4$ and the higher-order coefficients are chosen as

$$(c_1, c_2, c_3, c_4, c_5, c_6) = (\frac{17}{10}, \frac{3}{5}, -\frac{3}{5}, \frac{11}{5}, \frac{2}{5}, 0). \tag{3.23}$$

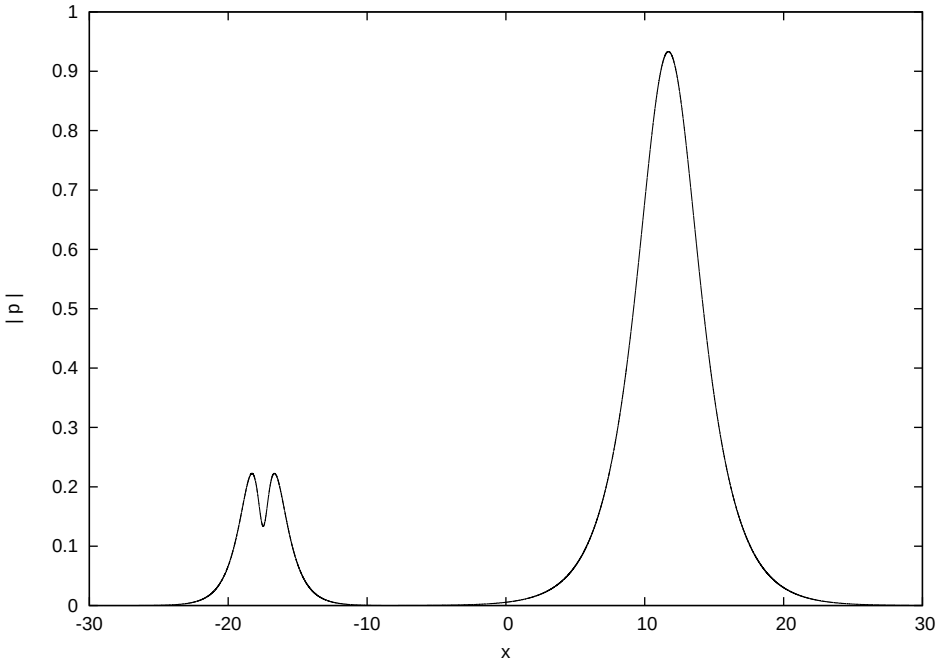

Figure 3.1: $|p|$ at $t = 7$ for example 1

The spatial and temporal grid spacings used are $\Delta x = 1 \times 10^{-3}$ and $\Delta t = 1 \times 10^{-4}$. Initially the perturbation $p = 0$ at time $t = 0$, which corresponds to a time well before interaction of the solitary waves.

Figure (3.1) shows $|p|$ for example 1 after interaction, at $t = 7$. It shows that $|p|$ comprises two, well separated humps, which represent the phase and coordinate shifts of the two solitary waves. Examination of the free surface behind the humps after interaction shows that it essentially flat, with no dispersive wave train produced. The amplitude of the largest oscillation behind the symmetric and antisymmetric waves is $O(10^{-6})$. Richardson extrapolation indicates the converged amplitudes of oscillations are $O(10^{-7})$, confirming that it is merely a result of the discretization. Hence, no dispersive wave train occurs as a result of the collision, so it is elastic to $O(\epsilon)$.

Figure (3.2) shows the imaginary and real parts of $pe^{-i\varphi}$ for example 1 at $t = 7$. The perturbation has been scaled to eliminate the phase $e^{i\varphi}$ of the waves, so that the real and imaginary parts represent the coordinate and phase shifts, respectively. It can been seen from the figure that the real part is anti-symmetric and the imaginary part is symmetric, corresponding to the sech tanh and sech functions of the Taylor

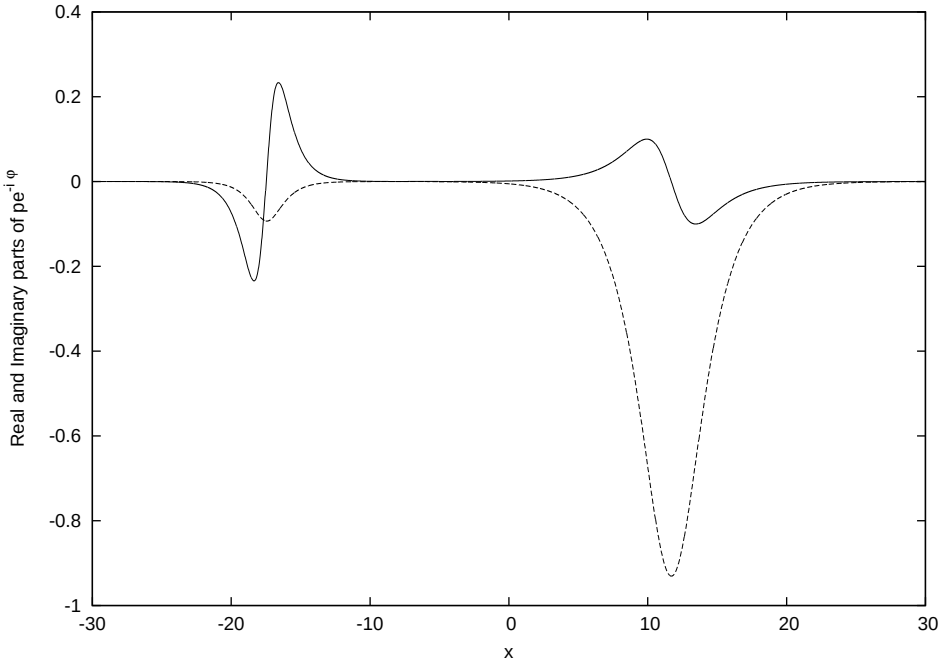

Figure 3.2: Real (solid lines) and imaginary parts (dashed lines) of $pe^{-i\varphi}$ at $t = 7$ for example 1

series expansion (2.26). Also, note that the expressions for the two waves have been scaled by slightly different forms of the phase, as Hirota solitons suffer different phase shifts, given by (3.15).

The numerical estimates of the higher-order phase and coordinate shifts are obtained by measuring the amplitudes of the symmetric and antisymmetric curves in figure (3.2). The amplitudes are also measured using values of Δx and Δt double the values quoted above. Richardson extrapolation is then used to obtain a converged estimate of the phase and coordinate phase shifts. The numerically obtained phase shifts are -0.0671 and -1.8667 for the larger and smaller waves, respectively. The corresponding theoretical predictions from (3.16) are -0.0667 and -1.8667. For the coordinate shifts the numerical predictions are 0.4000 and -0.7999, while the theoretical predictions are 0.4 and -0.8, for the larger and smaller waves, respectively. In absolute terms the largest error is 4×10^{-4}. The errors are extremely small, verifying the theoretical predictions and confirming the accuracy of the numerical scheme.

Figure (3.3) shows the first-order mass M_1, versus time t, for example 1. Shown

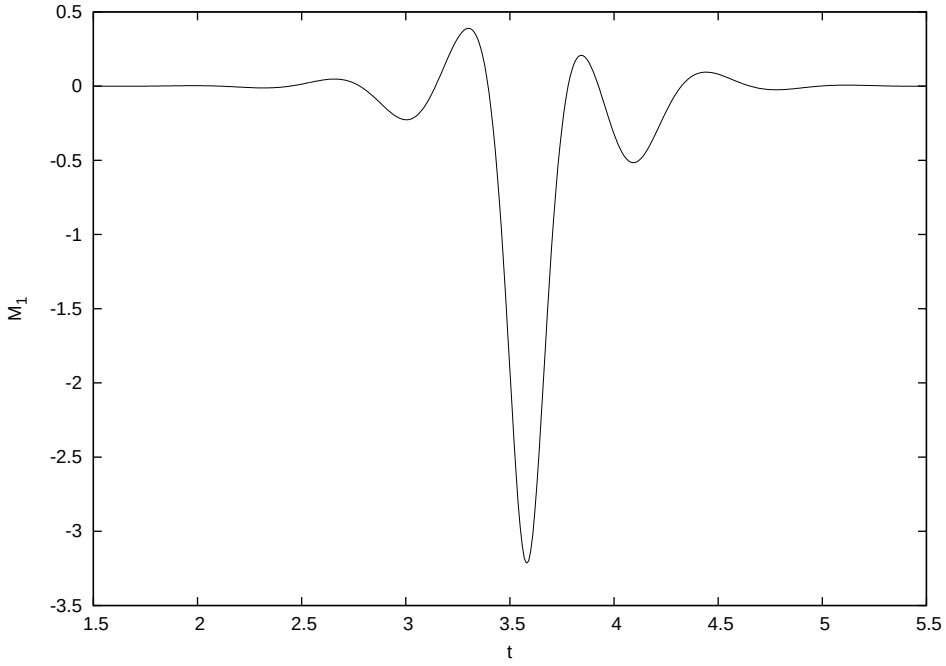

Figure 3.3: The first-order mass M_1, for example 1

is the solution of (3.22) with u being the Hirota two-soliton solution. The direct numerical calculation of M_1, from the finite-difference solution is not shown as it is the same as (3.22) to graphical accuracy. The value of M_1 is zero well before and after collision. As $c_7 = \frac{22}{5}$ the first-order mass varies during the collision. It varies in an oscillatory manner to a minimum value of -3.215614 at time $t = 3.58$. The difference between this prediction for mass, and that from the numerical scheme, is very small, being only 4.16×10^{-4} or 0.0129%. Hence the numerical scheme accurately predicts the first-order mass throughout the collision. Hence mass is not conserved during the collision but is conserved well before and after collision (as $t \to \pm\infty$).

In summary, it can be seen that the theoretical predictions have been confirmed for this example. The numerical results show that the collision is asymptotically elastic to first-order and the numerical estimates for coordinate and phase shifts are very close to the theoretical predictions.

3.4 Perturbation theory and solitary wave evolution

It was found in section 3.2 that a two-parameter family of higher-order asymptotic embedded solitons exists if (3.5) is true. As the higher-order waves are embedded in the linear wave spectrum, when (3.5) is not satisfied the solitary wave will decay as radiation is shed. Here soliton perturbation theory is used to determine the details of the evolving solitary wave, to first-order. An analytical expression is found for the tail of the solitary wave and comparisons are made with numerical solutions.

3.4.1 The perturbation solution

There are many applications of soliton perturbation theory in the literature, see Herman [12] for applications to perturbed KdV, NLS and mKdV equations, or Yang and Kaup [43] for an application to a generalized NLS equation. Also, Yang [41], outlines the application of the method to the higher-order Hirota equation (3.4).

The Hirota soliton is

$$\eta_0 = (\frac{2\gamma}{\alpha})^{\frac{1}{2}} \kappa e^{i(a\theta+\varphi)} \operatorname{sech} \kappa\theta, \quad \varphi = \lambda t - \varphi_0, \quad \theta = x - vt - \theta_0, \qquad (3.24)$$
$$\text{where} \quad v = \gamma(\kappa^2 - 3a^2), \quad \lambda = -2\gamma(a^2 + \kappa^2)a,$$

when κ, a, θ_0 and φ_0 are free parameters. For the higher-order Hirota equation (3.2) the perturbed solution can be written as

$$\eta = e^{i\varphi}\phi(\theta, t), \quad \theta = x - \int_0^t v dt - \theta_0, \quad \varphi = \int_0^t \lambda dt - \varphi_0. \qquad (3.25)$$

By substituting (3.25) in the higher-order Hirota equation (3.2) we obtain

$$\phi_t + i\lambda\phi - v\phi_\theta + \gamma\phi_{\theta\theta\theta} + 3\alpha|\phi|^2\phi_\theta = -\epsilon H(\phi), \qquad (3.26)$$

where H represents the perturbed terms in (3.2). The solution $\phi(\theta, t)$ can be expanded as a perturbation series

$$\phi = \phi_0(\theta) + \epsilon\phi_1(\theta, t) + \ldots, \qquad (3.27)$$

which is substituted into (3.26). The soliton parameters κ, a, θ_0 and φ_0 all vary on a slow time scale $T = \epsilon t$. The forms of the slow variations will be chosen to

eliminate the secular terms in the expansion. But the main focus here is to find the correction to the solitary wave profile ϕ_1, which allows the tail of the solitary wave to be determined. The expression for ϕ_1 depends only on the perturbation terms in H, not on any contributions from the slow time variations.

At $O(\epsilon)$ the equation

$$\begin{aligned} &\phi_{1_t} + i\lambda\phi_1 + (3\alpha|\phi_0|^2 - v)\phi_{1_\theta} + \gamma\phi_{1_{\theta\theta\theta}} \\ &+r(\theta)\phi_1 + q(\theta)\phi_1^* = -H(\phi_0), \qquad (3.28) \\ &\text{where} \quad r(\theta) = 3\alpha\phi_0^*\phi_{0_\theta}, \quad q(\theta) = 3\alpha\phi_0\phi_{0_\theta}, \\ &\qquad\qquad \phi_0 = \eta_0 e^{-i\varphi} = (\frac{2\gamma}{\alpha})^{\frac{1}{2}}\kappa e^{ia\theta}\,\mathrm{sech}\,\kappa\theta, \end{aligned}$$

with the initial value $\phi_1|_{t=0} = 0$ is solved. The linear equation (3.28) can be written in the matrix form $(\partial_t + L)\mathbf{w_1} = \mathbf{H}$ where

$$\begin{aligned} L = \begin{pmatrix} G(\theta) & q(\theta) \\ q^*(\theta) & G^*(\theta) \end{pmatrix}, \quad \mathbf{w_1} = \begin{pmatrix} \phi_1 \\ \phi_1^* \end{pmatrix}, \quad \mathbf{H} = \begin{pmatrix} \omega_1 \\ \omega_1^* \end{pmatrix}, \qquad (3.29) \\ \text{where} \quad G(\theta) = \gamma\partial_{\theta\theta\theta} + (3\alpha|\phi_0|^2 - v)\partial_\theta + r(\theta) + i\lambda, \\ \text{and} \quad \omega_1 = -H(\phi_0) - \phi_{0_{T_1}} + i\phi_0\varphi_{0_{T_1}} + \phi_{0_\theta}\theta_{0_{T_1}}. \end{aligned}$$

The technique used to solve (3.28) is similar to that applied to the perturbed KdV and NLS equations. The solution is expanded as the set of eigenfunctions for the linearisation operator. These eigenfunctions are just the squared eigenstates of the Zakharov-Shabat system with the soliton potential (see Yang [40] and Zakharov and Shabat [45]).

It is not difficult to show that non-localized (continuous) eigenstates are

$$\begin{aligned} \mathbf{w_2} &= \begin{pmatrix} -\kappa^2\,\mathrm{sech}^2\,\kappa\theta e^{i(2a-\xi)\theta} \\ (\kappa\tanh\kappa\theta + i\xi - ia)^2 e^{-i\xi\theta} \end{pmatrix}, \\ \mathbf{w_3} &= \begin{pmatrix} -(\kappa\tanh\kappa\theta - i\xi + ia)^2 e^{+i\xi\theta} \\ \kappa^2\,\mathrm{sech}^2\,\kappa\theta e^{-i(2a-\xi)\theta} \end{pmatrix}, \qquad (3.30) \end{aligned}$$

and the localized (discrete) of L are

$$\mathbf{w_4} = \begin{pmatrix} -\phi_0 \\ \phi_0^* \end{pmatrix} = (\frac{2\gamma}{\alpha})^{\frac{1}{2}} \begin{pmatrix} -e^{ia\theta} \\ e^{-ia\theta} \end{pmatrix} \kappa \operatorname{sech} \kappa\theta, \tag{3.31}$$

$$\mathbf{w_5} = \begin{pmatrix} \phi_{0_\theta} \\ \phi_{0_\theta}^* \end{pmatrix} = (\frac{2\gamma}{\alpha})^{\frac{1}{2}} \begin{pmatrix} (-\kappa \tanh \kappa\theta + ai)e^{ia\theta} \\ (-\kappa \tanh \kappa\theta - ai)e^{-ia\theta} \end{pmatrix} \kappa \operatorname{sech} \kappa\theta,$$

$$\mathbf{w_6} = (\frac{2\gamma}{\alpha})^{\frac{1}{2}} \begin{pmatrix} (-3a(1 - \kappa\theta \tanh \kappa\theta) - i\kappa^2\theta)e^{ia\theta} \\ (-3a(1 - \kappa\theta \tanh \kappa\theta) + i\kappa^2\theta)e^{-ia\theta} \end{pmatrix} \operatorname{sech} \kappa\theta,$$

$$\mathbf{w_7} = (\frac{2\gamma}{\alpha})^{\frac{1}{2}} \begin{pmatrix} (-2ia\kappa^2\theta + (\kappa^2 + 3a^2)(1 - \kappa\theta \tanh \kappa\theta))e^{ia\theta} \\ (2ia\kappa^2\theta + (\kappa^2 + 3a^2)(1 - \kappa\theta \tanh \kappa\theta))e^{-ia\theta} \end{pmatrix} \operatorname{sech} \kappa\theta,$$

where

$$\begin{gathered} L\mathbf{w_4} = L\mathbf{w_5} = 0, \\ L\mathbf{w_6} = 2i\kappa(\kappa^2 + 9a^2)\mathbf{w_4}, \;\; L\mathbf{w_7} = -2\kappa(\kappa^2 + 9a^2)\mathbf{w_5}, \\ L\mathbf{w_2} = i\vartheta\mathbf{w_2}, \qquad L\mathbf{w_3} = -i\vartheta\mathbf{w_3}, \end{gathered} \tag{3.32}$$

and the parameter ϑ is defined as

$$\vartheta = \gamma(\xi + 2a)k_1, \quad k_1 = \kappa^2 + (\xi - a)^2. \tag{3.33}$$

Also needed are the continuous eigenfunctions of the adjoint operator $L^\dagger$, which are related to (3.31) and (3.30) by $\mathbf{w_i}^\dagger = (-a^*, b^*)^T, \;\; i = 2, .., 7$, where $\mathbf{w_i} = (a, b)^T$ are the eigenfunctions in (3.31) and (3.30). Lastly, the inner product

$$\langle \mathbf{f}(\theta), \mathbf{g}(\theta) \rangle = \int_{-\infty}^{\infty} \mathbf{f}(\theta)^T \mathbf{g}(\theta) d\theta, \tag{3.34}$$

needs to be defined.

The only nonzero inner products of the (bounded) eigenstates and adjoint (bounded)

eigenstates are

$$\begin{aligned}
\langle \mathbf{w_4}, \mathbf{w_6}^\dagger \rangle &= \frac{12\gamma}{\alpha} a = -\langle \mathbf{w_6}, \mathbf{w_4}^\dagger \rangle, \\
\langle \mathbf{w_5}, \mathbf{w_6}^\dagger \rangle &= -\frac{4\gamma}{\alpha} i(\kappa^2 + 3a^2) = -\langle \mathbf{w_6}, \mathbf{w_5}^\dagger \rangle, \\
\langle \mathbf{w_4}, \mathbf{w_7}^\dagger \rangle &= -\frac{4\gamma}{\alpha} (\kappa^2 + 3a^2) = -\langle \mathbf{w_7}, \mathbf{w_4}^\dagger \rangle, \\
\langle \mathbf{w_5}, \mathbf{w_7}^\dagger \rangle &= -\frac{4\gamma}{\alpha} ia(\kappa^2 + 3a^2) = -\langle \mathbf{w_7}, \mathbf{w_5}^\dagger \rangle, \\
\langle \mathbf{w_2}(\theta;\xi), \mathbf{w_2}^\dagger(\theta;\xi') \rangle &= 2\pi k_1^2 \delta(\xi - \xi'), \\
\langle \mathbf{w_3}(\theta;\xi), \mathbf{w_3}^\dagger(\theta;\xi') \rangle &= -2\pi k_1^2 \delta(\xi - \xi'),
\end{aligned} \tag{3.35}$$

where δ is δ-*Dirac* function. Let us start by expanding the first-order solitary wave solution of (3.29) ,

$$\begin{aligned}
\mathbf{w_1} = &\int_{-\infty}^{\infty} [g_1(t;\xi)\mathbf{w_2} + g_2(t;\xi)\mathbf{w_3}] d\xi \\
&+ h_1(t)\mathbf{w_4} + h_2(t)\mathbf{w_5} + h_3(t)\mathbf{w_6} + h_4(t)\mathbf{w_7},
\end{aligned} \tag{3.36}$$

and also right hand site of (3.29),

$$\mathbf{H} = \int_{-\infty}^{\infty} [\Gamma_1(\xi)\mathbf{w_2} + \Gamma_2(\xi)\mathbf{w_3}] d\xi + p_1\mathbf{w_4} + p_2\mathbf{w_5} + p_3\mathbf{w_6} + p_4\mathbf{w_7}, \tag{3.37}$$

in the closure of L's eigenstates. Then it is not difficult to show that the coefficients p_j, $\Gamma_1(\xi)$ and $\Gamma_2(\xi)$ can be determined by applying inner product of eigenfunctions of $L^\dagger$ on (3.37) and then using orthogonality relations (3.35):

$$\begin{aligned}
p_1 &= \frac{\langle \mathbf{H}, \mathbf{w_7}^\dagger \rangle \langle \mathbf{w_5}, \mathbf{w_6}^\dagger \rangle - \langle \mathbf{H}, \mathbf{w_6}^\dagger \rangle \langle \mathbf{w_5}, \mathbf{w_7}^\dagger \rangle}{\langle \mathbf{w_4}, \mathbf{w_7}^\dagger \rangle \langle \mathbf{w_5}, \mathbf{w_6}^\dagger \rangle - \langle \mathbf{w_4}, \mathbf{w_6}^\dagger \rangle \langle \mathbf{w_5}, \mathbf{w_7}^\dagger \rangle}, \\
p_2 &= \frac{\langle \mathbf{H}, \mathbf{w_7}^\dagger \rangle \langle \mathbf{w_4}, \mathbf{w_6}^\dagger \rangle - \langle \mathbf{H}, \mathbf{w_6}^\dagger \rangle \langle \mathbf{w_4}, \mathbf{w_7}^\dagger \rangle}{\langle \mathbf{w_5}, \mathbf{w_7}^\dagger \rangle \langle \mathbf{w_4}, \mathbf{w_6}^\dagger \rangle - \langle \mathbf{w_5}, \mathbf{w_6}^\dagger \rangle \langle \mathbf{w_4}, \mathbf{w_7}^\dagger \rangle}, \\
p_3 &= \frac{\langle \mathbf{H}, \mathbf{w_5}^\dagger \rangle \langle \mathbf{w_7}, \mathbf{w_4}^\dagger \rangle - \langle \mathbf{H}, \mathbf{w_4}^\dagger \rangle \langle \mathbf{w_7}, \mathbf{w_5}^\dagger \rangle}{\langle \mathbf{w_6}, \mathbf{w_5}^\dagger \rangle \langle \mathbf{w_7}, \mathbf{w_4}^\dagger \rangle - \langle \mathbf{w_6}, \mathbf{w_4}^\dagger \rangle \langle \mathbf{w_7}, \mathbf{w_5}^\dagger \rangle}, \\
p_4 &= \frac{\langle \mathbf{H}, \mathbf{w_5}^\dagger \rangle \langle \mathbf{w_6}, \mathbf{w_4}^\dagger \rangle - \langle \mathbf{H}, \mathbf{w_4}^\dagger \rangle \langle \mathbf{w_6}, \mathbf{w_5}^\dagger \rangle}{\langle \mathbf{w_7}, \mathbf{w_5}^\dagger \rangle \langle \mathbf{w_6}, \mathbf{w_4}^\dagger \rangle - \langle \mathbf{w_7}, \mathbf{w_4}^\dagger \rangle \langle \mathbf{w_6}, \mathbf{w_5}^\dagger \rangle}, \\
\Gamma_1(\xi) &= \frac{\langle \mathbf{H}, \mathbf{w_2}^\dagger \rangle}{2\pi k_1^2}, \quad \Gamma_2(\xi) = -\frac{\langle \mathbf{H}, \mathbf{w_3}^\dagger \rangle}{2\pi k_1^2}.
\end{aligned} \tag{3.38}$$

Substituting (3.36) and (3.37) in (3.29) leads us to the governing differential equations for coefficients h_j, $g_1(t;\xi)$ and $g_2(t;\xi)$

$$h_{3_t} = p_3, \;\; h_{4_t} = p_4, \;\; h_{1_t} + 2i\kappa(\kappa^2 + 9a^2)h_3 = p_1, \;\; h_{2_t} - 2\kappa(\kappa^2 + 9a^2)h_4 = p_2, \tag{3.39}$$

with the initial conditions (because of (3.28))

$$h_1(t)|_{t=0} = h_2(t)|_{t=0} = h_3(t)|_{t=0} = h_4(t)|_{t=0} = 0. \tag{3.40}$$

In (3.36) the localized eigenstates' coefficients, h_j, are secular and therefore should be suppressed, leading to the secularity conditions

$$\langle \mathbf{H}, \mathbf{w_4}^\dagger \rangle = \langle \mathbf{H}, \mathbf{w_5}^\dagger \rangle = \langle \mathbf{H}, \mathbf{w_6}^\dagger \rangle = \langle \mathbf{H}, \mathbf{w_7}^\dagger \rangle = 0. \tag{3.41}$$

Under above assumption the relations (3.38) and the equations (3.39)-(3.40) will give

$$p_1(t) = p_2(t) = p_3(t) = p_4(t) = h_1(t) = h_2(t) = h_3(t) = h_4(t) = 0, \quad t \geq 0.$$

Thus, the ϵ-order correction (3.36) can be written as an integral of L's continues eigenstates. In view of the secularity conditions (3.41), with associated initial conditions

$$v|_{T_1=0} = \gamma(\kappa^2 - 3a^2), \lambda|_{T_1=0} = -2\gamma(\kappa^2 + a^2)a, \varphi_0|_{T_1=0} = 0, \theta_0|_{T_1=0} = 0, \tag{3.42}$$

we obtain the effects of the correction terms on the soliton parameters as:

$$\begin{aligned} v &= \gamma(\kappa^2 - 3a^2), \ \lambda = -2\gamma(\kappa^2 + a^2)a, \\ \theta_0 &= \gamma^2(\frac{2\gamma}{\alpha})^{\frac{1}{2}}[5c_6a^4 + (2c_2 - 4c_3 - 2c_4 + \frac{2}{3}c_5 + 10c_6)\kappa^2a^2 \\ &\quad + \frac{1}{45}(32c_1 + 10c_2 - 68c_3 - 2c_4 - 2c_5 + 105c_6)\kappa^4]\epsilon t, \\ \varphi_0 &= a\gamma^2(\frac{2\gamma}{\alpha})^{\frac{1}{2}}[-4c_6a^4 - \frac{8}{3}c_5\kappa^2a^2 + \\ &\quad \frac{1}{45}(128c_1 - 192c_3 - 48c_4 - 88c_5 + 420c_6)\kappa^4]\epsilon t. \end{aligned} \tag{3.43}$$

The quantity $\Gamma_1(\xi)$ (*i.e.* $\Gamma_2(\xi) = \Gamma_1(\xi)$), found using the residue theorem, is

$$\begin{aligned} 360\kappa^6\Gamma_1(\xi) &= i\gamma^2(\frac{2\gamma}{\alpha})^{\frac{1}{2}} \big[45\kappa^3(A_1 + A_2) - \kappa^2(15A_3 + 9A_4)(\xi - a) \\ &+5\kappa A_1(\xi - a)^2 - A_4(\xi - a)^3\big] \operatorname{sech}(\frac{\pi(\xi - a)}{2\kappa}), \end{aligned} \tag{3.44}$$

where the various parameters are

$$\begin{aligned}
A_1 &= (-4c_1 + 2c_2 + 20c_3 + 8c_4 - 120c_6)\kappa^5 a,\\
A_2 &= (-2c_2 + 4c_3 + 2c_4 + 2c_5 - 20c_6)\kappa^3 a^3\\
&\quad +(-2c_2 - 12c_3 - 6c_4 + 2c_5 + 100c_6)\kappa^5 a,\\
A_3 &= (6c_2 - 12c_3 - 6c_4 + 2c_5 + 60c_6)\kappa^4 a^2\\
&\quad +(6c_2 + 4c_3 + 2c_4 + 2c_5 - 60c_6)\kappa^6,\\
A_4 &= (4c_1 - 10c_2 - 16c_3 - 4c_4 - 4c_5 + 120c_6)\kappa^6.
\end{aligned}$$

And similar to (3.39) and (3.40), the evolution equations for continues eigenfunctions' coefficients in expansion (3.36) are found as

$$g_{1_t} + i\vartheta g_1 = \Gamma_1(\xi),\ \ g_{2_t} - i\vartheta g_2 = \Gamma_1(\xi), \tag{3.45}$$

when $g_1(0) = g_2(0) = 0$. By a simple computation one obtains

$$g_1 = -\frac{i\Gamma_1(\xi)}{\vartheta}(1 - e^{-i\vartheta t}),\ \ g_2 = -g_1^*. \tag{3.46}$$

And hence, the first-order solution (3.36) has the form

$$\mathbf{w_1} = \int_{-\infty}^{\infty} (g_1 \mathbf{w_2} + g_1^* \mathbf{w_3}) d\xi. \tag{3.47}$$

Rearranging (3.47) gives

$$\begin{aligned}
\phi_1(\theta, t) = &\int_{-\infty}^{\infty} i\Gamma_1(\xi)\frac{(1 - e^{-i\vartheta t})}{\vartheta}\kappa^2 \operatorname{sech}^2 \kappa\theta e^{-i(\xi - 2a)\theta} d\xi\\
&- \int_{-\infty}^{\infty} i\Gamma_1(\xi)\frac{(1 - e^{i\vartheta t})}{\vartheta}(\kappa \tanh \kappa\theta - i(\xi - a))^2 e^{i\xi\theta} d\xi,
\end{aligned} \tag{3.48}$$

as an integral expression for the first-order correction to the solitary wave profile. It is easy to show that (3.48) satisfies in (3.28). Note that for integrable coefficients (3.3), the first-order solution ϕ_1 in (3.48) is zero and therefore (3.27) becomes (3.8).

We also note that

$$\lim_{\vartheta \to 0} \frac{(1 - e^{\pm i\vartheta t})}{\vartheta} = \mp it, \tag{3.49}$$

so the integrand of (3.48) is singular at $\vartheta = 0$ ($\xi = -2a$) in the limit of large time, as $t \to \infty$.

3.4.2 The solitary wave tail

As radiation is shed from the solitary wave, it propagates in the negative x-direction, according to $c_g = -3k^2$, the group velocity of the linear KdV equation. Hence for right-moving waves, $\kappa^2 > 3a^2$, the radiation forms a tail behind the evolving solitary wave. For left-moving waves, $3a^2 > \kappa^2$, and the radiation and the wave move in the same direction, with the radiation forming a front ahead of the solitary wave. For convenience we call the region, $\theta \ll -1$, the solitary wave tail for both right and left-moving solitary waves. The asymptotic analysis considered here is similar to that of Herman [12] (see his Appendix B) and Pelinovsky and Yang [33] (see their section 4).

The Riemann-Lebesgue lemma implies that the integral (3.48) will decay to zero, as $t \to \infty$, except near any singular points. Hence for large time, the leading-order behaviour of (3.48) can be found by considering contributions near $\xi = -2a$. We substitute the transformation $\xi = -2a + z/t$ into (3.48) and obtain

$$\phi_1(\theta, t) \sim ie^{-2ia\theta}\Gamma_1(-2a)\frac{(\kappa(\pm 1) + i3a)^2}{\gamma(\kappa^2 + 9a^2)} \left(\int_{-\infty}^{\infty} \frac{e^{izc_p}}{z}dz - \int_{-\infty}^{\infty} \frac{e^{iz(\gamma(k^2+9a^2)+c_p)}}{z}dz\right), \quad |\theta| \gg 1, \quad t \to \infty, \tag{3.50}$$

where the $\pm$ in the expression refers to the regions well in front $(+)$ and behind $(-)$ the solitary wave. Also we let $\theta/t = c_p$, an $O(1)$ constant. Also, the integral

$$\int_{-\infty}^{\infty} \frac{e^{izp}}{z}dz = i\pi \mathrm{sgn}(p), \tag{3.51}$$

is needed to evaluate (3.50). Well in front of the soliton, $c_p > 0$, so both integrals within (3.50) have the same value. So the cancellation of the two integrals implies $\phi \sim 0$ well ahead of the solitary wave. This is physically consistent with the fact that the group velocity of the linear radiation is negative.

Behind the wave we choose $-\gamma(k^2 + 9a^2) < c_p < 0$. Then the integrals within (3.50) have the opposite sign and

$$\phi_1 \sim he^{-2ia\theta}, \quad \text{where} \quad h = \frac{1}{5}ia\pi(\kappa^2 + a^2)\gamma(\frac{2\gamma}{\alpha})^{\frac{1}{2}} (2c_1 - 3c_3 - 2c_4 - 2c_5 + 10c_6)\frac{\kappa - 3ia}{\kappa + 3ia}\,\mathrm{sech}(\frac{3\pi a}{2\kappa}), \quad \theta \ll -1, \quad t \to \infty, \tag{3.52}$$

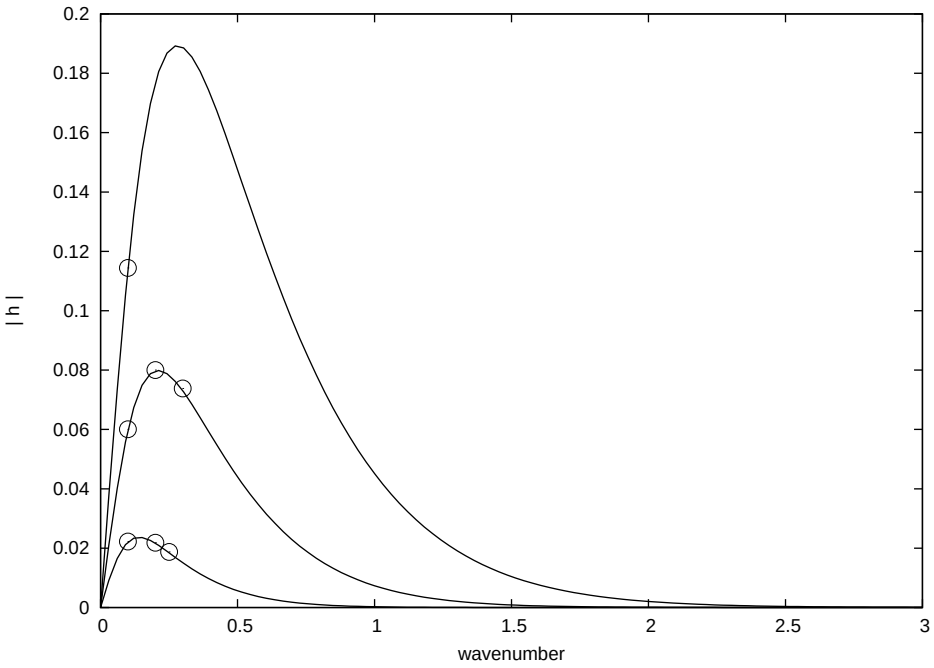

Figure 3.4: tail amplitude $|h|$ versus wavenumber a and comparison with numerical simulations

is obtained as the steady-state tail of the solitary wave at first-order. The tail (3.52) is qualitatively similar to the expression found by Yang [41] for the tail of an evolving solitary wave governed by (3.4). For the higher-order Hirota equation (3.4) it was found that a one-parameter family of embedded solitons occurred for fixed values of the wavenumber a.

Figure (3.4) shows the tail amplitude $|h|$ versus wavenumber a for $\kappa = 0.5$ (lower curve), $\kappa = 0.75$ and $\kappa = 1$ (upper curve). The other parameters are $\alpha = 2$, $\gamma = 1$, $c_1 = 1$ with the other $c_i = 0$. For a given value of the solitary wave amplitude ($A = \kappa$ for these parameter choices) the tail amplitude is zero at wavenumber $a = 0$, increases to a maximum, before decreasing to zero as $a \to \infty$. When $a = 0$ the Hirota soliton is the real-valued mKdV soliton. In this limit $h = 0$ as the higher-order mKdV equation has localised solitary wave solutions for all choices of higher-order coefficients. It can be also seen from the figure that the tail amplitude increases as the wave amplitude increases. Moreover, the numerical simulations for right-moving waves have been carried out and the comparison between the numerical tail amplitudes and (3.52) are shown in the figure, see 3.4.3 for details of the numerical

scheme.

For (3.2) the tail (3.52) is zero if (3.5) is satisfied and a two-parameter family of asymptotic embedded solitons occurs. Note that this two-parameter family only exists up to first-order, as the second-order tail, at $O(\epsilon^2)$, may be non-zero. The tail amplitude (3.52) is also zero if $a = 0$, hence a one-parameter family of embedded solitons (the real mKdV soliton family) also exists. This family are part of the one-parameter family of embedded solitons found by Yang [41].

Also noteworthy is the fact that the condition (3.5) from the asymptotic transformation is the condition in (3.52) for the tail amplitude to be zero. This is the same two-parameter family of embedded solitons identified using the asymptotic transformation, so there is agreement between the two analytical methods.

The leading-order transient terms in the tail region will occur due to contributions from (3.48) at points of stationary phase. The relevant phase of (3.48) is

$$\vartheta_1 = \vartheta + \xi c_p = \gamma(\xi + 2a)(\kappa^2 + (\xi - a)^2) + \xi c_p, \tag{3.53}$$

and points of stationary phase, which occur when $\frac{d\vartheta_1}{d\xi} = 0$, are

$$\xi_s^{\pm} = \pm\sqrt{-\frac{1}{3}(\kappa^2 - 3a^2 + \frac{c_p}{\gamma})}. \tag{3.54}$$

Using the method of stationary phase gives

$$\phi_1 \sim he^{-2ia\theta} + i\pi^{\frac{1}{2}}\frac{[\kappa + i(\xi_s^{\pm} - a)]^2}{(3t|\xi_s^{\pm}|)^{\frac{1}{2}}\vartheta(\xi_s^{\pm})}\Gamma_1(\xi_s{}^{\pm})e^{i[(\vartheta(\xi_s^{\pm}) + \xi_s^{\pm}c_p)t \mp \frac{\pi}{4}]}, \tag{3.55}$$
$$\theta \ll -1, \quad t \to \infty.$$

The tail (3.55) consists of the steady-state result (3.52) plus the two leading order transient terms, which are contributions from the points of stationary phase (one term for each of the roots (3.54)). The points of stationary phase (3.54) only exist when $c_p < \gamma(3a^2 - \kappa^2)$. For left-moving waves $3a^2 > \kappa^2$, and the slowly decaying transient terms, of $O(t^{-\frac{1}{2}})$, occur along the whole of the tail (for all $c_p < 0$). For right-moving waves $\kappa^2 > 3a^2$, and the $O(t^{-\frac{1}{2}})$ transient terms only occur on the far edge of the tail, between $-\gamma(\kappa^2 + 9a^2) < c_p < -\gamma(\kappa^2 - 3a^2)$. For the near tail of a right moving wave the transient terms decay more quickly than those in

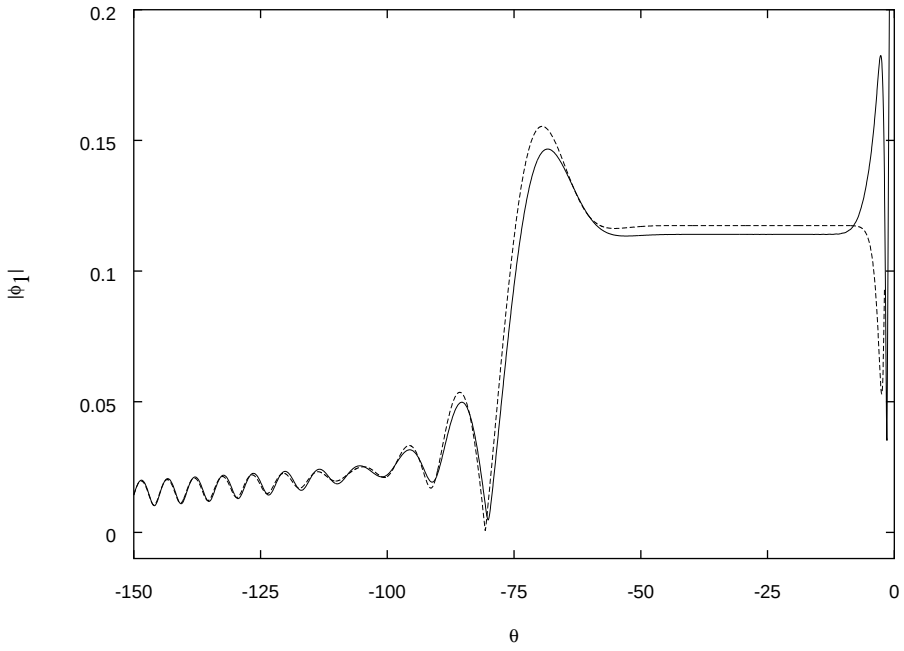

Figure 3.5: The first-order correction $|\phi_1|$ versus θ at $t = 70$ for a right-moving wave. Shown is the perturbation solution (3.48) (solid curve) and numerical solution of (3.2) (dashed curve)

(3.55) (presumably they are $O(t^{-1})$) and the flat steady-state tail will be quickly approached.

The group velocity of linear radiation is $c_g = -3\gamma k^2$, while the soliton velocity is $v = \gamma(\kappa^2 - 3a^2)$. For tails with wavenumber $k = -2a$, the difference between the soliton velocity and the group velocity of shed radiation, $v - c_g = \gamma(\kappa^2 + 9a^2)$, which is the length of the solitary wave tail. Hence the tail length has a clear physical meaning.

3.4.3 Numerical solutions and discussion

Figure (3.5) shows the first-order correction $|\phi_1|$ versus θ at time $t = 70$. The parameters are $\kappa = 1$, $a = 0.1$, $\gamma = 1$, $\alpha = 2$, $\epsilon = 0.1$, $c_1 = 1$ and all the other $c_i = 0$. The perturbation solution (3.48), was solved numerically using a high-order quadrature scheme. The higher-order Hirota equation (3.2) was solved numerically using an implicit finite-difference scheme. The initial condition used in the numerical scheme was a Hirota soliton. The quantity $\epsilon^{-1}|\eta|$ is plotted from the

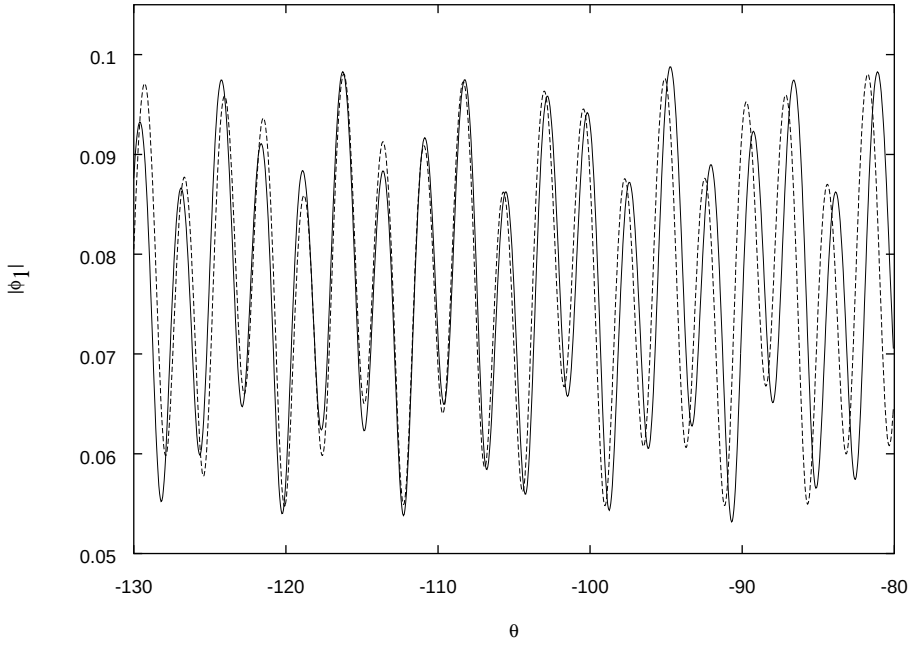

Figure 3.6: The first-order correction $|\phi_1|$ versus θ at $t = 150$ for a left-moving wave. Shown is the perturbation solution (3.48) (solid curve) and numerical solution of (3.2) (dashed curve)

numerical solution as it allows a comparison with the perturbation solution in the tail region.

As $\kappa^2 > 3a^2$ this is an example of a right-moving wave. There is an excellent comparison between the numerical and perturbation solutions. The figure shows the surface elevation behind the evolving solitary wave with the flat steady-state tail clearly visible. The amplitude of this tail, as predicted by the perturbation solution (3.48), is $|\phi_1| = 0.1140$, which is the same as the analytical expression (3.50) for the steady-state tail amplitude. The numerical results show that the tail has amplitude $|h| = 0.1185$, a difference of about 4%.

The figure shows that the tail amplitude drops from its steady-state value, to near zero at $\theta \approx -75$. The asymptotic theory implies that the length of the solitary wave tail is $(\kappa^2 + 9a^2)t = 76.3$, which is close to numerical tail length, of about 80. The tail will be flat for $\theta > -\gamma(\kappa^2 - 3a^2)t = -67.9$, as no slowly-decaying transients exist on the near tail. There is an oscillation right at the end of the tail, so again the asymptotic result is consistent with the perturbation and numerical solutions.

Figure (3.6) shows the first-order correction $|\phi_1|$ versus θ at time $t = 150$. The parameters are the same as for figure (3.5), except that $a = 0.8$. Shown are the perturbation solution (3.48) and the quantity $\epsilon^{-1}|\eta|$ from the numerical solution of (3.2).

The figure shows a portion of the region $(-130 < \theta < -80)$ in front of the left-moving solitary wave. The comparison between the numerical and perturbation solutions is very good, with some slight differences in phase and amplitude noticeable. Also the asymptotic expression (3.55) is the same as the perturbation solution (3.48) over this region of the tail, confirming the validity of the asymptotic expression (3.55).

In contrast to the flat tail for the right-moving wave, here the tail is highly oscillatory. The superposition of the steady-state tail wavelength (of $\lambda = \pi/a \approx 3.93$) with the two different transient wavelengths leads to a classical beating-like phenomena where the tail has multiple peaks and troughs of higher and lower amplitudes. The steady-state tail amplitude is 7.60×10^{-2}. An average taken of the numerical solution, over the range $-200 < \theta < -50$, is 7.74×10^{-2}, which is within 2% of the analytical steady-state tail amplitude. The maximum amplitude (crest to trough) of the tail oscillations is 4.56×10^{-2} at $t = 150$. As the oscillations decay like $O(t^{-\frac{1}{2}})$, a relatively flat tail will not be reached until $t = O(10^6)$, when the amplitude of the oscillations will have decayed to less than 1% of this value. Physically, the occurrence of slowly decaying transients on the tail of the left-moving wave, is related to the fact the wave is moving in the same direction as its shed linear radiation, while the right-moving wave moves in the opposite direction.

In summary the perturbation theory results, both direct numerical solutions of (3.48) and the further asymptotic results derived from (3.48) are in good agreement with each other and numerical solutions of the governing pde (3.2) for examples of right and left-moving solitary waves.

3.5 Conclusion

Firstly, an asymptotic transformation has been applied to the higher-order Hirota equation (3.2) when (3.5) is satisfied. Applied to a single soliton, it enables a two-parameter family of higher-order asymptotic embedded solitons to be identified. For a two-soliton collision it enables the details of the higher-order collision to be determined. The higher-order collision is found to be elastic and the higher-order coordinate and phase shifts, after interaction of the solitary waves, were also found.

Secondly, soliton perturbation theory has been applied to (3.2) with an integral expression found for the first-order correction to the solitary wave profile. An asymptotic expansion, valid for large time, allows a simple analytical expression to be found for the solitary wave tail. The theoretical results clearly explain the differences which occur for right and left-moving solitary waves. A flat tail occurs for the right-moving case while the tail for the left-moving wave is highly oscillatory, due to slowly decaying transient terms.

The solitary wave tail is zero when (3.5) is satisfied. Hence the two-parameter family of higher-order asymptotic embedded solitons can be identified using two different analytical methods, the asymptotic transformation and soliton perturbation theory. The two analytical methods provide a useful cross-validation of the theoretical results. Moreover, it illustrates the usefulness of the asymptotic transformation in providing theoretical results in a simple manner.

Chapter 4

Gray soliton interaction and evolution for a higher-order Hirota equation

In contrast to the focusing Hirota equation (3.1), the defocusing Hirota equation

$$\eta_t + 6|\eta|^2\eta_x - \eta_{xxx} = 0, \tag{4.1}$$

has dark and gray soliton solutions which are stable on a background of periodic waves of constant amplitude. In this chapter, gray solitary wave interaction and evolution for a higher-order defocusing Hirota equation is examined. The higher-order Hirota equation is asymptotically transformed to a higher-order member of the Hirota hierarchy of integrable equations, if the higher-order coefficients satisfy an algebraic relationship. The transformation is used to derive higher-order one and two-soliton solutions. It is shown that the interaction is asymptotically elastic and analytical expressions for the higher-order corrections to the coordinate shifts, which occur due to the interaction, are derived. The asymptotic theory and direct analysis identify a three-parameter and a two-parameter family of higher-order embedded gray solitary waves. Soliton perturbation theory is used to determine the detailed behavior of an evolving higher-order gray Hirota solitary wave; an integral expression for the first-order correction to the wave is found and analytical expressions for the solitary wave tail are derived. A subtle and complex picture of the development of

solitary wave tails emerges. For solitary wave interaction strong agreement is found between the prediction of the asymptotic transformation and numerical solutions. For the solitary wave evolution strong agreement is found between the theoretical predictions of the perturbation theory, the results of the asymptotic transformation of (4.1) and also numerical solutions.

4.1 Introduction

Dark solitons in the normal dispersive regimes, which appear as a localized intensity dip on a stable or travelling wave background, have been extensively studied by several authors. Kivshar and Luther-Davies [19] presents a historical overview of the optical dark solitons and the physical origins of the defocusing cubic nonlinear Schrödinger (NLS) equation. By analyzing the modulational instability they discussed the differences between bright and dark solitons and showed that small excitations of the nonzero background wave are absolutely stable for the defocusing NLS equation and unstable for focusing case. The stability considerations apply to the focusing and defocusing Hirota equations also, see section 4.4.

Li *et. al.* [24], by applying inverse scattering transform (IST) method, and Mahalingam and Porsezian [25], by using the Painlevé analysis and the Hirota bilinearization method constructed a generalized dark solitary wave solution of the higher-order nonlinear Schrödinger (NLS) equation

$$\eta_t + i(\alpha_1\eta_{xx} + \alpha_2|\eta|^2\eta) + \alpha_3\eta_{xxx} + \alpha_4(|\eta|^2\eta)_x + \alpha_5\eta(|\eta|^2)_x = 0, \tag{4.2}$$

where the real coefficients, the α_i, are determined by the physical model under consideration. Li *et. al.* [24] also showed that the absolute value ($|\eta|$) of the dark two-soliton solution of (4.2) can be considered as the superposition of the absolute values of two interacting dark one-soliton solutions; the only effects of the collision are the coordinate shifts that the solitons suffer.

The defocusing Hirota equation (4.1) considered in this chapter, has the form (4.2) with $\alpha_1 = \alpha_2 = 0$, $\alpha_3 = -1$, and $\alpha_4 = -\alpha_5 = 6$. These restrictions are called the *Hirota conditions*, and result in (4.2) being integrable. The defocusing Hirota equation has a number of physical applications, such as ultrashort light pulses in

the subpicosecond regime, whose duration is shorter than 100 femtoseconds, see Li *et. al.* [24] and Mahalingam and Porsezian [25]. The defocusing Hirota equation also is part of the NLS hierarchy of integrable equations, and its soliton solution has a very similar form to the defocusing NLS soliton. This is similar to the relation between the focusing Hirota and NLS equations, see Li *et. al.* [24].

The higher-order defocusing Hirota equation

$$\begin{aligned}&\eta_t + 6|\eta|^2\eta_x - \eta_{xxx} + \epsilon(c_1|\eta|^4\eta_x + c_2(\eta|\eta_x|^2)_x + c_3\eta^*(\eta\eta_{xx})_x \\ &+c_4\eta^*\eta_x\eta_{xx} + c_5\eta\eta_x\eta^*_{xx} + c_6\eta_{5x}) = 0, \quad \epsilon \ll 1,\end{aligned} \tag{4.3}$$

is considered in this chapter. When the higher-order coefficients are given by

$$(c_1, c_2, c_3, c_4, c_5, c_6) = (1, -\frac{1}{3}, -\frac{1}{3}, -\frac{1}{3}, 0, \frac{1}{30}), \tag{4.4}$$

then (4.3) is a member of the Hirota integrable hierarchy. The integrable hierarchy is obtained using the Lax hierarchy of the Hirota equations. Hence (4.3) represents a generalization of a member of the integrable hierarchy (4.4).

The pioneering works of Chen *et. al.* [3] on soliton perturbation theory for the dark soliton of the NLS equation overcame the difficulties caused by divergency of the perturbations to the soliton parameters. By applying the IST method, the non-localized (continuous) eigenfunction of the linearization operator based on the squared Jost solution, and its adjoint state, were found and, by using an appropriate inner product in a manner similar to bright solitons (3.34) the orthogonality relationships between the non-localized and localized eigenstates and their adjoint counterparts were established. Then, as an application of Jordan's lemma, it was proved that the first-order correction to the solitary wave profile can be expanded by the squared Jost solutions. Using the similarity between the first Lax pair of the defocusing Hirota and NLS equations, the process can be extended to (4.3), for more details, see section 4.4 and Appendix A.

In this chapter, we examine solitary wave interaction and evolution for the higher-order Hirota equation (4.3). In section 4.2 the Hirota bilinearization method is modified to find the single dark soliton solution of the defocusing Hirota equation (4.1). In section 4.3 a nonlocal asymptotic transformation is used to transform (4.3)

to the integrable member of the Hirota hierarchy (4.4). Note that the asymptotic transformation for the higher-order Hirota equation (4.3) is valid if

$$c_1 + 3c_3 + 2c_4 + 2c_5 + 20c_6 = 0, \tag{4.5}$$

is satisfied. As for the bright solitary wave interaction discussed in chapter 3, the interaction is elastic if the algebraic relationship is satisfied, but the relationship (4.5) is different from that found for the higher-order focusing Hirota equation, see (3.3). In section 4.3 higher-order single and two-soliton solutions are generated explicitly, using the transformation.The higher-order two-soliton collision, is found to be asymptotically elastic for the special case (4.5) and analytical expressions are derived for the higher-order coordinate shifts, due to the collision. In section 4.3.3, numerical simulations of elastic higher-order gray solitary wave collisions are presented, with the theoretical and numerical values for the higher-order coordinate shifts in close agreement.

The bright Hirota soliton is embedded, as its frequency is embedded in the linear wave spectrum, see the discussion on p.32 in chapter (3). The gray Hirota solitons considered here are similarly embedded in the linear wave spectrum, so the gray Hirota solitons represent a three parameter family of embedded solitons. The asymptotic transformation and direct solutions show that a three parameter family of higher-order asymptotic embedded gray solutions exists, when (4.5) is satisfied. Also, an additional two-parameter family of higher-order asymptotic embedded solutions is identified.

In section 4.4, soliton perturbation theory is used to derive the details of an evolving gray solitary wave at first-order. An integral expression for the first-order correction to the solitary wave and explicit expressions for tail amplitudes, for different values of the background wave number, are found. The links between the perturbation theory and the asymptotic transformation are explored. Also, an excellent comparison is found between the theoretical and numerical solutions for the first-order solitary wave correction.

4.2 The gray one-soliton solution

Here, by using Hirota bilinearization method, the single soliton solution for the Hirota equation (4.1) is found. We consider the transformation

$$\eta = e^{i\delta(x-bt)}\frac{G(x,t)}{F(x,t)}, \tag{4.6}$$

where $G(x,t)$ is a complex valued function and $F(x,t)$ is a real valued function and δ is a free parameter and b shall be determined. By using the transformation (4.6) in (4.1), the bilinearized relations for G and F

$$\begin{aligned}\{D_t + (2\delta^2 + b)D_x - 3i\delta D_x^2 - D_x^3\}G.F = 0,\\ \{3D_x^2 + (\delta^2 - b)\}F.F = -6|G|^2,\end{aligned} \tag{4.7}$$

are found, where the Hirota bilinear operator is defined as

$$D_x^m D_t^n f.g = (\frac{\partial}{\partial x} - \frac{\partial}{\partial x_1})^m(\frac{\partial}{\partial t} - \frac{\partial}{\partial t_1})^n f(x,t)g(x_1,t_1)|_{x_1=x,t_1=t}. \tag{4.8}$$

The functions G and F are defined by

$$G = g_0(1 + \beta g_1) \quad \text{and} \quad F = 1 + \beta f_1. \tag{4.9}$$

By substituting (4.9) in (4.7) and collecting β-orders, at β^0, g_0 satisfies

$$\{D_t + (2\delta^2 + b)D_x - 3i\delta D_x^2 - D_x^3\}g_0.1 = 0, \quad |g_0|^2 = \frac{1}{6}(b - \delta^2), \tag{4.10}$$

which can be solved as

$$g_0 = \frac{(a - i\kappa)^2}{\sqrt{\frac{1}{6}(b-\delta^2)}} \quad \text{where} \qquad b = 6\mu^2 + \delta^2, \quad \mu^2 = a^2 + \kappa^2, \tag{4.11}$$

and a and κ are two free parameters. The coefficients of β and β^2 lead to

$$\begin{aligned}\{g_0(D_x^3 - 2\delta^2 D_x - bD_x - 3i\delta D_x^2 - D_t) + g_{0_x}(-3D_x^2 + 2\delta^2 + b + 6i\delta D_x)\\ +g_{0_{xx}}(3D_x - 3i\delta) - (D_x^3 - D_t)g_0.1\}(f_1.1 + 1.g_1) = 0,\\ \{3D_x^2 + (\delta^2 - b)\}f_1.1 = -3|g_0|^2(g_1 + g_1^*),\\ \{g_0(D_x^3 - 2\delta^2 D_x - bD_x - 3i\delta D_x^2 - D_t) + g_{0_x}(-3D_x^2 + 2\delta^2 + b + 6i\delta D_x)\\ +g_{0_{xx}}(3D_x - 3i\delta) - (D_x^3 - D_t)g_0.1\}f_1.g_1 = 0,\\ \{3D_x^2 + (\delta^2 - b)\}f_1.f_1 = -6|g_0|^2|g_1|^2,\end{aligned} \tag{4.12}$$

which can be solved by assuming

$$g_1 = \frac{a+i\kappa}{a-i\kappa}, \quad f_1 = \frac{a+i\kappa}{a-i\kappa}e^{2\kappa(x-vt)},$$
$$\text{where} \quad v = 3\delta^2 + 6a^2 - 6\delta a + 2\kappa^2. \tag{4.13}$$

Hence,

$$\eta = \frac{a-i\kappa}{\mu}e^{i\varphi}(a + i\kappa\tanh\kappa\theta), \quad b = 6\mu^2 + \delta^2,$$
$$\text{where} \quad \varphi = \delta(x-bt) + \varphi_0, \quad \theta = x - vt - \theta_0, \tag{4.14}$$

is the Hirota gray soliton solution. Note that (4.14) can be also derived using the IST approach, see Li *et. al.* [24]. This is a gray soliton solution with three free parameters (a, κ, δ). a is the minimum intensity of the wave, δ is the background wave number and κ is the wavenumber of the soliton envelope. The boundary values for (4.14) are

$$\eta \to \frac{(a-i\kappa)^2}{\mu}e^{i\varphi}, \quad \text{as} \quad x \to -\infty, \quad \eta \to \mu e^{i\varphi}, \quad \text{as} \quad x \to \infty,$$

hence the amplitude of the background travelling wave is μ.

4.3 The asymptotic theory

Consider the transformation

$$\begin{aligned}
&\eta = \psi + \frac{\epsilon}{6}(2c_2 - c_3 - c_4 + c_5)|\psi|^2\psi \\
&+\frac{\epsilon}{24}(-c_1 - 4c_2 - c_3 + 2c_4 - 4c_5)\psi_{xx} \\
&\tau = t - \frac{\epsilon}{24}(c_1 + 2c_2 + c_3 + 2c_5)x, \\
&\xi = x - \epsilon c_7\left[\int_{-\infty}^{x}(|\psi(p,t)|^2 - \mu^2)dp + \mu^2 x - 3\mu^4 t - 3\delta^2\mu^2 t\right], \quad \epsilon \ll 1, \\
&\text{where} \quad c_7 = \frac{1}{12}(c_1 - 2c_2 + c_3 + 4c_4 + 2c_5).
\end{aligned} \tag{4.15}$$

This form of transformation is appropriate for solutions which approach a mean level of μ far up and downstream, such as the solitary wave solutions considered here. Note that when $\mu = 0$, this transformation is qualitatively similar to that one was used in chapter 3, for the higher-order focusing Hirota equation.

When the transformation (4.15) is substituted into (4.3) and terms of $O(\epsilon^2)$ are neglected, then $\psi(x,t)$ is a solution of the higher-order member of the Hirota hierarchy of integrable equations

$$\begin{aligned}
&\psi_\tau + 6\psi|^2\psi_\xi - \psi_{\xi\xi\xi} + \epsilon^{'}|\psi|^4\psi_\xi - \frac{\epsilon^{'}}{3}(\psi|\psi_\xi|^2)_\xi - \frac{\epsilon^{'}}{3}\psi^*(\psi\psi_{\xi\xi})_\xi \\
&-\frac{\epsilon^{'}}{3}\psi^*\psi_\xi\psi_{\xi\xi} + \frac{\epsilon^{'}}{30}\psi_{\xi\xi\xi\xi\xi} = 0, \\
&\text{where } \epsilon^{'} = \frac{3\epsilon}{4}(3c_1 + 10c_2 - c_3 - 4c_4 + 6c_5) \ll 1,
\end{aligned} \tag{4.16}$$

if the algebraic relationship (4.5) is satisfied. The integrability of (4.16) can be shown in a similar manner to Kano [17]. In fact, the conserved quantity $I_6^0[\psi,\psi^*]$ for the focusing Hirota (see his Appendix) can be modified to the conserved quantity for (4.1) by

$$I_6^0[\psi,\psi^*] = \int_{-\infty}^{\infty} 10\psi^3\psi^{*^2}\psi_\xi^* + 10\psi\psi_\xi\psi^*\psi_{\xi\xi}^* + 5\psi\psi_\xi\psi_\xi^{*^2} + 5\psi_\xi^2\psi^*\psi_\xi^* + \psi_{\xi\xi}\psi_{\xi\xi\xi}^* d\xi,$$

and hence the related $K_6(\psi,\psi^*)$ will be the higher-order terms in (4.16).

4.3.1 A higher-order gray one-soliton solution

The higher-order solitary wave solution of (4.3) can be found by direct substitution, as

$$\begin{aligned}
\eta &= \frac{a-i\kappa}{\mu}(a + i\kappa\tanh\kappa\theta)e^{i\varphi} + \\
&\quad \epsilon\frac{a-i\kappa}{\mu}(B_0 + iB_1\tanh\kappa\theta + B_2\tanh^2\kappa\theta + iB_3\tanh^3\kappa\theta)e^{i\varphi}, \\
\text{where } \theta &= x + \epsilon c_7\kappa - s[1 + \frac{\epsilon}{6}(c_1 + 4c_2 + c_3 - 2c_4 + 2c_5)a^2 \\
&\quad + \frac{\epsilon}{8}\delta(\delta - 2a)(c_1 + 2c_2 + c_3 + 2c_5) + \frac{\epsilon}{3}(c_2 - c_4)\kappa^2] - v_h t, \\
\varphi &= \delta(x + \epsilon c_7\kappa - s[1 + \frac{\epsilon}{6}\mu^2(c_1 + 4c_2 + c_3 - 2c_4 + 2c_5) \\
&\quad + \frac{\epsilon}{24}(c_1 + 2c_2 + c_3 + 2c_5)\delta^2] - b_h t) + \varphi_0,
\end{aligned} \tag{4.17}$$

and the various parameters are

$$\begin{aligned}
B_1 &= \frac{1}{3}(c_1+c_2+c_3+c_4+2c_5)\kappa\delta a - \frac{1}{12}(c_1+c_2+c_3+c_4+c_5)\delta^2\kappa \\
&\quad +\frac{1}{6}(c_1-c_2+c_3+3c_4+3c_5)\kappa^3 + \frac{1}{6}(-c_1-2c_2-2c_3+c_4-c_5)\kappa a^2, \\
B_2 &= \frac{1}{6}(2c_2-c_3-c_4+c_5)\kappa^2 a - \frac{1}{6}(c_1+c_2+c_3+c_4+3c_5)\delta\kappa^2, \\
B_3 &= \frac{1}{6}\kappa^3(-c_1+c_2-2c_3-2c_4-2c_5),
\end{aligned}$$

with the velocity v_h and parameter b_h given by

$$\begin{aligned}
v_h &= 3\delta^2+6a^2-6\delta a+2\kappa^2 \\
&\quad +(c_1a^4+\frac{1}{5}(c_1+2c_4-2c_3+2c_5)\kappa^4+(3c_2-c_5-6c_3-3c_4)\delta^2a^2 \\
&\quad +\frac{1}{4}(-c_1-2c_4-3c_3-2c_5)\delta^4+\frac{1}{2}(3c_4+c_1-c_2+3c_5+5c_3)a\delta^3 \\
&\quad +(c_4-c_1-c_5+4c_3-2c_2)a^3\delta-2c_3\kappa^2a^2+(2c_3-2c_5)a\kappa^2\delta \\
&\quad +(-2c_3+c_2+c_5-c_4)\kappa^2\delta^2+(12a-6\delta)B_0)\epsilon, \qquad (4.18) \\
b_h &= 6\mu^2+\delta^2 \\
&\quad +(c_1a^4+(2c_4-2c_3+c_1+2c_5)\kappa^4+(-c_4+c_2-2c_3-c_5)\delta^2a^2 \\
&\quad +\frac{1}{20}(-c_1-3c_3-2c_5-2c_4)\delta^4+(2c_3+2c_5+2c_1+2c_4+2c_2)a\kappa^2\delta \\
&\quad -6c_3\kappa^2a^2+12aB_0+(-c_1-2c_4-3c_3-2c_5)\kappa^2\delta^2)\epsilon.
\end{aligned}$$

The parameter B_0 is arbitrary and represents a higher-order correction to the background wave.

For (4.17), the first-order corrections in the background are not zero. This form of solution can be rescaled back to a wave with a zero higher-order mean-level with an suitable choice for B_0, if required. The explicit form of B_0 for this case is

$$B_0 = -B_2 - \frac{\kappa}{a}(B_1+B_3), \quad \text{for} \quad a \neq 0. \qquad (4.19)$$

The higher-order gray one-soliton solution (4.17) can only be derived if the algebraic relationship (4.5) is satisfied or

$$2\kappa^2+3\kappa\delta-\delta^2=0, \qquad (4.20)$$

is satisfied. The algebraic relationship (4.5) is the condition for the asymptotic transformation to apply and implies that a three-parameter family (4.17) of higher-order

asymptotic embedded solitons exists. The condition (4.20) represents a relationship between the three free parameters. Physically (4.20) implies that the soliton velocity is the same as the phase velocity of the background wave, *i.e.* $v = b$ from (4.14) and implies an additional two-parameter family of embedded asymptotic soliton exists.

The single soliton solution of the integrable higher-order Hirota equation (4.16) is

$$\begin{aligned}
&\psi = \frac{a - i\kappa}{\mu} e^{i\varphi}(a + i\kappa \tanh \kappa\theta), \qquad (4.21)\\
&\theta = \xi - s - v\tau, \quad \varphi = \delta(\xi - b\tau - s) + \varphi_0,\\
&\text{where} \quad b = 6\mu^2 + \delta^2 + (\mu^4 + \frac{1}{30}\delta^4 + \frac{2}{3}\delta^2\mu^2)\epsilon', \quad \mu^2 = a^2 + \kappa^2,\\
&\qquad v = 3a^2 + 2\kappa^2 + 3(a - \delta)^2\\
&+(\frac{2}{3}\delta^2\kappa^2 + \frac{1}{6}\delta^4 + \frac{2}{3}a^2\kappa^2 - \frac{2}{3}\delta^3 a + \frac{1}{5}\kappa^4 + a^4 - 2a^3\delta - \frac{2}{3}a\kappa^2\delta + 2a^2\delta^2)\epsilon',
\end{aligned}$$

and δ, a and $\kappa > 0$ are free parameters. The single soliton solution (4.21) is (4.14) with the higher-order corrections to the velocity v and the parameter b. This is similar to NLS soliton (2.9) and Hirota bright soliton (3.8) for higher-order integrable equations.

The soliton solution (4.21) is substituted into (4.15). The phases θ and φ are implicit. They can be made explicit by expanding in a Taylor series. Also, parameters δ, κ and a are rescaled by

$$\begin{aligned}
\delta &= \delta^*[1 - \frac{1}{6}\epsilon(a^{*^2} + \kappa^{*^2})(c_1 + 4c_2 + c_3 - 2c_4 + 2c_5)\\
&\quad -\frac{1}{24}(c_1 + 2c_2 + c_3 + 2c_5)\epsilon\delta^{*^2}],\\
\kappa &= \kappa^*[1 - \frac{1}{6}(c_1 + 4c_2 + c_3 - 2c_4 + 2c_5)\epsilon a^{*^2}\\
&\quad -\frac{1}{8}\epsilon\delta^*(\delta^* - 2a^*)(c_1 + 2c_2 + c_3 + 2c_5) - \frac{1}{3}(c_2 - c_4)\epsilon\kappa^{*^2}], \qquad (4.22)\\
a &= a^*[1 - \frac{1}{6}(c_1 + 4c_2 + c_3 - 2c_4 + 2c_5)\epsilon a^{*^2}\\
&\quad -\frac{1}{8}\epsilon\delta^*(\delta^* - 2a^*)(c_1 + 2c_2 + c_3 + 2c_5) - \frac{1}{3}(c_2 - c_4)\epsilon\kappa^{*^2}],
\end{aligned}$$

which, after dropping the stars and using the algebraic relation (4.5) gives the di-

rectly derived higher-order solitary wave (4.17), if the choice

$$\begin{aligned} B_0 &= \frac{1}{12}(-c_1-c_2-c_3-c_4-c_5)\delta^2 a+\frac{1}{12}(c_1+4c_2+c_3-2c_4+4c_5)\delta\kappa^2 \\ &+\frac{1}{4}(c_1+2c_2+c_3+2c_5)\delta a^2+\frac{1}{3}(-c_2+c_4)\kappa^2 a \\ &+\frac{1}{6}(-c_1-2c_2-2c_3+c_4-c_5)a^3, \end{aligned}$$

is used in (4.17). This represents the appropriate correction to the background travelling wave that the asymptotic transformation generates. Moreover, the higher-order solitary wave has been shifted from $\xi = s$ at $\tau = 0$ to

$$\begin{aligned} x = -\epsilon c_7\kappa + s[1+\frac{1}{6}(c_1+4c_2+c_3-2c_4+2c_5)\epsilon a^2 \\ +\frac{1}{8}\epsilon\delta(\delta-2a)(c_1+2c_2+c_3+2c_5)+\frac{1}{3}(c_2-c_4)\epsilon\kappa^2] \end{aligned} \tag{4.23}$$

at $t = 0$.

4.3.2 The higher-order gray two-soliton solution

In this section the dark two-soliton solution of the higher-order Hirota equation (4.3) is derived for the higher-order coefficients satisfied in (4.5). The explicit gray two-soliton solution for the integrable Hirota hierarchy (4.4) is

$$\begin{aligned} &\Omega = \mu[1+\frac{\Psi(\xi,\tau)}{\Phi(\xi,\tau)}]e^{i\varphi}, \quad \text{where} \quad \Psi(\xi,\tau) = \\ &4\mu(\phi_1(\xi,\tau)+\phi_2(\xi,\tau)-2\mu)-4i(\nabla+i)(\phi_1(\xi,\tau)-\mu)(\phi_2(\xi,\tau)-\mu), \\ &\Phi(\xi,\tau) = 4\mu^2+(\nabla+i)^2(\phi_1(\xi,\tau)-\mu)(\phi_2(\xi,\tau)-\mu), \\ &\phi_j(\xi,\tau) = \frac{a_j-i\kappa_j}{\mu}(a_j+i\kappa_j\tanh\kappa_j\theta_j), \quad j=1,2. \end{aligned} \tag{4.24}$$

The various other parameters are

$$\begin{aligned} &\varphi = \delta(\xi-b\tau), \quad b = 6\mu^2+\delta^2+(\mu^4+\frac{1}{30}\delta^4+\frac{2}{3}\delta^2\mu^2)\epsilon', \\ &\mu^2 = a_1^2+\kappa_1^2 = a_2^2+\kappa_2^2, \\ &\nabla = \frac{a_1+a_2}{\kappa_1+\kappa_2}, \quad \theta_j = \xi-s_j-v_j\tau+\theta_{0_j}, \\ &v_j = 3\delta^2+6a_j^2+2\kappa_j^2-6\delta a_j+(\frac{2}{3}\delta^2\kappa_j^2+\frac{1}{6}\delta^4+\frac{2}{3}a_j^2\kappa_j^2 \\ &\quad -\frac{2}{3}\delta^3 a_j+\frac{1}{5}\kappa_j^4+a_j^4-2a_j^3\delta-\frac{2}{3}a_j\kappa_j^2\delta+2a_j^2\delta^2)\epsilon', \quad j=1,2, \end{aligned}$$

where δ, a_1, a_2, κ_1 and κ_2 are free real constants, see Li *et. al.* [24].

The velocity of the jth soliton is v_j and its position is s_j at $\tau = 0$. When $\epsilon^{'} = 0$, it becomes the Hirota gray two-soliton solution. The higher order terms only affect the velocities v_j and the parameter b. This is similar to the bright two-soliton solution of the integrable higher-order Hirota equation (3.13), for which only the velocities have a correction term at $O(\epsilon)$.

We assume that the soliton with minimum intensity a_2 is initially well to the left of the soliton with minimum intensity $a_1(< a_2)$ and $\delta < \frac{2}{3}(a_1 + a_2)$. Hence before interaction the wave on the left (with minimum intensity a_2) will overtake the other wave after interaction. As figure 4.1 shows, well before and after collision the gray two soliton solution (4.24) is just the sum of two well separated solitons; hence the collision is elastic with no radiation being shed. However, the gray two-soliton solution (4.24) can be written as

$$|\Omega|^n = |\psi_1(\xi,\tau)|^n + |\psi_2(\xi,\tau)|^n - \mu^n, \quad n = 1, 2, ... \tag{4.25}$$

well before and after collision, where the single soliton $\psi_j, (j = 1, 2)$ have the form (4.21). The only effects of the collision are coordinate shifts that the solitons suffer, these are

$$\frac{\ln\chi}{2\kappa_1}, \quad -\frac{\ln\chi}{2\kappa_2}, \quad \text{where } \chi = 1 - (\nabla^2 + 1)\frac{\kappa_1\kappa_2}{\mu^2}. \tag{4.26}$$

Substituting the two soliton solution (4.24) in the asymptotic transformation (4.15) gives the higher-order two-soliton solution for (4.3), but due to the complicated form of (4.24), the higher-order two-soliton solution is investigated well before and after interaction. Expression (4.25) describes the integrable Hirota two-soliton solution (4.24) before and after interaction; using relation (4.25) , for example for $|\eta|^2$, in (4.15) gives

$$|\eta|^2 = |\eta_1|^2 + |\eta_2|^2 - \mu^2 - \frac{\epsilon}{3}(2c_2 - c_3 - c_4 + c_5)\mu^4 - \frac{\epsilon}{12}(c_1 + 4c_2 + c_3 - 2c_4 + 4c_5)\delta^2\mu^2. \tag{4.27}$$

Here the single higher-order solitons η_1 and η_2 have the form (4.17) but the transformation (4.15) modifies the coordinate shifts as

$$-2\epsilon c_7\kappa_2, \qquad 2\epsilon c_7\kappa_1, \tag{4.28}$$

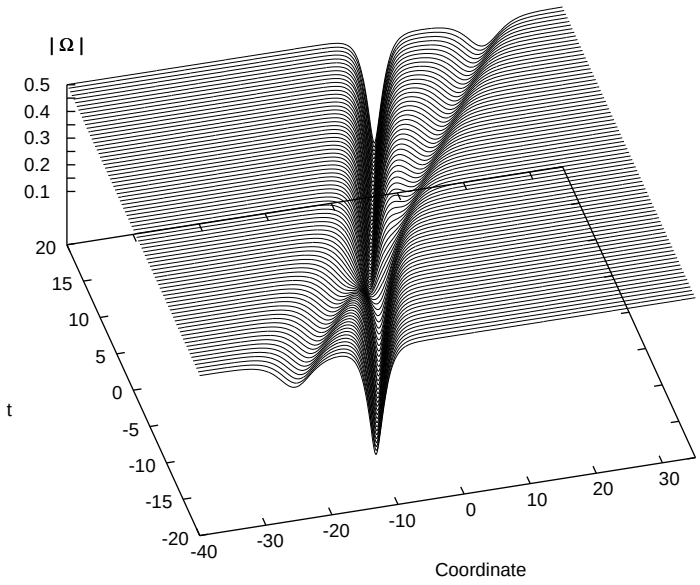

Figure 4.1: Gray soliton interaction for Hirota (4.1) equation

for η_1 and η_2, respectively. The coordinate shifts (4.28) are due to the integration in the transformation over the trailing wave, which involves

$$\int_{-\infty}^{\infty}(|\Omega(p,t)|^2-\mu^2)dp. \tag{4.29}$$

Also, there is some contribution from the rescalings (4.22), to the higher-order coordinate shifts. Combining these contributions gives

$$\frac{\ln\chi}{2\kappa_1}-2\epsilon\kappa_2 c_7+\epsilon\kappa_2\Lambda c_8, \qquad -\frac{\ln\chi}{2\kappa_2}+2\epsilon\kappa_1 c_7-\epsilon\kappa_1\Lambda c_8, \tag{4.30}$$

$$\text{where}\quad \Lambda=\frac{\nabla}{12}\frac{(a_1-a_2)(a_1\kappa_2-a_2\kappa_1)(2a_1+2a_2-3\delta)}{(a_1\kappa_1-a_2\kappa_2)^2+(\kappa_1^2-\kappa_2^2)^2},$$

$$c_8=c_1+2c_2+c_3+2c_5,$$

as the higher-order coordinate shifts of the slower and faster gray solitary waves, respectively. Note that in the integrable case where the higher-order coefficients satisfy (4.5), then $c_7=c_8=0$, and the higher-order shifts are all zero.

4.3.3 Numerical interaction of higher-order gray solitary waves

In section 4.3 the effects of the interaction of higher-order gray solitary waves were identified. The main effect of the collision is the higher-order coordinate shifts, when the relationship (4.5) is satisfied. Here numerical interaction of the higher-order solitary wave solutions of (4.3) are undertaken and the coordinate shifts found in (4.30) are numerically verified. The numerical scheme is a hybrid Runge-Kutta finite-difference scheme with fourth-order accuracy in space and time, see Appendix B. The spatial and temporal grid spacings used are $\triangle x = 8\times10^{-2}$ and $\triangle t = 1\times10^{-4}$. The initial higher-order solitary waves are in the form (4.17). The soliton parameters are $\delta = 0$, $\kappa_1 = a_2 = \frac{\sqrt{3}}{2}$ and $a_1 = \kappa_2 = \frac{1}{2}$, for two solitons with initial positions $s_1 = -10$ and $s_2 = -25$, and the perturbation parameter is $\epsilon = 0.1$. A constant phase shift φ_0 is applied to make the background wave in front of the trailing wave match the background wave behind the leading wave. The $O(1)$ coordinate shifts (4.26) of Hirota solitons, for these parameter values, are -1.160 and 2.010 for the slower wave ($\kappa_1 = \frac{\sqrt{3}}{2}$) and the faster wave ($\kappa_2 = \frac{1}{2}$), respectively. Also note that the parameter B_0 is chosen as in (4.19), so that the backgrounds at $O(\epsilon)$ remain unchanged.

We consider the case where $c_1 = -5$ and $c_3 = c_4 = 1$ and the other $c_i = 0$, which satisfies (4.5). Numerical runs are done for cases with and without interaction. The phase shift is taken as the difference in position between the two runs. As the grid spacing is $\triangle x = 8 \times 10^{-2}$, a quadratic curve is fitted to the solitary wave peak, in order to obtain a more accurate estimate of the coordinate shift. The positions of the two waves at $t = 20$, well after interaction for the slower and faster waves are $\theta_1^{'} = 44.91$ and $\theta_2^{'} = 69.29$. For numerical runs with no collisions the positions are $\theta_1^{''} = 46.11$ and $\theta_2^{''} = 67.21$, after $t = 20$. Hence the numerical coordinate shifts after the interaction for the slower and faster waves are $\triangle\theta_1 = \theta_1^{'} - \theta_1^{''} = -1.20$ and $\triangle\theta_2 = \theta_2^{'} - \theta_2^{''} = 2.08$. The coordinate shifts predictions from the asymptotic theory in (4.30) are -1.19 and 2.07. An excellent agreement is achieved for the higher-order coordinate shifts of both waves. The agreement is much better than that

provided by the Hirota coordinate shifts (4.26), hence the higher-order predictions are verified.

The minimum intensities of $|\eta|$, (which occur at $\theta = 0$) for the slower wave, before and after interaction are 0.4875 and 0.4876, respectively, with an increase in amplitude of about 1×10^{-4}. The minima for the faster wave are 0.8588 and 0.8592, with a change about 4×10^{-4}. The $O(\epsilon)$ change in minimum intensity between the Hirota soliton and the higher-order solitary wave is $0.5 - 0.49 \approx 0.01$, as the intensity of the Hirota soliton is just a. For the faster wave the $O(\epsilon)$ correction to the minimum intensity is 6×10^{-3}. The changes in intensity due to the collision are much smaller than these measures of an $O(\epsilon)$ change in intensity, hence the collision is elastic to $O(\epsilon)$.

4.4 Perturbation theory and solitary wave evolution

It was found from the asymptotic theory and direct calculations in section 4.3 that a three-parameter and a two-parameter family of higher-order Hirota embedded solitons exist if (4.5) or (4.20) is satisfied. Here direct soliton perturbation theory based on the Jost solution of the defocusing Hirota equation, is used to determine the details of the evolving solitary wave, to first-order. Analytical expressions are found for the tails of the solitary wave. It is found that tails form for two reasons; one reason is the shedding of radiation due to non-existence of a higher-order asymptotic embedded soliton, the second is related to first-order corrections to the background travelling wave. Comparisons of the solitary wave tails are made with numerical solutions and an excellent agreement is found.

4.4.1 The perturbation solution based on Jost solution

Given the similarity between the dark Hirota and NLS solitons, the technique for analysing them is closely related. We first investigate the linear stability of the background radiation for the Hirota equation, see Kivshar and Luther-Davies [19] for

the application to the NLS equation. The travelling-wave solution of the defocusing Hirota equation (4.12) is given by

$$\eta = \rho_0 e^{i\delta x - i\beta t}, \quad \beta = 6\rho_0^2\delta + \delta^3, \tag{4.31}$$

where ρ_0 and δ are free parameters. To investigate the stability we substitute

$$\eta = (\rho_0 + \nu)e^{i\delta x - i\beta t + i\varphi}, \tag{4.32}$$

as a small excitation of the exact travelling wave solution (4.31) in the defocusing Hirota equation (4.1), where the function ν and derivatives of φ are small. By taking $\nu, \varphi \sim e^{ipt-iqx}$, the dispersion relation

$$(q^3 - p + 3q\delta^2 + 6\rho_0^2 q)^2 = 9q^2\delta^2(q^2 + 4\rho_0^2), \tag{4.33}$$

is obtained. Solving (4.33) gives

$$p = q^3 + 3q\delta^2 + 6\rho_0^2 q \pm 3q\delta\sqrt{q^2 + 4\rho_0^2}, \tag{4.34}$$

as the wave number of the perturbed wave. As p is real, small excitations of the background wave (4.31) are absolutely stable. Note that for the focusing Hirota equation the excitation (4.32) is unstable.

As $p, q \ll 1$ (it has been assumed the derivatives of φ are small), we apply a Taylor series expansion to (4.34) and obtain

$$\frac{p}{q} = 6\mu^2 + 3\delta^2 \pm 6\delta\mu, \tag{4.35}$$

as the phase velocity of the perturbation. To this level of approximation, the phase and group velocities are equal. Hence there are two different phase velocities for small perturbations propagating on the background wave. This is similar to the case of the defocusing NLS equation, see (2.14) of Kivshar and Luther-Davies [19], for which two phase velocities are also identified.

The single soliton solution (4.14) can be considered as an excitation on the background wave (4.31) and may be formulated as

$$\begin{aligned} &\psi_0 = \frac{a - i\kappa}{\mu}(a + i\kappa\tanh\kappa\theta)e^{i(\delta\theta+\varphi)}, \\ &\varphi = 2\delta(-3a\delta + \delta^2 - 2\kappa^2)t - \varphi_0, \quad \theta = x - vt - \theta_0, \\ &\text{where} \quad v = 3a^2 + 2\kappa^2 + 3(a-\delta)^2, \ \mu^2 = a^2 + \kappa^2, \end{aligned} \tag{4.36}$$

where a, κ, δ, φ_0 and θ_0 are all free parameters. Similar to (4.36), the perturbed solution of the higher-order Hirota equation (4.3) is written

$$\psi = e^{i\varphi}\eta(\theta, t, T_1, T_2, ...),\ \theta = x - \int_0^t v dt - \theta_0,\ \varphi = \int_0^t \lambda dt - \varphi_0. \quad (4.37)$$

The soliton parameters κ, a, δ, θ_0 and φ_0 all vary on the slow time scales $T_n = \epsilon^n t, n = 1, 2, ...$ The forms of the slow variation are chosen to eliminate the secular terms in the expansion. In fact, some integrals are divergent, hence the coefficients of these divergent terms must be equal to zero, see for example Chen *et. al.* [3]. This feature in dark soliton perturbation is different from the counterpart for the bright soliton. In our analysis below, these slow variations, which are not explicitly shown, are determined to let η_1 in (4.49) rest on a zero mean level. Hence, the mean level of the background (4.31) does not change in the presence of the perturbed terms in (4.3). The only effect of the higher-order terms on the travelling wave background (4.31) is a phase shift, at $O(\epsilon)$, which is given by

$$\beta = 6\rho_0^2\delta + \delta^3 + \epsilon\delta(c_1\rho_0^4 + c_2\delta^2\rho_0^2 - 2c_3\delta^2\rho_0^2 - c_4\delta^2\rho_0^2 - c_5\delta^2\rho_0^2 + c_6\delta^4). \quad (4.38)$$

Note that the theoretical development here is for gray solitons only. For black solitons where $a = 0$, the details of the analysis are slightly changed. The main focus here is to find the first-order correction (η_1) to the solitary wave profile, which allows the tails of the solitary wave to be determined.

By substituting (4.37) in (4.3) one obtains

$$\eta_t + i\lambda\eta - v\eta_\theta - \eta_{\theta\theta\theta} + 6|\eta|^2\eta_\theta = -\epsilon H(\eta) - \epsilon(\eta_{T_1} - i\eta\varphi_{0_{T_1}} - \eta_\theta\theta_{0_{T_1}}), \quad (4.39)$$

where H represents the perturbed terms in (4.3). The solution $\eta(\theta, t, T_1, T_2, ...)$ can be found by expanding as

$$\eta = \eta_0(\theta) + \epsilon\eta_1(\theta, t, T_1, T_2, ...) + ..., \quad (4.40)$$

and substituting in (4.39), where initial solution $\eta_0(\theta) = \frac{a-i\kappa}{\mu}(a + i\kappa\tanh\kappa\theta)e^{i\delta\theta}$. At the zeroth-order, the equation is satisfied automatically, and at first-order,

$$\eta_{1_t} + i\lambda\eta_1 + (6|\eta_0|^2 - v)\eta_{1_\theta} - \eta_{1_{\theta\theta\theta}} + r(\theta)\eta_1 + q(\theta)\eta_1^* = \omega_1, \quad (4.41)$$

$$\text{where} \quad r(\theta) = 6\eta_0^*\eta_{0_\theta}, \quad q(\theta) = 6\eta_0\eta_{0_\theta},$$

$$\omega_1 = -H(\eta_0) - \eta_{0_{T_1}} + i\eta_0\varphi_{0_{T_1}} + \eta_{0_\theta}\theta_{0_{T_1}},$$

is obtained. The linearized equation (4.41) can be written in the matrix form $(\partial_t + L)\mathbf{w_1} = \mathbf{H}$ and is solved using the initial condition $\eta_1|_{t=0} = 0$, where

$$L = \begin{pmatrix} G(\theta) & q(\theta) \\ q^*(\theta) & G^*(\theta) \end{pmatrix}, \quad \mathbf{w}_1 = (\eta_1, \eta_1^*)^T, \quad \mathbf{H} = (\omega_1, \omega_1^*)^T, \tag{4.42}$$
$$G(\theta) = -\partial_{\theta\theta\theta} + (6|\eta_0|^2 - v)\partial_\theta + r(\theta) + i\lambda.$$

It is not difficult to show that the non-localized (continuous) eigenstate of L is found as $\Phi = \mathbf{S} \bigcirc \mathbf{S} = (\mathbf{S}_1^2, \mathbf{S}_2^2)^T$, where $\mathbf{S} = (\mathbf{S}_1, \mathbf{S}_2)^T$ is a Jost solution of Hirota equation. Thus the non-localized eigenstates can be found similar to Chen *et. al.* [3] by

$$\mathbf{w}_2 = \frac{(a - i\kappa)^2}{\mu^4(\alpha - a + i\kappa)^2} \times \tag{4.43}$$
$$\begin{pmatrix} \mu^2(\alpha - a - i\kappa + i\kappa \operatorname{sech} \kappa\theta e^{-\kappa\theta})^2 e^{i(\delta - 2\omega)\theta} \\ (i\mu^2\alpha^{-1}(\alpha - a - i\kappa) - \kappa(a + i\kappa) \operatorname{sech} \kappa\theta e^{-\kappa\theta})^2 e^{-i(\delta + 2\omega)\theta} \end{pmatrix},$$

see Appendix A. The continuous eigenfunction of the adjoint operator $L^\dagger = -\sigma_2 L \sigma_2$ is also needed, where

$$\sigma_2 = \begin{pmatrix} 0 & -i \\ i & 0 \end{pmatrix}, \tag{4.44}$$

is a *Pauli* matrix. It is not difficult to show that $\mathbf{w}_2^\dagger = (-a^*, b^*)^T$ is a continuous eigenfunction for $L^\dagger$ where $\mathbf{w}_2 = (a, b)^T$ is the eigenfunction for L in (4.42). Again the inner product

$$\langle \mathbf{f}(\theta), \mathbf{g}(\theta) \rangle = \int_{-\infty}^{\infty} \mathbf{f}(\theta)^T \mathbf{g}(\theta) d\theta, \tag{4.45}$$

is used to find nonzero inner products of the non-localized and localized eigenstates and their adjoint eigenstates. Note that the forms of two localized eigenfunctions can be determined explicitly by calculating $\mathbf{w}_2|_{\alpha=a+i\kappa}$ and $\frac{d\mathbf{w}_2}{d\alpha}|_{\alpha=a+i\kappa}$.

The completeness of the set of eigenstates can be proved in an analogous manner to the proof for the counterpart set of the NLS equation which has been presented in Yan *et. al.* [39], using Green's function theory, and in Chen *et. al.* [3], by using Jordan's lemma and in Huang *et. al.* [16] by applying a generalized Marchenko equation. For example, the completeness relationships in Chen *et. al.* [3] (see their section 4.1) can be extended to the Hirota equation by including $e^{i\delta\theta}$ in the proof.

The first-order solution has the form

$$\begin{aligned}
&\mathbf{w}_1 = \int_{-\infty}^{+\infty} g\mathbf{w}_2 d\alpha, \quad \text{where} \quad g = \frac{iM(\alpha)}{\vartheta}(1 - e^{i\vartheta t}), \\
&\vartheta = 8\omega(\xi + a - \frac{3}{2}\delta)(\xi - a), \quad M(\alpha) = -\frac{\langle \mathbf{H}, \mathbf{w}_2^\dagger \rangle}{k(\alpha)}, \\
&k(\alpha) = 2\pi \frac{(a - i\kappa)^2}{\mu^2} (\frac{\alpha - a - i\kappa}{\alpha - a + i\kappa})^2 (1 - \mu^2 \alpha^{-2}),
\end{aligned} \tag{4.46}$$

and the auxiliary variables are defined as

$$\omega = \frac{1}{2}(\alpha - \mu^2 \alpha^{-1}), \quad \xi = \frac{1}{2}(\alpha + \mu^2 \alpha^{-1}). \tag{4.47}$$

The quantity $M(\alpha)$, found using the residue theorem, is

$$\begin{aligned}
M(\alpha) \;=\; & \frac{i(\alpha^2 - \mu^2)(a + i\kappa)(\alpha - a + i\kappa)^2}{360\mu} \times \\
& \frac{(\alpha + \mu^6 \alpha^{-5})E_1 + (1 + \mu^4 \alpha^{-4})E_2 + (\alpha^{-1} + \mu^2 \alpha^{-3})E_3 + \alpha^{-2} E_4}{\sinh(\frac{\pi\omega}{\kappa})},
\end{aligned} \tag{4.48}$$

where the various coefficients are given by

$$\begin{aligned}
E_1 \;=\; & -(c_1 + 5c_2 + 8c_3 + 2c_4 + 2c_5 + 120c_6), \\
E_2 \;=\; & (5c_1 + 5c_2 + 50c_3 + 20c_4 + 600c_6)\delta \\
& + (-2c_1 + 10c_2 - 26c_3 - 14c_4 + 6c_5 - 240c_6)a, \\
E_3 \;=\; & (31c_1 + 25c_2 + 88c_3 - 8c_4 + 12c_5 + 120c_6)a^2 \\
& + (-10c_1 - 100c_2 + 80c_3 + 50c_4 - 30c_5 + 600c_6)a\delta \\
& + (45c_2 - 90c_3 - 45c_4 + 15c_5 - 900c_6)\delta^2 \\
& + (15c_1 - 15c_2 + 60c_3)\kappa^2, \\
E_4 \;=\; & (-80c_1 + 10c_2 - 260c_3 - 50c_4 - 90c_5 - 600c_6)\kappa^2\delta \\
& + (-45c_2 + 90c_3 + 45c_4 + 45c_5 + 900c_6)\delta^3 \\
& + (90c_2 - 180c_3 - 90c_4 - 150c_5 - 1800c_6)\delta^2 a \\
& + (64c_1 + 20c_2 + 212c_3 + 8c_4 + 8c_5 + 480c_6)a^3 \\
& + (-120c_1 - 30c_2 - 300c_3 - 30c_4 + 30c_5)a^2\delta \\
& + (32c_1 + 20c_2 + 116c_3 - 16c_4 + 24c_5 + 240c_6)a\kappa^2.
\end{aligned}$$

And finally, (4.46) gives

$$\begin{aligned}
\eta_1(\theta, t) \;=\; & \frac{i(a - i\kappa)^2}{\mu^2} \int_{-\infty}^{+\infty} \frac{M}{\vartheta} \frac{(1 - e^{i\vartheta t})}{(\alpha - a + i\kappa)^2} \times \\
& (\alpha - a - i\kappa + i\kappa \operatorname{sech} \kappa\theta e^{-\kappa\theta})^2 e^{i(\delta - 2\omega)\theta} d\alpha,
\end{aligned} \tag{4.49}$$

which is qualitatively similar to the second integral in the first-order correction to the bright Hirota solitary wave profile in (3.48). We note the limit (3.49), so the integrand of (4.49) is singular at $\vartheta = 0$ as $t \to \infty$.

4.4.2 The solitary wave tail

In contrast to the bright Hirota solitons, dark solitons are right-moving only. The analysis below shows that the evolution of the solitary wave tails for the higher-order defocusing Hirota equation is subtle and complicated. For some parameter ranges, tails only appear in front of the soliton, whilst for other parameter choices tails appear in front of and behind the solitary wave. For bright solitons non-zero tails only occur when embedded asymptotic solitons do not exist and hence radiation is shed. For gray solitons tails also occur for another reason; the first-order correction of the background wave, well ahead and behind the solitary wave. The asymptotic analysis considered here is similar to that of section 3.4.2, and references therein.

The contribution to (4.49) for large time comes entirely from the neighborhood of the singularities. Note that for

$$\delta \in I = [\frac{2}{3}(a-\mu), \frac{2}{3}(a+\mu)], \tag{4.50}$$

the leading expression for (4.49) can be found by considering the singular points $\alpha = \pm\mu$, and for $\delta \in I^c$, the extra singular points

$$\alpha = -a + \frac{3}{2}\delta \pm \frac{1}{2}(9\delta^2 - 12a\delta - 4\kappa^2)^{\frac{1}{2}} \equiv \alpha_c^{\pm}, \tag{4.51}$$

are needed. Hence when $\delta \in I$, there are two singular points and when $\delta \in I^c$, there are four. We suppose $\mu\delta \geq 0$ and define the quantities

$$S^{\pm} = (\mu \pm (a - \frac{3}{2}\delta))(\mu \mp a), \quad h_{\text{tail}}^{\pm} = \frac{\pi}{4}\frac{(a-i\kappa)^2}{\mu^2}\frac{M(\pm\mu)}{S^{\pm}}(\frac{\pm\mu - a - i\kappa}{\pm\mu - a + i\kappa})^2. \tag{4.52}$$

The length of the solitary wave tails is $4S^{\pm}$, while their respective amplitudes are $h_{\text{tail}}^{\pm}$. It should be noted that when $\mu\delta < 0$, the procedure is slightly modified by replacing $h_{\text{tail}}^{\pm}$ and $S^{\pm}$ in (4.52) by $h_{\text{tail}}^{\mp}$ and $S^{\mp}$.

For $\delta \in I$ we begin our analysis by making the substitution $\alpha = \pm\mu + z/t$ and obtain

$$\eta_1 \sim \frac{i}{2\pi}h_{\text{tail}}^{\pm}e^{i\delta\theta}\int_{-\infty}^{+\infty}(\frac{e^{-2izc_p} - e^{-2iz(c_p - 4S^{\pm})}}{z})dz, \tag{4.53}$$

where $c_p = \theta/t$ is an $O(1)$ constant. Using the integral (3.51), well behind of the soliton, $\theta \ll -1$ and $c_p < 0$, so both integrals within (4.53) have the same value. So the cancellation of the two integrals implies $\eta_1 \sim 0$ well behind the solitary wave. Hence tails only form ahead of the solitary wave for $\delta \in I$.

Ahead of the wave ($\theta \gg 1$, $t \to \infty$), we choose two intervals, $0 < c_p < 4S^+$ and $4S^+ < c_p < 4S^-$. Then the leading-order expression for (4.49) has the form as

$$\eta_1 \sim \begin{cases} (h^+_{\text{tail}} + h^-_{\text{tail}})e^{i\delta\theta}, & 0 < c_p < 4S^+, \\ h^-_{\text{tail}} e^{i\delta\theta}, & 4S^+ < c_p < 4S^-. \end{cases} \tag{4.54}$$

We note that for particular case $\delta = 0$, (*i.e.* $S^+ = S^-$), η_1 over the second tail's region vanishes and (4.54) yields a single tail which propagates ahead of the solitary wave.

The length of the solitary wave tails $4S^\pm$, is the difference between the soliton velocity (4.13) and the phase velocity of perturbations on the background wave (4.35). The two tails correspond to the two different phase velocities in (4.35). Moreover, for $\delta \in I$, both background phase velocities are greater than the soliton velocity, so tails only form ahead of the wave.

For $\delta \in I^c$ a similar procedure for large time yields

$$\eta_1 \sim \begin{cases} h^-_{\text{tail}} e^{i\delta\theta} + h^\pm_c e^{i(\delta - \triangle^\pm_1)\theta} + T^+, & 0 < c_p < 4S^-, \\ -(\frac{b\mu - a + i\kappa}{b\mu - a - i\kappa})^2 h^+_{\text{tail}} e^{i\delta\theta} + T^-, & 4S^+ < c_p < 0, \end{cases} \tag{4.55}$$

where $b = \text{sgn}(\delta\mu)$. A new tail component is now generated ahead of the solitary wave. Its amplitude is

$$\begin{aligned} h^\pm_c \;=\; & \frac{i\delta(a - i\kappa)\pi}{10\mu} \frac{(\alpha^\pm_c - a - i\kappa)^2}{\alpha^{\pm 3}_c (\triangle^\pm_2 - 2a)\triangle^\pm_1} (c_1 + 3c_3 + 2c_4 + 2c_5 + 20c_6) \times \\ & [(4\frac{S^+S^-}{\kappa^2} - 3\mu^2)\alpha^\pm_c + \mu^2 \triangle^\pm_2] \frac{2\kappa^2 + 3a\delta - \delta^2}{\sinh(\frac{\pi\triangle^\pm_1}{2\kappa})}, \end{aligned} \tag{4.56}$$

where $\triangle^\pm_1 = \frac{\alpha^{\pm 2}_c - \mu^2}{\alpha^\pm_c}$, $\triangle^\pm_2 = \frac{\alpha^{\pm 2}_c + \mu^2}{\alpha^\pm_c}$. Note that in (4.55),

$$h^\pm_c = 0, \quad \text{in} \quad 4\frac{\triangle^{+2}_1}{\triangle^+_2}(\triangle^+_2 - 2a) < c_p < 4S^-, \tag{4.57}$$

if $\frac{\triangle^{+2}_1}{\triangle^+_2}(\triangle^+_2 - 2a) < S^-$.

The fact that tails now occur in front of and behind the soliton is due to one of the phase velocities (4.35) now being less than the soliton velocity, while the other is greater than the soliton velocity. Moreover the tail in front of the soliton now consists of components with three different wavenumbers, hence the long-time tail is oscillatory in nature. In contrast, behind the solitary wave the long-time tail will be flat, as it consists of a component with a single wavenumber.

The two leading transient terms are calculated from contributions at points of stationary phase. The relevant phase of (4.49) is $\vartheta_1 = \vartheta - 2\omega c_p$, which has the stationary point when $\vartheta_1' = \frac{d\vartheta_1}{d\alpha} = \frac{R}{\alpha^4} = 0$, where

$$R = 3\alpha^6 - 6\delta\alpha^5 + (6\delta a - c_p + \mu^2 - 4a^2)\alpha^4 + \mu^2(6\delta a - c_p + \mu^2 - 4a^2)\alpha^2 - 6\delta\mu^4\alpha + 3\mu^6. \tag{4.58}$$

Due to the high order of the polynomial R in (4.58), the solutions of R are found numerically for constant parameters a, k, δ and different values of c_p. It is not difficult to show that $\frac{\mu^2}{\alpha_s}$ is a stationary point when α_s is a stationary point. Numerical solutions of R show that for finite c_p, which is analyzed here, there are just two roots for R. Using the method of stationary phase gives

$$T^{\pm} = -i\frac{(2\pi)^{\frac{1}{2}}}{t^{\frac{1}{2}}}\frac{(a-i\kappa)^2}{\mu^2|\vartheta_1''(\alpha_s)|^{\frac{1}{2}}}\frac{M(\alpha_s)}{\vartheta(\alpha_s)(\alpha_s - a + i\kappa)^2}[(\alpha_s - a \mp i\kappa)^2 \tag{4.59}$$
$$e^{i(\vartheta_1(\alpha_s)t \pm \mathrm{sgn}(\vartheta_1''(\alpha_s))\frac{\pi}{4})} - (\frac{\mu^2}{\alpha_s} - a \mp i\kappa)^2 e^{-i(\vartheta_1(\alpha_s)t \pm \mathrm{sgn}(\vartheta_1''(\alpha_s))\frac{\pi}{4})}]e^{i\delta\theta}.$$

It is noteworthy that the tail component $h_c^{\pm}$ vanishes if (4.5) or (4.20) is satisfied. These conditions imply the existence of higher-order asymptotic embedded solitons, hence the tail components $h_c^{\pm}$ are associated with radiation shedding due to linear resonance. The other tail components, with amplitudes $h_{\mathrm{tail}}^{\pm}$, have the same wavenumber, δ, as the background wave, so can be associated with corrections to the background wave at first-order.

4.4.3 Numerical solutions and discussion

In this section (4.3) is solved numerically and compared with the numerical solution of η_1 in (4.49). The main analytical features of the solitary tails, for different values

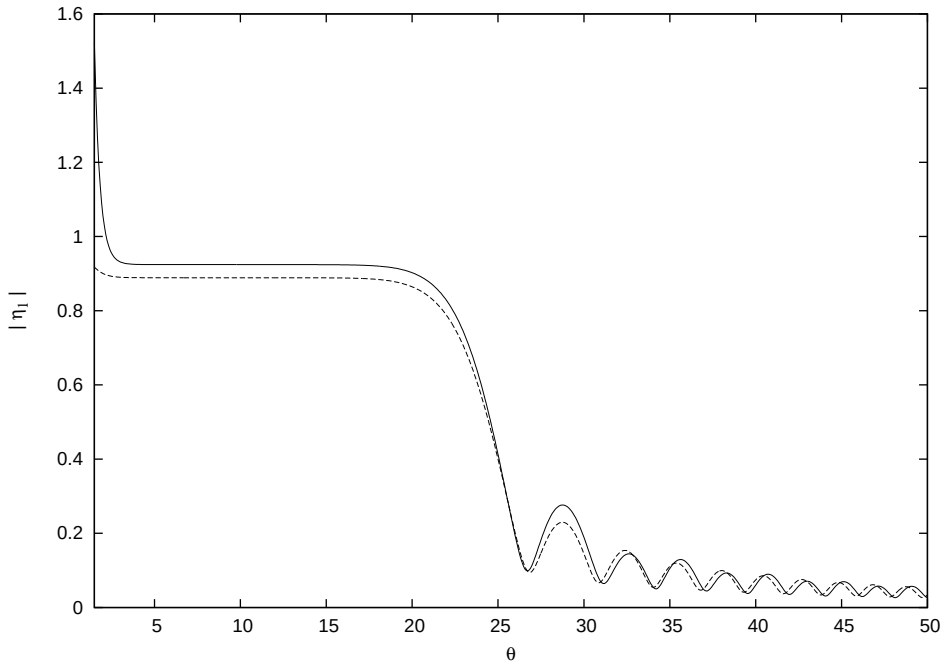

Figure 4.2: The first-order correction $|\eta_1|$ versus θ at $t = 3$ for wavenumber $\delta = 0$. Shown is the perturbation solution (4.49) (dashed curve) and numerical solution of (4.3) (solid curve)

of wavenumber δ, are also verified. For all the examples we choose $\epsilon = 0.05$ and use the soliton parameters $\kappa = a = \sqrt{2}$ and $\mu = 2$. The perturbation solution (4.49), is solved numerically by a higher-order quadrature scheme, and the higher-order Hirota equation (4.3), is solved using the fourth-order hybrid scheme, see Appendix B. The spatial and temporal gridspacings used are the same as in section 4.3.3. The quantity $\epsilon^{-1}|\eta - \eta_0|$ is plotted from the numerical solution as it allows a comparison with the perturbation solution in the tail region. Note that η_0 has the form (4.14) with b modified to include the higher phase corrections of the background radiation (4.38).

For the first example, we choose $\delta = 0 \in I$. Figure (4.2) shows the first-order correction $|\eta_1|$ versus θ at time $t = 3$. The higher-order coefficients used are $c_1 = c_4 = 1$ with all the other $c_i = 0$. There is an excellent comparison between the numerical and perturbation solutions. The figure shows the surface elevation ahead the evolving solitary wave with the flat steady-state tail clearly visible. For this

example the tail is

$$(h^{+}_{\text{tail}} + h^{-}_{\text{tail}})e^{i\delta\theta} = \frac{2i\kappa^5 a\mu}{9S^+S^-}(-2c_2 + c_4 + c_3 - c_5). \tag{4.60}$$

The amplitude of this tail, as predicted by the perturbation solution (4.49), is $|\eta_1| = 0.89$, which is the same as the analytical expression (4.60) for the steady-state tail amplitude. The numerical results that show that the tail has amplitude of 0.924, a difference of about 3%. The maximum amplitude of the real part of the numerical tail is 5×10^{-4}, which represents a small error compared with the analytical tail amplitude (4.60), which has a real zero part.

The asymptotic theory implies that the length of the solitary wave tail is $4tS^+ \approx 24$, which matches closely with the numerical results. For this example ,where $\delta = 0$, there is only one phase velocity in (4.35), so only one tail forms. Moreover, as (4.35) is greater than the soliton velocity, the tail only forms in front of the wave.

This example does not satisfy (4.5), but for examples which do satisfy (4.5), the long time expression for η_1 is not the first-order correction to the embedded solitary wave profile (4.17). This is because the embedded solitary waves have first-order corrections to the background wave in front of and behind the wave, whilst the evolving wave (for $\delta \in I$) only has first-order corrections in front of the wave.

The special case, where $c_2 = c_4 = 1$, $c_5 = -1$ and the other $c_i = 0$, has no higher-order corrections to the background level in (4.17), so $\eta_1 = 0$. In this case the perturbation theory predicts no tails occur and the perturbation and asymptotic theories correspond.

Figure (4.3) shows the first-order correction $|\eta_1|$ versus θ at $t = 3$, for $\delta = 1 \in I$, and $c_1 = 1$, with the other $c_i = 0$. The other soliton parameters are the same as for figure (4.2). Again, tails only appear in front of solitary wave. The figure shows the region in front of the moving solitary profile. For this example $\delta \neq 0$, so the two distinct phase velocities (4.35) result in two different tail regions. The comparison between the numerical and perturbation solutions is again very good, with some very slight differences in amplitude and phase. The tail closest to the wave occurs in the region $0 < \theta < 4tS^+ \approx 13.45$, with amplitude $|h^{+}_{\text{tail}} + h^{-}_{\text{tail}}| = 0.387$. The numerical amplitude is 0.375, which is a difference of about 3%.

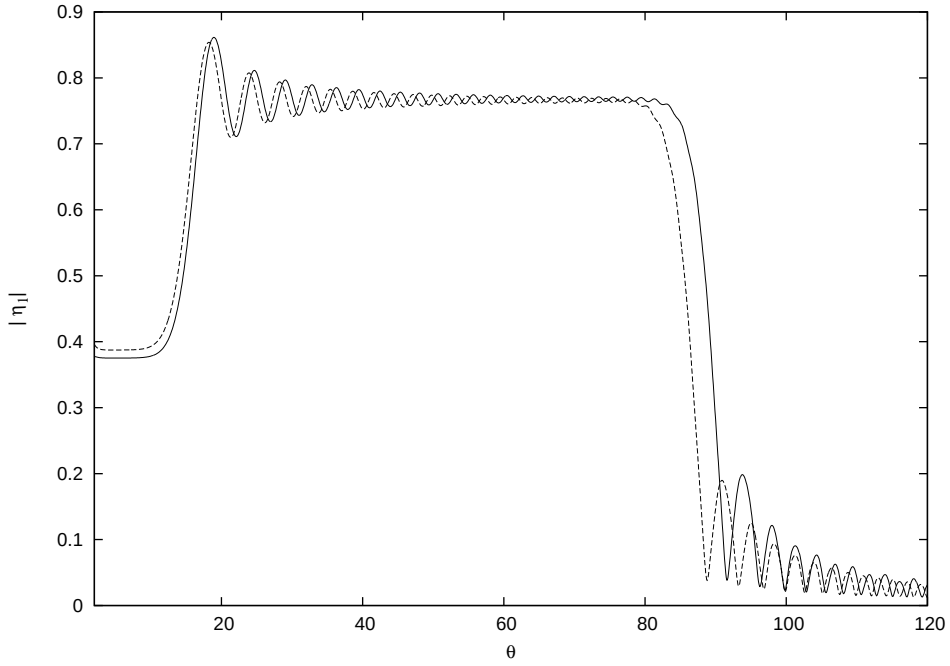

Figure 4.3: The first-order correction $|\eta_1|$ versus θ at $t = 3$ for wavenumber $\delta = 1$. Shown is the perturbation solution (4.49) (dashed curve) and numerical solution of (4.3) (solid curve)

The second tail region which occurs in $13.45 \approx 4tS^+ < \theta < 4tS^- \approx 85.45$, the average taken of the numerical solution is 0.762, which is within 0.4% of the analytical steady-state tail amplitude of 0.766. Some oscillations occur on the second tail. These oscillations represent a undular bore, which links together the different amplitudes of the two tails, see, for example, Marchant and Smyth [29].

Lastly, we investigate the tail evolution for an example of $\delta \in I^c$. The parameters and numerical scheme are the same as the figure (4.3) except we choose $\delta = -1$. Similar to figure (4.3), the figure (4.4) shows a schematic of the first-order solution $|\eta_1|$ versus θ at $t = 3$. Shown are the perturbation solution (4.49) and the quantity $\epsilon^{-1}|\eta - \eta_0|$ from the numerical solution of (4.3).

Again, the numerical solution is very close to the perturbation solution (4.49), with slight phase and amplitude differences. The average taken of the numerical solution over the tail for $\theta \ll -1$, is 0.8668. As $\mu\delta < 0$, the corresponding perturbation theory prediction is $|(\frac{-\mu-a+i\kappa}{-\mu-a-i\kappa})^2 h^+_{\text{tail}}| = 0.8608$, a difference of about 0.6%. A similar average taken in front of the solitary wave is 0.8044, which is about 1%

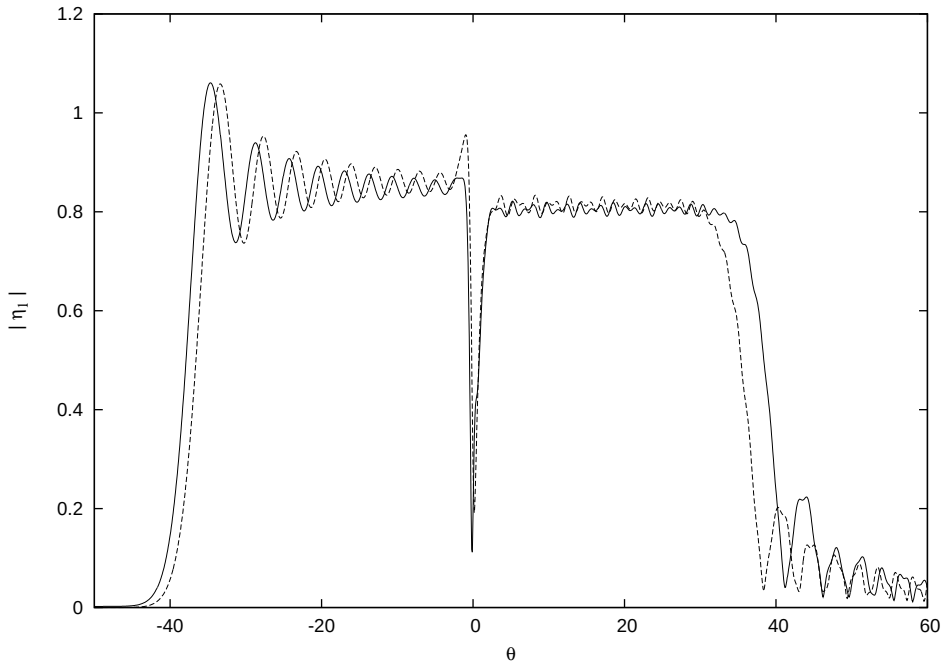

Figure 4.4: The first-order correction $|\eta_1|$ versus θ at $t = 3$ for wavenumber $\delta = -1$. Shown is the perturbation solution (4.49) (dashed curve) and numerical solution of (4.3) (solid curve)

different from the perturbation theory prediction of $|h^-_{\text{tail}}| = 0.8133$. Note that for this example, the $h^\pm_c$ contributions are negligible. In fact the amplitudes of h^+_c, h^-_c for figure (4.4) is $O(10^{-2})$.

For this example, the solution velocity lies between the two phase velocities (4.35), so tails occur behind and in front of the solitary wave.

The figure shows that the numerical tails occur between $-40 \leqslant \theta \leqslant 35$. The asymptotic results (4.55) yields tail length of $4tS^+ = -37.5$ and $4tS^- \approx 34.5$, which are very close to the numerical values. In contrast to the flat tails for the wavenumbers $\delta \in I$, the tails here are highly oscillatory. In front of the soliton, the superposition of the steady-state tail components of different wavenumbers with the transients of form (4.59) leads to a classical beating-like phenomena where the tail has multiple peaks and troughs of higher and lower amplitudes. For the tail behind the soliton the oscillations, generated by T^- form a undular bore, which links the mean level of zero, well behind the solitary wave, with tail amplitude of $|h^-_{\text{tail}}|$. The maximum amplitude (crest to trough) of the oscillations behind the soliton is 0.33

at $t = 3$. As the oscillations decay like $O(t^{-\frac{1}{2}})$, a relatively flat tail will not be reached until $t = O(10^6)$, when the amplitude of the oscillation will have decayed to less than 1% of this value.

In summary, for a number of examples the soliton perturbation theory (both analytical results and direct numerical solutions of (4.49)), the results from the asymptotic transformation (4.49), and numerical solutions of the governing pde (4.3) are in good agreement.

4.5 Conclusion

An asymptotic transformation and soliton perturbation theory have been used to investigate the interaction and evolution of the gray solitons of a higher-order Hirota equation. It is found that the higher-order solitary waves are asymptotic embedded solitons when an algebraic relationship (4.5) involving the higher-order coefficients is satisfied. An additional two-parameter family of asymptotic embedded solitary waves, which exist when (4.20) is satisfied, is also identified. By using the asymptotic theory the higher-order coordinate shifts, after interaction of the solitary waves, were also found. Numerical simulations of the higher-order gray solitary wave interaction confirm these coordinate shift corrections.

The soliton perturbation theory has been applied to evaluate the higher-order gray soliton profile for Hirota equation with an integral expression found for the first-order correction to the solitary wave profile. Asymptotic expansions, valid for large time, allows analytical expressions to be found for the solitary wave tails for the two different parameter regions. An extremely complicated picture of tail evolution emerges. In some cases, tails only form in front of the solitary wave, while in other cases they occur on both sides of the wave. Moreover, tails form for two reasons; shedding of radiation due to linear resonance and corrections to the background wave at first-order.

Appendix A

Lax equations and Jost solutions for Hirota equation

In this Appendix the Lax pairs and Jost solutions for the defocusing Hirota equation (4.1) are presented. In section 4.4.1 it is shown that the non-localised (continuous) eigenfunction (4.43) of the linearized operator L (4.42) is just the squared Jost solution of the Hirota equation.

It can be shown that the representation of Hirota equation in terms of the so-called Lax equations is

$$\mathbf{S}_x = \mathbf{M}\mathbf{S}, \quad \mathbf{S}_t = \mathbf{N}\mathbf{S}, \text{ where } \quad \mathbf{S} = (\mathbf{S}_1(x,t), \mathbf{S}_2(x,t))^T \tag{A.0.1}$$

and the Lax pair is

$$\begin{aligned} \mathbf{M} &= -i(\xi - \frac{1}{2}\delta)\sigma_3 + U, \\ \mathbf{N} &= 4i(\xi - \frac{1}{2}\delta)^3\sigma_3 - 4(\xi - \frac{1}{2}\delta)^2 U + 2i(\xi - \frac{1}{2}\delta)(U^2 + U_x)\sigma_3 \\ &\quad -2U^3 + U_{xx} + UU_x - U_x U, \\ \text{where } \ U &= \begin{pmatrix} 0 & \eta \\ \eta^* & 0 \end{pmatrix}, \text{ and } \sigma_3 = \begin{pmatrix} 1 & 0 \\ 0 & -1 \end{pmatrix} \end{aligned} \tag{A.0.2}$$

is a *Pauli* matrix. It is easy to verify that Hirota equation is tantamount to the zero curvature representation $\mathbf{M}_t - \mathbf{N}_x + [\mathbf{M}, \mathbf{N}] = 0$ of the Lax equations (A.0.1). Now the affine auxiliary parameter α is introduced to make $\omega = \sqrt{\xi^2 - \mu^2}$ as a single-valued function. Hence the parameters ω and ξ are functions of α as in (4.47). As

$x \to \infty$ (*i.e.*, $\eta \to \mu e^{i\delta x}$) the Jost solution of (A.0.1) approaches

$$E_+(x,\alpha) = e^{\frac{1}{2}i\delta x\sigma_3} \begin{pmatrix} 1 & -i\mu\alpha^{-1} \\ i\mu\alpha^{-1} & 1 \end{pmatrix} e^{-i\omega x\sigma_3}, \tag{A.0.3}$$

and as $x \to -\infty$ the asymptotic solution can be chosen as $E_-(x,\alpha) = e^{\frac{1}{2}i\theta_s\sigma_3}E_+(x,\alpha)$, where, θ_s, the phase difference between each end of the boundary values, is determined as

$$\eta \to \mu e^{i\theta_s}, \quad \text{as} \quad x \to -\infty. \tag{A.0.4}$$

In other words the relationships between the Jost solutions of the Lax pair (A.0.1) and the asymptotic solutions $E_+(x,\alpha)$ and $E_-(x,\alpha)$ can be found as

$$\begin{aligned} \Psi(x,\alpha) &= (\tilde{\psi}(x,\alpha), \psi(x,\alpha)) \to E_+(x,\alpha) \ \text{ as } \ x \to +\infty, \\ \Phi(x,\alpha) &= (\phi(x,\alpha), \tilde{\phi}(x,\alpha)) \to E_-(x,\alpha) \ \text{ as } \ x \to -\infty. \end{aligned} \tag{A.0.5}$$

Also noteworthy is that the asymptotic behavior of Jost solutions (A.0.3) are exactly the same as NLS equation counterparts. This equivalence is resulted from the fact that the first Lax equation (A.0.1) and (A.0.2) are common for the Hirota and NLS equations. For example, in the single-soliton case (*i.e.* $\mu^2 e^{i\theta_s} = (a - i\kappa)^2$), the explicit expressions of the Jost solutions can be found as

$$\psi(x,\alpha) = \begin{pmatrix} (-i\mu\alpha^{-1} - \frac{\kappa}{\alpha-\alpha_1^*}e^{\frac{1}{2}i\theta_s}\operatorname{sech}\kappa x e^{-\kappa x})e^{i(\frac{1}{2}\delta+\omega)x} \\ (1 - \frac{i\kappa}{\alpha-\alpha_1^*}\operatorname{sech}\kappa x e^{-\kappa x})e^{-i(\frac{1}{2}\delta-\omega)x} \end{pmatrix},$$

$$\phi(x,\alpha) = \begin{pmatrix} (\frac{\alpha-\alpha_1}{\alpha-\alpha_1^*}e^{\frac{1}{2}i\theta_s} + \frac{i\kappa}{\alpha-\alpha_1^*}e^{\frac{1}{2}i\theta_s}\operatorname{sech}\kappa x e^{-\kappa x})e^{i(\frac{1}{2}\delta-\omega)x} \\ (i\mu\alpha^{-1}\frac{\alpha-\alpha_1}{\alpha-\alpha_1^*}e^{\frac{1}{2}i\theta_s} - \frac{\kappa}{\alpha-\alpha_1^*}\operatorname{sech}\kappa x e^{-\kappa x})e^{-i(\frac{1}{2}\delta+\omega)x} \end{pmatrix},$$

and

$$\tilde{\phi}(x,\alpha) = -i\mu\alpha^{-1}\phi(x,\mu^2\alpha^{-1}), \quad \tilde{\psi}(x,\alpha) = i\mu\alpha^{-1}\psi(x,\mu^2\alpha^{-1}),$$

where $\alpha_1 = a + i\kappa$, see Chen *et. al.* [3].

Appendix B

The numerical scheme for the higher-order defocusing Hirota equation

The numerical solutions for the higher-order defocusing Hirota equation (4.3) were obtained by using fourth-order centered finite differences in the spatial coordinate x and a fourth-order Runge-Kutta method for the temporal coordinate t. The numerical scheme described below is stable for reasonable choices of the space and time discretization units $\triangle x$ and $\triangle t$. Various straight finite-difference methods considered by the authors were found to be unstable for nearly all nonzero values of ϵ.

Given that the solution at the time t_i is

$$\eta_{i,j} = \eta(x_j = j\triangle x, t_i = i\triangle t), \quad (j = 1, ..., M), \tag{B.0.1}$$

then the numerical solution at time t_{i+1} is given by

$$\eta_{i+1,j} = \eta_{i,j} + \frac{1}{6}(k^a_{i,j} + 2k^b_{i,j} + 2k^c_{i,j} + k^d_{i,j}) + D(x_j), \quad (j = 1, ..., M), \tag{B.0.2}$$

where the various functions are

$$k^a_{i,j} = \triangle t f(\eta_{i,j}), \quad k^b_{i,j} = \triangle t f(\eta_{i,j} + \tfrac{1}{2}k^a_{i,j}), \tag{B.0.3}$$
$$k^c_{i,j} = \triangle t f(\eta_{i,j} + \tfrac{1}{2}k^b_{i,j}), \quad k^d_{i,j} = \triangle t f(\eta_{i,j} + k^c_{i,j}),$$

and $D(x)$ is the damping function used at the boundaries, so the boundaries do not affect the wave evolution being studied. The function f is the finite-differenced form of all the terms in (4.3) involving spatial derivatives,

$$\begin{aligned} f(p_{i,j}) = &-\frac{|p_{i,j}|^2}{12\triangle x}(6+\epsilon c_1|p_{i,j}|^2)A_1 - \frac{1}{8\triangle x^3}(-1+\epsilon c_3|p_{i,j}|^2)A_3 \\ &-\frac{\epsilon(c_2+c_5)p_{i,j}}{124\triangle x^3}A_2^*A_1 - \frac{\epsilon(c_3+c_4)p_{i,j}^*}{124\triangle x^3}A_2A_1 \\ &-\frac{\epsilon c_2 p_{i,j}}{124\triangle x^3}A_2A_1^* - \frac{\epsilon c_2}{124\triangle x^3}|A_1|^2A_1 - \frac{\epsilon c_5}{6\triangle x^5}A_4, \end{aligned} \tag{B.0.4}$$

where the fourth-order centered finite-difference formulas are given by

$$\begin{aligned} A_1 &= p_{i,j-2} - 8p_{i,j-1} + 8p_{i,j+1} - p_{i,j+2}, \\ A_2 &= -p_{i,j-2} + 16p_{i,j-1} - 30p_{i,j} + 16p_{i,j+1} - p_{i,j+2}, \\ A_3 &= p_{i,j-3} - 8p_{i,j-2} + 13p_{i,j-1} - 13p_{i,j+1} + 8p_{i,j+2} - p_{i,j+3}, \\ A_4 &= p_{i,j-4} - 9p_{i,j-3} + 26p_{i,j-2} - 29p_{i,j-1} + 29p_{i,j+1} - 26p_{i,j+2} \\ &\quad +9p_{i,j+3} - p_{i,j+4}. \end{aligned}$$

The function

$$D(x_j) = \operatorname{sech}^2[(j-1)\frac{\triangle x}{10}] + \operatorname{sech}^2[(j-M)\frac{\triangle x}{10}], \tag{B.0.5}$$

damps the boundary values to zero which stops the reflection of the small-amplitude dispersive radiation back into the solution domain. The accuracy of the numerical method is fourth-order in time and space *i.e.* $O(\triangle t^4, \triangle x^4)$.

References

[1] T. Benjamin and J.F. Feir. The disintegration of wavetrains on deep. *J. Fluid Mech.*, 27:417–430, 1967.

[2] A. R. Champneys, B. A. Malomed, J. Yang, and D. J. Kaup. Embedded solitons: solitary waves in resonance with the linear spectrum. *Phys. D*, 152:340–354, 2001.

[3] X-J Chen, Z-D Chen, and N-N Huang. A direct perturbation theory for dark solitons based on a complete set of the squared Jost solutions. *J. Phys. A: Math. Gen.*, 31:6929–6947, 1998.

[4] S. V. Dmitriev, D. A. Semagin, A. A. Sukhorukov, and T. Shigenari. Chaotic character of two-soliton collisions in the weakly perturbed nonlinear Schrödinger equation. *Phys. Rev. E*, 66(046609), 2002.

[5] K. B. Dysthe, E. Mjolhus, H. L. Pecseli, and L. Stenflo. Langmuir solitons in magnetised plasmas. *Plamsa Phys.*, 20:1087–1099, 1978.

[6] H. A. Erbay. Nonlinear transverse waves in a generalized elastic solid and the complex modified Korteweg-de Vries equation. *Phys. Scr.*, 58:9–14, 1998.

[7] A. S. Fokas and Q. M. Liu. Asymptotic integrability of water waves. *Phys. Rev. Lett.*, 77(12):2347–2351, Sep 1996.

[8] H. Frauenkron, Y. S. Kivshar, and B. A. Malomed. Multisoliton collisions in nearly integrable systems. *Phys. Rev. E*, 54:R2244–R2247, 1996.

[9] C. Gilson, J. Hietarinta, J. Nimmo, and Y. Ohta. Sasa-Satsuma higher-order nonlinear Schrödinger equation and its bilinearization and multisoliton solution. *Phys. Rev. E*, 68(016614), 2003.

[10] J. P. Gordon. Dispersive perturbations of solitons of the nonlinear Schrödinger equation. *J. Opt. Soc. Am. B*, 9:91–97, 1992.

[11] A. Hasegawa and F. Tappert. Transmission of stationary nonlinear optical pulses in dispersive dielectric fibres. I. Anomalous dispersion. *Appl. Phys. Lett.*, 23:142–144, 1973.

[12] Russell L Herman. A direct approach to studying soliton perturbation. *J. Phys. A: Math. Gen.*, 23:2327–2362, 1990.

[13] R. Hirota. Exact envelope-soliton solutions of a nonlinear wave equation. *J. Math. Phys.*, 14:805–809, 1973.

[14] S. M. Hoseini and T. R. Marchant. Solitary wave interaction and evolution for a higher-order Hirota equation. *Wave Motion*, 44:92–106, 2006.

[15] S. M. Hoseini and T. R. Marchant. Solitary wave interaction for a higher-order nonlinear Schrödinger equation. *IMA J. Appl. Math.*, 72:206–222, 2007.

[16] N-N. Huang, S. Chi, and X-J. Chen. Foundation of direct perturbation method for dark solitons. *J. Phys. A: Math. Gen.*, 32:3939–3945, 1999.

[17] T. Kano. Normal form of nonlinear Schrödinger equation. *J. Phys. Soc. Jap.*, 58:4322–4328, 1989.

[18] L. Kavitha and M. Daniel. Integrability and soliton in a classical one dimensional site dependent biquadratic Heisenberg spin chain ans the effect of nonlinear inhomgeneity. *J. Phys. A: Math. Gen.*, 36:10471–10492, 2003.

[19] Y. S. Kivshar and B. Luther-Davies. Dark optical solitons: physics and applications. *Phys. Rep.*, 298:81–197, 1998.

[20] Y. S. Kivshar and M. Salerno. Modulational instabilities in the discrete deformable nonlinear Schrödinger equation. *Phys. Rev. E*, 49:3543–3546, 1994.

[21] Y. Kodama. On integrable systems with higher order corrections. *Phys. Lett.*, 107A(6):245–249, February 1985.

[22] Y. Kodama. On solitary wave interaction. *Phys. Lett. A*, 123:276–282, 1987.

[23] Y. Kodama and A. V. Mikhailov. *Obstacles to asymptotic integrability.* in *I. G. A. Fokas (ed.)*, volume 26 of *Progress in nonlinear differential equations and their applications*, pages 173–204. Birkhauser, 1997.

[24] L. Li, Z. Li, Z. Xu, G. Zhou, and K. H. Spatschek. Gray optical dips in the subpicosecond regime. *Phys. Rev. E*, 66(046616), 2002.

[25] A. Mahalingam and K. Porsezian. Propagation of dark solitons with higher-order effects in optical fibers. *Phys. Rev. E*, 64(046608), 2001.

[26] T. R. Marchant. Asymptotic solitons for a higher-order modified Korteweg-de Vries equation. *Phys. Rev. E*, 66(046623):1–8, October 2002.

[27] T. R. Marchant. Asymptotic solitons on a non-zero mean level. *Chaos, Solitons and Fractals*, 32:1328–1336, 2007.

[28] T. R. Marchant and N. F. Smyth. Soliton interaction for the extended Korteweg-de Vries equation. *IMA J. Appl. Math.*, 56:157–176, April 1996.

[29] T. R. Marchant and N. F. Smyth. The initial boundary problem for the Korteweg-de Vries equation on the negative quarter-plane. *Proc. R. Soc. Lond. A*, 458, 2002.

[30] Y. Matsuno. Dynamics of interacting algebraic solitons. *Int. J. Mod. Phys. B*, 9:1985–2081, 1995.

[31] D. Mihalache, L. Torner, F. Moldoveanu, N.-C. Panoiu, and N.Truta. Inverse-scattering approach to femtosecond solitons in monomode optical fibers. *Phys. Rev. E*, 48(6):4699–4709, 1993.

[32] A. A. Minzoni, N. F. Smyth, and A. L. Worthy. A variational approach to the stability of an embedded NLS soliton at the edge of the continuum. *Phys. D*, 206:166–179, 2005.

[33] D. E. Pelinovsky and J. Yang. A normal form for nonlinear resonace of embedded solitons. *Proc. Roy. Soc. Lond. A*, 458:1469–1497, 2002.

[34] D. E. Pelinovsky and J. Yang. Stability analysis of embedded solitons in the generalized third-order nonlinear Schrödinger equation. *Chaos*, 15(037115), 2005.

[35] D. H. Peregrine. Water waves and their development in space and time. *Proc. Roy. Soc. Lond. A*, 400:1–18, 1985.

[36] R. F. Rodriguez, J. A. Reyes, A. Espinosa-Ceron, J. Fujioka, and B. A. Malomed. Standard and embedded solitons in nematic optical fibers. *Phys. Rev. E*, 68(036606), 2003.

[37] T. R. Taha and M. J. Ablowitz. Analytical and numerical aspects of certain nonlinear evolution equations. II. Numerical, nonlinear Schrödinger equation. *J. Comp. Phys.*, 55:231–253, 1984.

[38] S. Wabnitz, Y. Kodama, and A. B. Aceves. Control of optical soliton interactions. *Opt. Fibr. Tech.*, 1:187–217, 1995.

[39] T. Yan, H. Cai, and N-N. Huang. Direct perturbation theory for nearly integrable nonlinear equation with application to dark-soliotn solutions. *J. Phys. A: Math. Gen.*, 39:9493–9502, 2006.

[40] J. Yang. Complete eigenfunctions of linearized integrable equation expanded around a soliton solution. *J. Math. Phys.*, 41:6614–6638, 2000.

[41] J. Yang. Stable embedded solitons. *Phy. Rev. Lett.*, 91(143903):1–4, 2003.

[42] J. Yang and T. R. Akylas. Continuous families of embedded solitons in the third-order nonlinear Schrödinger Equation. *Stud. Appl. Math.*, 111:359–375, 2003.

[43] J. Yang and D. J. Kaup. Stability and evolution of solitary waves in perturbed generalized nonlinear Schrödinger equations. *SIAM J. Appl. Math.*, 60:967–989, 2000.

[44] H. C. Yuen and B. M. Lake. Nonlinear dynamics of deep-ware gravity waves. *Adv. Appl. Mech.*, 22:67–229, 1982.

[45] V. E. Zakharov and A. B. Shabat. Exact theory of two-dimensional self-focusing and one-dimensional self-modulation of waves in nonlinear media. *Sov. Phys. JETP*, 34:62–69, 1971.

[46] Y. Zhu and J. Yang. Universal fractal structures in the weak interaction of solitary waves in generalized nonlinear Schrödinger equations. *Phys. Rev. E.*, 75(036605), 2007.

[47] Q. Zou and C. H. Su. Overtaking collision between two solitary waves. *Phys. Fluids*, 29:2113–2123, 1986.